Kaunas University of Technology

Faculty of Mechanical Engineering and Design

Aircraft Propeller blade quality evaluation using ultrasound NDT

Master's Degree Final Project

Paulius Jakas
Author

Prof. Dr. Elena Jasiūnienė
Supervisor

Kaunas University of Technology

Faculty of Mechanical Engineering and Design

Aircraft Propeller blade quality evaluation using ultrasound NDT

Master's Degree Final Project

Aeronautical engineering (6211EX024)

Paulius Jakas
Author

Prof. Dr. Elena Jasiūnienė
Supervisor

Doc. Marius Rimašauskas
Reviewer

Kaunas, 2019

Kaunas University of Technology

Faculty of mechanical engineering and design

Aircraft Propeller blade quality evaluation using ultrasound NDT

Declaration for academic integrity

I do confirm that mine , Paulius Jakas , final master thesis, topic „Aircraft propeller blade quality evaluation using ultrasound NDT“ was written sollely by myself and all given data and research results are valid and received honestly. In this thesis non of the parts were plagiarised from any written or online sources and all sources direct and indirect citations are marked as such in the literature links. I did not pay any monetary amounts except established by law while doing this thesis.

I do understand that if inconsistency with honestly principles are detected , penalties will be applied as per KTU internal law.

Kaunas University of Technology

Faculty of mechanical engineering and design

Aeronautical engineering (6211EX024)

Master's degree final project task

Student Paulius Jakas

1. Final project topic:

In lithuanian : Propelerio mentės kokybės įvertinimas naudojant ultragarso neardomąją kontrolę

In english : Propeller blade quality evaluation using ultrasound NDT

2. Project aim :

To create propeller blade computerised inspection model in order to check ultrasonic inspection method validity and certify method experimentally.

3. Project tasks :

1. To do literature review regarding similar tasks already analysed, NDT techniques available to be utilised for complex shape and material composition parts, review sound attenuation in composites
2. Determine propeller blade geometry, structure and materials
3. Design propeller blade computerised model in CIVA NDT software
4. Determine and utilise correct NDT probe for complex propeller blade shape analysis
5. Utilise ultrasonic inspection techniques on physical blade using model data

4. Project structure :

Introduction, literature review, computer model of the propeller blade inspection , experimental analysis.

5. Project consultants :

Final project author _____

(name, surname, signature and date)

Final project supervisor _____

(name, surname, signature and date)

Paulius Jakas. PROPELLER BLADE QUALITY EVALUATION USING ULTRASOUND NDT. Final project of Aeronautical engineering, *Master's degree* /supervisor prof. dr. Elena Jasiūnienė, Kaunas University of Technology, Faculty of Mechanical engineering and design .
Kaunas, 2019. 77 p.

SUMMARY

In this work, aircraft ATR42 propeller blade consisting of composite materials and aluminium spar overall ultrasound NDT inspection technique has been determined. Propeller blade computerised inspection model has been established and experimentally examined for validation. Propeller blade each of single material acoustic characteristcs have been found. Artificial flaws in all layers of the propeller blade examined experimentally and electronic scanning graphs provided. Most suitable propeller inspection probe has been concluded.

CONTENTS

List of Figures

List of Tables

1. INTRODUCTION

Composite propeller blades are widely used on turbogas propeller driven aircrafts around the globe. Blades are exposed to high variety of environmental issues like sand erosion, weather driven water ingress, dents and nicks at the leading edge and tips, burns caused by lightning strike and other. Line maintenance usually have no other means to inspect propeller blade but to replace it, in case of doubt. This most often happens when blade is mechanically damaged by foreign object (stone, sand) - dents are caused on the leading edge of the blade which in turn can cause delamination between outer fiberglass composite shell and polyurethane foam. Maintenance manuals do not provide any other serviceability inspection method but visual and tap test and there are no other NDT means provided in order to inspect serviceability of the blade while in service. Propeller blade price is very high and usually there are 8 to 12 blades installed on the aircraft. Finding more precise means for non-destructive inspection on site to determine blades serviceability would reduce unnecessary removals of the propeller blade and save the costs involved.

This thesis was motivated by the factors that project involves complex shaped part subjected to mechanical and ageing defects - made of composite and solid materials conjunction, so such fields as acoustic attenuation and materials acoustic characteristics determination would be concurrent requirements for propeller blade experimental and theoretical inspection model. Thesis examines propeller blade flaws detectability chances in all material layers and analyse the materials separately.

Project aim – to create propeller blade computerised inspection model in order to check ultrasonic inspection method validity and certify method experimentally.

Project tasks:

1. To do literature review regarding similar tasks already analysed, NDT techniques available to be utilised for complex shape and material composition parts, review sound attenuation in composites
2. Determine propeller blade geometry, structure and materials
3. Design propeller blade computerised model in CIVA NDT software
4. Determine and utilise correct NDT probe for complex propeller blade shape analysis
5. Utilise ultrasonic inspection techniques on physical blade using model data

2. THEORY OF ULTRASONIC NDT

2.1 SCHEDULED PROPELLER BLADES INSPECTION TECHNICS

Composite propeller blade manufacturing scheme was published in patent WO 1993008017 A1 in 1992 and since then its modifications are widely used in various types of aircrafts. Composite propeller blade materials composition and distribution is showed in figure 2.1.

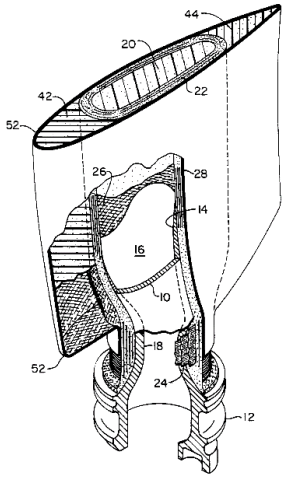

Figure 2-1. Blade structure [2]

Table 2.1 provides detailed information about the materials which incorporate any composite propeller blade.

Table 2-1. Propeller blade materials [2]

Item number	**Material**
Metal retention, item 12	Lightweight metal alloy
Composite aerofoil - 52	Glass composite fibers
leading edge filler – item 42	Polyurethane foam
trailing edge filler- item 44	Polyurethane foam,
Metal spar, item 20	Lightweight metal alloy
Blade spar - wrap – item 22	Kevlar aramid fibres or fiberglass

Every 7 years blades are subjected to major checks regarding erosion/corrosion and internal debonding damages. If blade does not pass the ultrasonic inspection on blade tulip location or its glass fiber layer is delaminated – propeller blade must be scrapped. Blade inspections scope is identified in table 2.2.

Table 2-2. Current propeller blade zones inspections methods [1].

Blade Root Metallization	Visual inspection for corrosion
Blade Foam	If foam leading edge or trailing edge damage is less than or equal to two square inches in area and up to 0.125 inch in depth it must be repaired
Blade Composite Shell	Examination of the composite shell for any evidence of damage – impact, delamination, cracks.
Blade Composite Shell	Examination for fatigue cracks
Blade Tulip Flange	Visual examination of the tulip flange for evidence of mechanical damage.
Blade Nikel Sheath	Examination for dents
Blade Composite Shell	Examination the blade shell for evidence of blistering

Propeller blades are subjected for tap test, ultrasonic and visual tests. As composite blade is made mainly of composite materials, so numerous other techniques could be used including ultrasonic testing thermographic testing, infrared thermography testing ,radiographic testing, visual testing or visual inspection, acoustic emission testing, acoustic-ultrasonic, shearography testing ,optical testing, electromagnetic testing, liquid penetrant testing ,and magnetic particle testing [4]. A composite material is a consolidation of two (or more) unique materials that are bonded together which gives final mechanical and chemical features of the bond. Composite materials are widely used in aerospace for weight saving and usually involves glass, aramid or carbon fiber reinforced materials. [5]. Composite materials are equally important for propulsion systems a and are currently widely used in turbofan engines design (Low pressure stages like fan blades) and gives good thrust-to-weight ratio. Propeller blade is not an exception and glass fiber composite is used as structural shell while polyurethane foam is used as filler. Combination of metal spar which is embraced and bonded to glass fiber shell and foam filler gives good structural characteristics, low maintenance needs and weight saving, also enables to make so needed complex air foil propeller design blade is so dependable on [49].

The tap test area must have a nominal intensity of 72 decibels with a maximum intensity of 75 decibels (Kevlar shell) on the camber and face sides [1]. Inspection zoning as identified on figure 2.2.

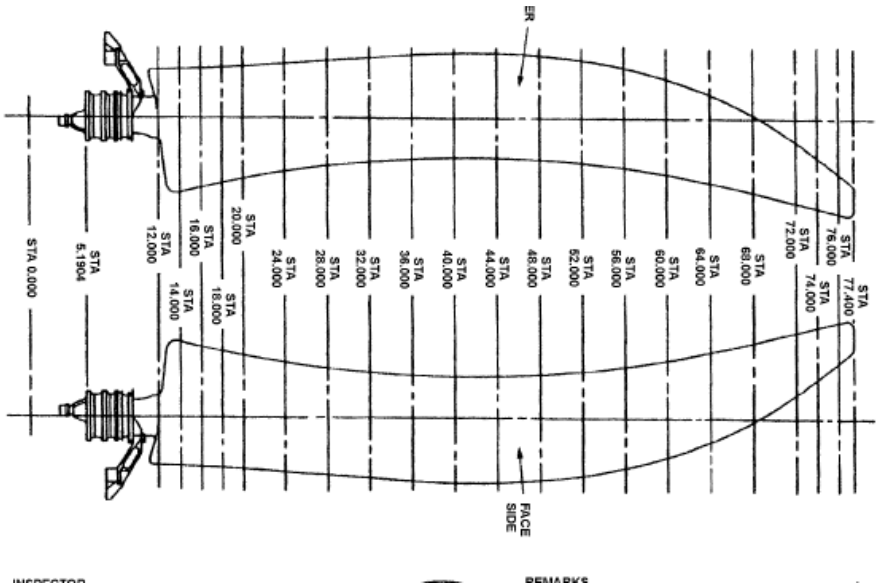

Figure 2-2. Blade stations [1]

Audible sounds and ultrasonic waves are of the same physical nature; both are acoustic vibrations. Ultrasonic waves have frequencies greater than 20 Kilohertz (KHz). In most of the tests, the frequency range is from 1 to 25 Megahertz (MHz). Ultrasonic inspection can be carried out on almost every type of material used in the construction of aircraft. It is an extremely sensitive method of detecting surface and subsurface flaws and has few limitations. From the different basic methods of ultrasonic testing, pulse-echo is the most frequently used [3] .

2.2 ULTRASONIC NDT METHODS FOR COMPOSITES

In it's the most basic explanation of ultrasonic NDT technician utilise piezo-electric probe which sends and receives ultrasonic pulses. If there are any flaws or imperfection if the ultrasound beam path echoes are generated from the flaw surface which is sent back to the probe. Technician by looking in the ultrasonic detector (Omniscan or similar models) tries to understand the echoes received and interpret them accordingly. Technician will adhere to standardisation instructions which are well established within the industry [13].

The pulse-echo ultrasonic inspection method is conducted using the principle of reflected sound waves. Sound has a stable velocity in a given material, therefore a change in the acoustical impedance of the material causes a change in the sound velocity at that point, generating an echo. The distance of the acoustical impedance change (defect-flaw) can be determined if the velocity of the sound in the test material and the time taken for the sound to reach and return from the flaw is known. The ultrasonic flaw detection equipment comprises the following basic elements [4] and principle schamatic is showed in figure 2.3.

- US monitor – rate generator with RF pulser
- Transducer probe (search unit) with piezoelectric crystal
- Specimen
- Coupling fluid or wedge

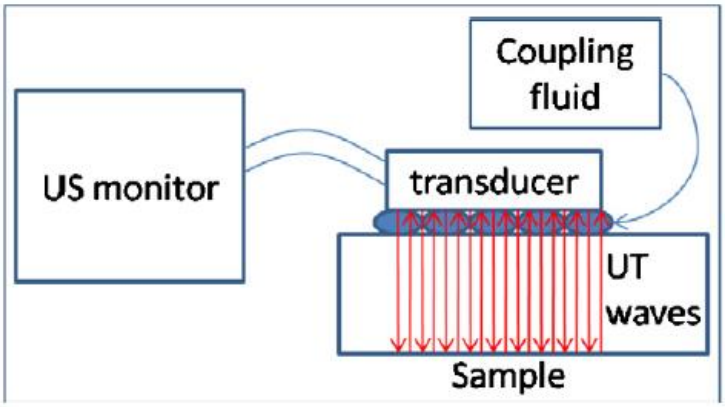

Figure 2-3. Flaw detection equipment elements [24]

Ultrasonic rate generator within the equipment electrically energize the RF pulser causing it to emit electrical pulses. The probe oscillates on receipt of the pulses and converts them into ultrasonic waves, which are transmitted through the specimen which is inspected. Any change in the acoustical impedance, caused by a defect in the materials or interface between them reflects the sound back in the form of an echo and piezoelectric crystal in the search unit receives the wave [4]. The piezoelectric crystal has two functions: - to transform the electric energy into mechanical energy (sound) - to change the mechanical energy of the return signal (echo) back to electrical energy for display and evaluation. The search unit functions as a receiver for reflected energy between pulses. [4].

The time base, which is triggered simultaneously with each transmission pulse, causes a spot to move rapidly across the instrument screen. The motion of this spot, controlled by a sweep generator, is called sweep and provides a time-base for the analysis of information. The spot sweeps from left to right across the face of the scope 50 to 5000 times per second, or higher if required for high-speed automated scanning. The earliest time is represented at the left side of the sweep and time increases towards the right. The time displayed on the instrument screen can be controlled and ranges, for test purposes, from 3 microseconds to 4000 microseconds. A sweep delay control enables the sweep to be moved back and forth, allowing the operator to start the area of main interest at the left-hand side of the instrument screen. [3].

Sharp vertical spikes, called pips, are produced by voltages applied to the instrument screen. The voltages are generated by the initial pulse and also by the transducer when struck by return echoes from reflections within the test piece. These are spaced along the baseline according to their time of receipt. The first echo received appears as a pip on the left of the screen and later echoes are spaced towards the right, the distance between them is proportional to the time elapsed between their respective times of arrival. Sound travels through a material at a constant speed, therefore the spacing of the pips indicates distance. The relative proportions of spacing to elapsed time can be varied. [3].

The test equipment may have a graduated screen or may have electronic range markers which are generated within the equipment and are used to provide a time or distance reference along the instrument screen baseline. The spacing of the range markers can be adjusted to provide convenient divisions along the sweep and may be controlled without affecting other adjustments of the instrument. [3].

Generation of ultrasonic pulses is accomplished in several ways. In practical testing, the selection of frequency depends on the sensitivity desired and sound penetration required, e.g. high frequency for sensitivity and low frequency for penetration. There are several ways of deriving the required frequency at the search unit, by a short burst of sound waves or by pulses. [3].

High variety of methods has been already analysed for composites flaws detection including phased array, immersion UT, radiographic testing, active thermographic testing, infrared, visual inspection, non-contact methods, vibration methods, shearography [21-37].

Phased array ultrasonic testing (PAUT) is different from conventional ultrasonic inspection because the probes contain multiple transducers which are controlled by sophisticated computer programs. This allows the operator to control the type of sound beam that is issued by the probe. The beam can be focused to give high sensitivity or steered to cover a larger area than normal. For angled beam inspections the probe can be programmed to emit a range of beam angles not just one. These capabilities make PAUT a powerful inspection tool which is available in a portable instrument of similar size and weight to conventional ultrasonic flaw detectors [22]

Figure 2-4. Single element versus Phased array elements [50]

Basically, a 1-D *phased array* probe is a transceiver composed of many small individual elements (transducers), each with a width much smaller than its length as showed in figure 2.4. In order to minimize transverse modes causing unwanted cross-talk effects, the individual elements are embedded in a special sealing compound which acoustically isolates them from one another [22].

Each of these transducers represents a line-shaped source for cylindrical waves, which interfere with each other under appropriate excitation. These individual wavelets combine to produce a new, coherent wave front.

Due to the slightly delayed excitation of the individual elements, the phases of the wavelets can be synchronized. In this way, sound beams with special characteristics (e.g. angle, focusing) as showed in figure 2.5.

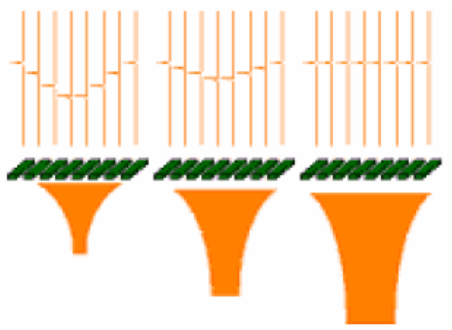

Figure 2-5. PA focusing [50]

Basic Specification of Any Ultrasonic unit having the following general specification [4]:

- Linear Horizontal and Vertical Deflection Frequency Range 0.5 to 15 MHz (0.5 to 25 MHz)
- Amplification 0 to 80 dB (0 to 100 dB) in 2 dB steps
- Mode -Pulse echo/through transmission
- Display -High frequency rectified signal display
- Depth- Range Variable between 10 mm - 250 mm (0.394 in - 9.84 in), in steel
- Sound Velocity- 2000-7000 m/sec, in steel
- Delay Range- 0 - 200 mm (0 - 7.87 in), in steel

Composite structures are subject for ageing, interlayer cracks and delamination. Excessive studies conducted for polyurethane aging effects through the foam usage in aerospace industry. Foam ageing effects starts at molecular dimensions which continues to load loss and consequential micro voids in the foam. Foam ageing also contributes to foam hardness, density change and consequential water ingress [38].

Glass fiber reinforced composites as a homogeneous materials experience thermoelastic effects during the operating life which causes the variation of material volume and causes stress. [40] Thermoelastic effects and dynamic loads throughout the propeller blade operating life are one the they main contributors to propeller blade glass fiber composite shell natural ageing. Ageing visual example is showed in figure 2.6.

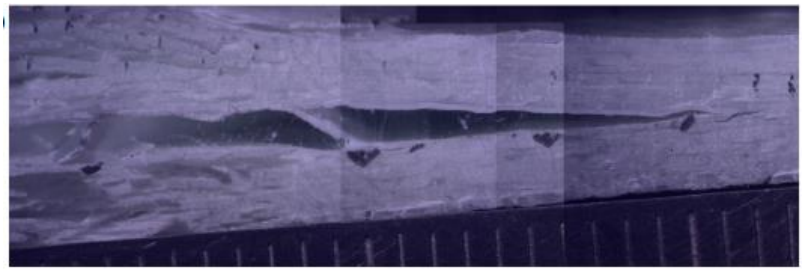

Figure 2-6. Composite material ageing effects [40]

Undetected mechanical damages are another contributor for composite materials ageing. Especially in aircraft industry investigations have been conducted to increase the accuracy of ultrasonic inspection on composite materials, increase efficiency. C and S electronical scanning techniques are widely used for characterisation of composite plies and both method of plotting utilise signal amplitude. The combination of time of flight, material density mutation and attenuation give mapping

where flaws can be seen. Investigation of A scan commonly phased out and C and S-scan is used more to gain inspection efficiency and speed [41].

Incorrectly performed adhesively bonded repairs (principal schematic is showed in figure 2.7) were also investigated by industry for better monitoring and ultrasonic scanning utilised to detect repairs flaws [42-43]. Common damages can arise from accidental mechanical damage by tooling, bird strike, lightning strike, hail damage. Propeller blade shell as other composite materials are subject for external bonded patches and scarf bonded patches which if incorrectly done would cause repair delamination.

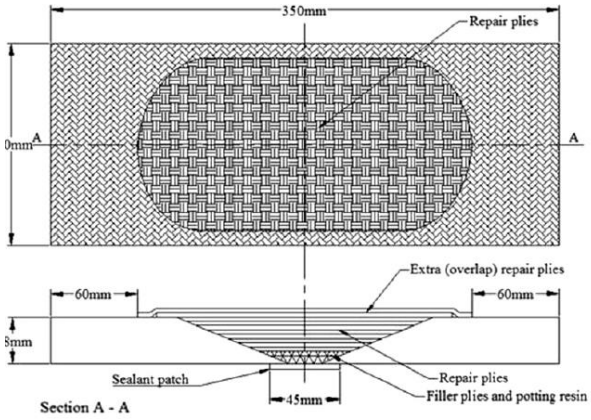

Figure 2-7. Composite repair patch [42]

As not only Ultrasonic tools can be used, thermographic inspection of the impact damages can be used as well, refer to figure 2.8 [43]. Researches are conducted for ultrasonic imaging of C and S scans and impact energy comparison [43].

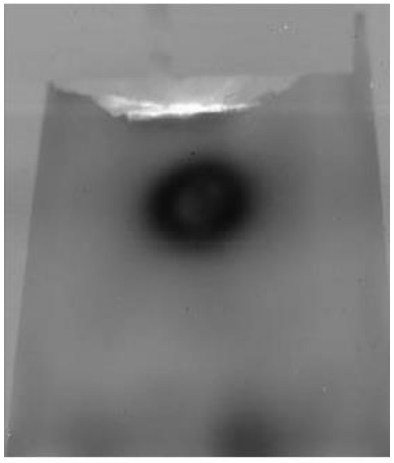

Figure 2-8. Thermographic image of impact damage [43]

Assessment of uncertainty in damage evaluation when ultrasonic means are used are widely researched. The key elements in damage detectability are angle of the inspection beam, delay line usage, transducer frequency, transducer diameter, near surface discontinuity detection by probe near

field elimination by usage of wedge and transducer calibration (usage of approved standards) [44]. Phased array probes have advantage here comparing to single element as more precise mapping of the damage can be done in S or C scan. Depending on the specimen linear array or annular array can be used as showed in figure 2.9.

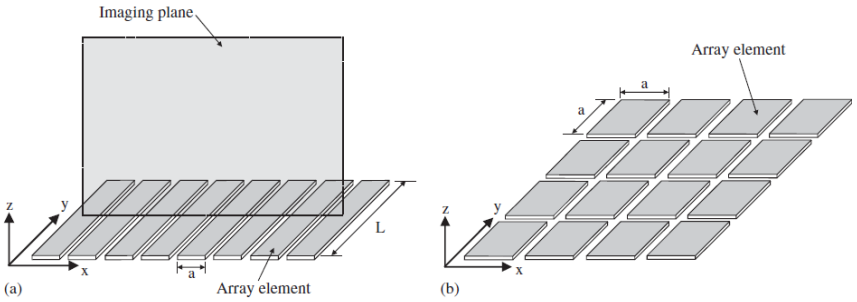

Figure 2-9. Arrays (a) - linear, (b) - annular array, where a is single element size [21]

Phased arrays are commonly used for composites compressed cracks in glass and carbon fibre reinforced plastic composites [47] as per schematic and result as showed in figure 2.10.

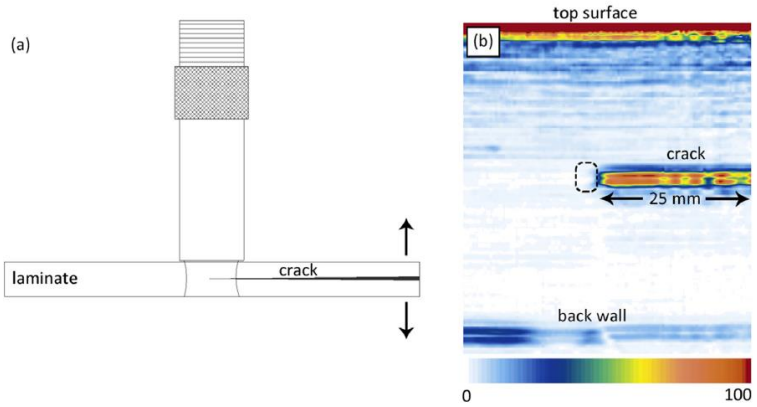

Figure 2-10. Phased array electronic scanning. a) schematic presentation b) S scan image [47]

Pulse-Echo single probe can be also used for fatigue damages detection within thick composites. During researches it was concluded that at high normalised stresses the amplitude rapidly rises due to cracks within the plies and increasing number of short delamination [45]. NDT using THz waves is an option when composite is made using soft epoxy resin in order to improve resolution [5].

This thesis was motivated by the factors that project involves was evaluating foam flaws detectability chances, glass fiber flaws detectability chances and interface flaws between the different material layers, attenuation effects and best inspection frequency.

2.2 Ultrasonic Recordings

Reflected ultrasonic energy can be presented (displayed), or recorded, in three ways [24] :

- A-Scan Presentation: uses standard cathode ray display equipment and is most commonly used in non-destructive testing.
- B-Scan Presentation: requires special equipment which is not easily used on aircraft. B-Scan presentation shows a cross-sectional plot of material thickness and internal discontinuities displayed on an image retention CRT or displayed on LCD screen.

- C-Scan Presentation: requires equipment manufactured for specific applications. C-Scan provides a recorded facsimile flat plane view of the scanned area.
- S-scan or sectorial scanning utilises phased array for electronic scanning in the entire length of the array or at the required angle taking all elements into account

When using the A Scan presentation, the first deflection (left to right), on the instrument screen baseline, is caused by the signal received from the front surface or interface of the part. The deflection farthest to the right is caused by the signal received by the back surface or interface. Deflections between these two indicate discontinuities. Refer to figure 2.11.

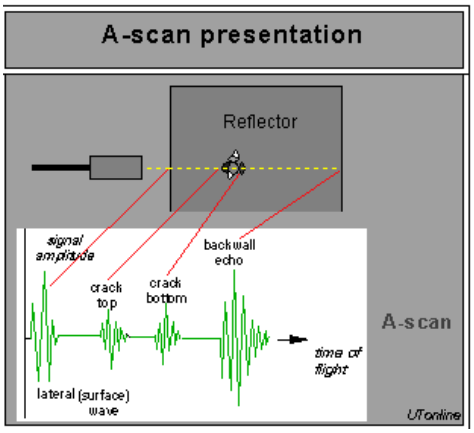

Figure 2-11. A-scan principle [4]

The amplitude of the echoes is related to the amount of receiver gain and to the size, and orientation, of the cause of the reflection. The amplitude of the deflection can, by comparison with a duplicate or standard part with a discontinuity of known dimension, be used to estimate the size of the discontinuity [3].

The B-scan is a cross-sectional profile of the specimen presentation as showed in figure 2.12. The time-of-flight of the sound wave is displayed on the vertical axis and the position of the transducer is showed along the horizontal axis. From the B-scan, the depth of the defect and approximate dimensions in the scan direction can be determined. The B-scan is typically used together with A-scan where amplitude trigger is observed. The echo is triggered by the sound reflecting from the backwall of the specimen and by defects which generate smaller reflections within the material. When the probe is over flaws *B* and *C*, profiles that are similar to the length of the defects and at similar depths within the specimen are displayed on the B-scan. It should be noted that larger flaws near the surface might mask smaller defects which are just above the near surface flaw.

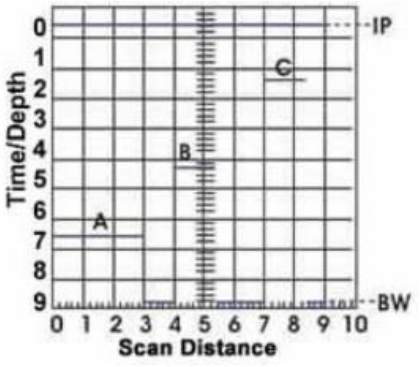

Figure 2-12. B-scan principle [4]

Like the B-scan, the S-scan shows a 2-D cross section of the test object in beam direction, refer to figure 2.13. But unlike the B-scan, the probe sweeps through a specific angular sector; with conventional ultrasonic systems, this process is based on mechanical control, and with *phased* arrays, it is based on electronic control. The reflectors existing in this sector are then displayed accordingly. The *phased array* S-scan is commonly defined as a scan of a complete sector without probe movement.

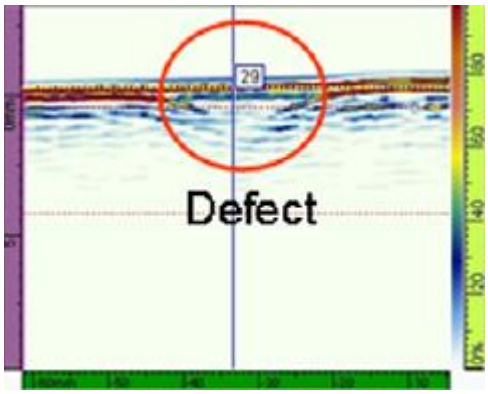

Figure 2-13. S-scan principle [24]

2.3 WAVE MODES

There are many wave forms and modes of ultrasonic vibration which can travel through metals. The pulse-echo technique can be employed in several wave modes (figure 2.14) [1] :

- Longitudinal wave mode,
- Shear (transverse) mode,
- Surface beam mode.

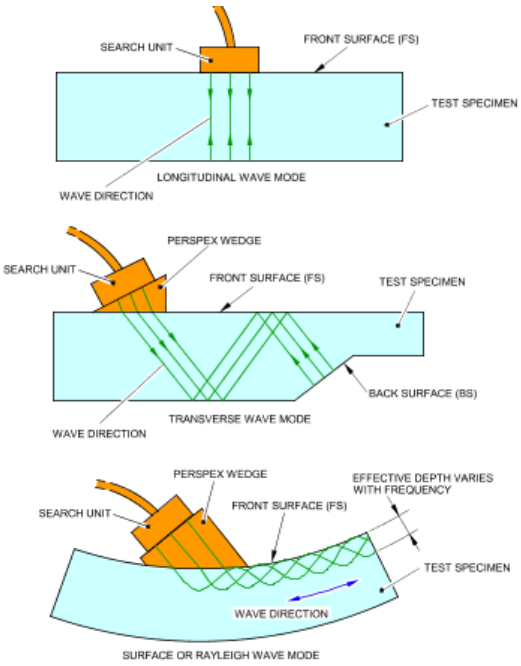

Figure 2-14.Wave modes [51]

2.3.1 Longitudinal (Compression) Wave Mode

Following modes can be excluded [1] :

(a) In the longitudinal wave mode, the particles vibrate in the direction of propagation. This is similar to audible sound waves, which are also compressional in character. Longitudinal waves are produced when the search unit is positioned so that the angle of entry into the part is at 90 degrees, or normal, to the surface (refer to figure 2.15)

(b) When inspecting parts having a back interface not parallel to the front, the longitudinal waves will be reflected and refracted internally, which could result in ghost signals on the instrument screen and lead to misinterpretations.

(c) By using a perspex wedge to obtain an incident angle of entry, the longitudinal wave may be used as a refracted angular beam. The longitudinal wave should not be used with incident angles greater than 15 degrees to ensure that no interference from shear wave mode occurs.

(d) Longitudinal wave mode can be used to detect laminar orientated discontinuities and for thickness measurement. Thickness measurements from 0.25 mm (0.010 in) to several centimetres (inches) can be accomplished.

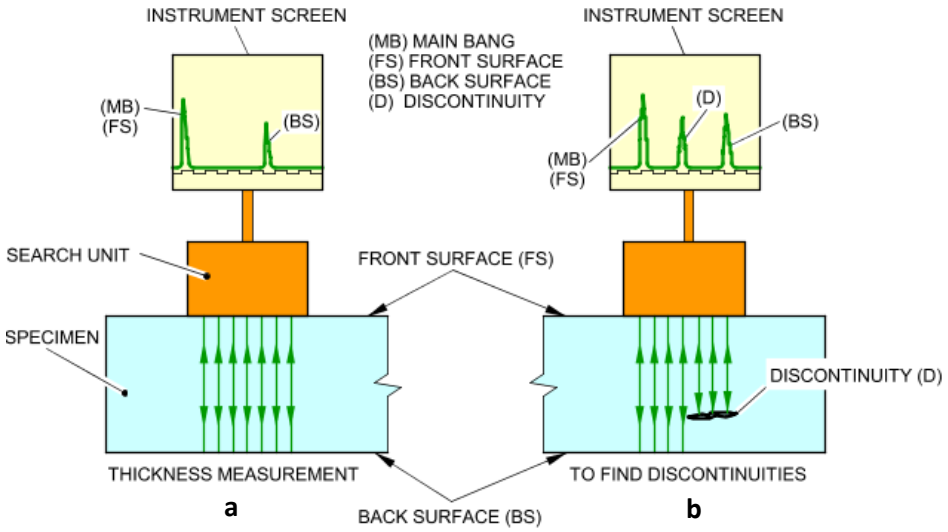

Figure 2-15. Longitudinal wave principles. a) for thickness measurement principle; b) flaw detection principle [51]

2.3.2 Shear Wave (Transverse) Mode

(a) In shear wave mode, particles vibrate transversely to the direction of wave propagation, with a velocity approximately half that of longitudinal waves. Shear waves are produced when longitudinal waves are refracted at the front interface. Refraction occur whenever an angle of entry is established. As a result of the compound wave motion, the shear wave mode has a high degree of sensitivity (refer to figure 2.16) [1].

(b) An advantage of shear wave mode is its versatility, since, by using various angles of perspex wedges, a variety of beam angles can be produced, which enables defects located within the part and in opposite extremities to be detected [1].

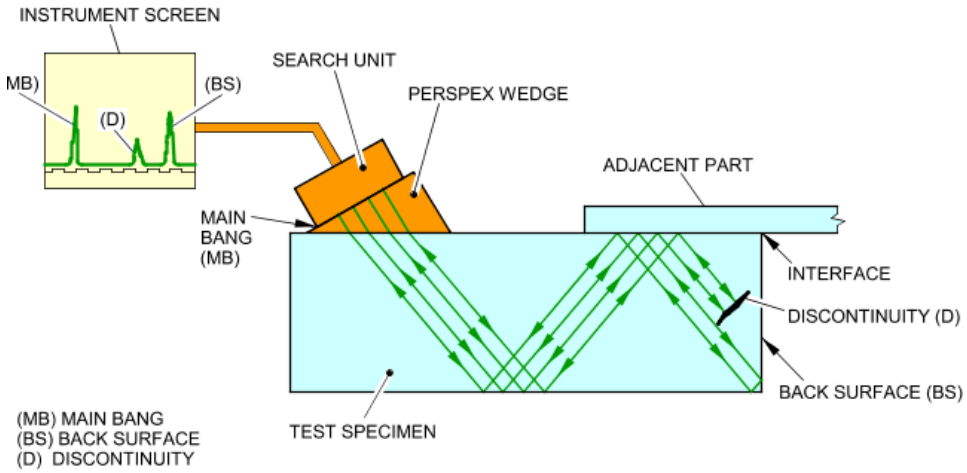

Figure 2-16. Shear wave principle [51]

2.3.3 Surface Wave Mode

Surface (Rayleigh) waves are elastic vibration whose energy is directed to narrow region just below the surface of a solid specimen like showed in figure 2.17. Surface waves propagation is independent from frequency and is defined by elastic modulus and density of a solid. There is a little attenuation effect, however energy decreases rapidly to due waves penetration deeper below the surface [1, 22].

(b) The waves are produced by increasing the angle of incidence sufficiently to refract all of the energy into the surface of the part. The surface wave mode can be useful in detecting discontinuities open to the accessible surface. The optimum angle for producing surface wave mode is 64 degrees. The crystal most suitable for surface wave mode is lithium sulphate which oscillates at a frequency of 2.25 MHz [1, 22].

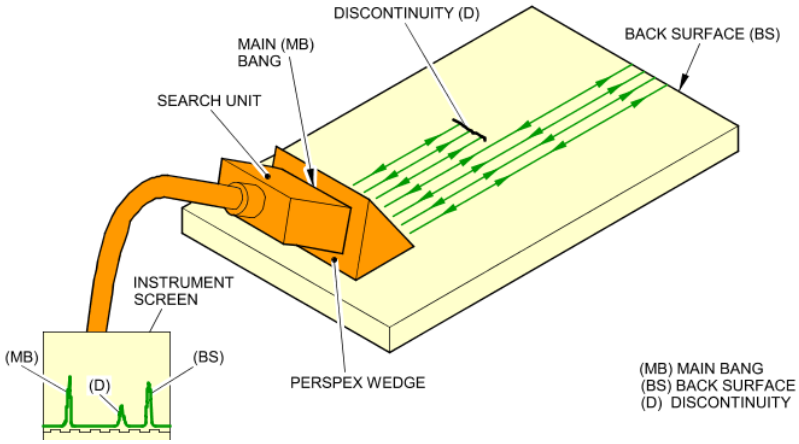

Figure 2-17.Surface wave [51]

2.4 Reflection and Transmission Energy at Interfaces

Ultrasonic energy incident upon an interface between two media of differing acoustic impedance (Z) may be partially or totally reflected or transmitted across the interface. C. The proportion of signal reflected or transmitted can be determined from the acoustic impedances of the two media using formula 2.1 [4]:

$$Z = \zeta \; x V \qquad (2.1)$$

Where: ζ = material density and V = velocity.

Some of the known reflections are listed in table 2.3.

Table 2-3. Reflection and transmission energy [3]

Material 1	Material 2	Reflection	Transmission *
Water	Aluminum	83.8 %	183.8 %
	Steel	93.6 %	193.6 %
Aluminum	Air	-99.9 %	0.01 %
Steel		-99.9 %	0.01 %

When ultrasonic vibrations are reflected from boundaries of two materials with different acoustic properties, this can be compared to a beam of light travelling through space and being reflected from a number of mirrors. The path travelled by the beam of ultrasonic energy is dependent upon the angle at which it impinges upon the reflecting surface as well as the number and Locations of these surfaces. In cases where ultrasonic waves strike a surface at an angle to the normal, the reflected angle is equal to the angle of incidence, refer to figure 2.18 [4].

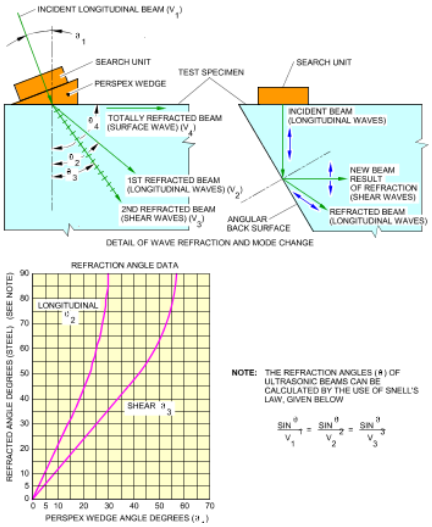

Figure 2-18. Waves refraction [51]

Refraction and mode conversion of the ultrasonic waves, when passing at an angle from one material to another, is analogous to the refraction of light beams when passing from one medium to another. Reflection at certain angles from a boundary also results in a mode conversion of ultrasonic waves. The ultrasonic sound waves are introduced at an angle into the material to be inspected by mounting the crystal on a plastic wedge. If the acoustic velocities in the test material and the plastic wedge differ, the longitudinal wave passing through the wedge will be refracted in the test material. At certain angles of entry of the ultrasonic sound wave into the test material, mode conversion takes place if the acoustic velocities of the wedge and the test material differ substantially. Some of the known acoustic velocities are identified in table 2.4 [4].

Table 2-4. Acoustic properties [51]

ACOUSTIC PROPERTIES OF MATERIALS						
MATERIALS	ACOUSTIC VELOCITIES m/s V_1 & V_2	V_3	V_4	ACOUSTIC IMPEDANCE (Pa s/mx10^6)	WAVELENGTH (mm AT 5 MHz)	DENSITY (kg / m^3)
METALS						
ALUMINUM ALLOY	6350	3100	2900	17.2	1.27	2710
BERYLLIUM	12800	8710	7870	12.8	2.56	1820
BRONZE, PHOSPHOR	3530	2230	2010	31.2	0.71	8860
COPPER	4660	2260	1930	41.8	0.93	8900
LEAD, ANTIMONY	2160	810	740	23.6	0.43	10900
MAGNESIUM (AM35)	5790	3100	2870	10.1	5.79	1740
MOLYBDENUM	6290	3350	3110	63.5	1.26	10090
INCONEL	7820	3020	2790	64.5	1.56	8250
MONEL	6020	2720	1960	53.1	1.20	8830
STEEL	5850	3230	2790	45.6	1.17	7800
TITANIUM	6100	3120	2790	27.7	1.22	4540
NONMETALS						
AIR	330	–	–	0.0033	0.07	1.0
OIL	1360	–	–	1.27	0.28	920
LUCITE	2670	1120	–	3.2	0.53	1180
WATER	1490	–	–	1.49	0.30	1000
CARBONFIBER						
RESIN	3000	1500	1350	45	0.60	2500
ADHESIVE	3000	1500	1350	33	0.60	1100
GLASSFIBER						
KEVLAR						

The wedge angle and resultant refraction angle (θ) which is showed in figure 2.19 can be calculated by applying the formula (Snell's Law).

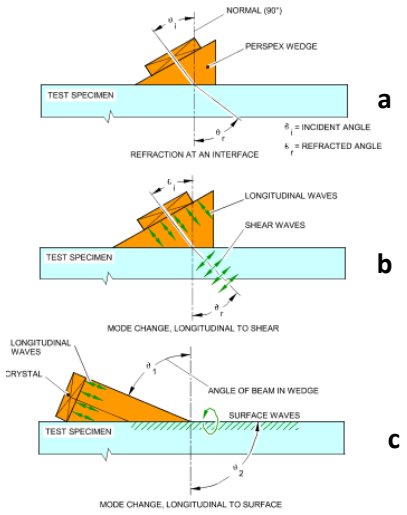

Figure 2-19.Refraction angle and wave mode change: a) longitudinal wave b) shear wave c) surface wave [51]

2.5 Detection Sensitivity of the Technique

This depends on different factors: - the orientation of planar discontinuities [3]:

- the frequency of the ultrasound,

- the size of the ultrasonic beam etc.

(a) The sensitivity is optimum when the discontinuity is perpendicular to the direction of the ultrasound beam, and this should determine the orientation of the transducer.

(b) In metallic materials, due to the various orientations of the discontinuities, compression, shear or surface waves can be used, depending on the shape and configuration of the part.

(c) In composite materials, most of the discontinuities to be detected are delaminations and disbonding in bonded parts. These discontinuities are always parallel to the surface of the part so composite materials, and disbonded parts, are usually checked using compression waves.

(d) As a general rule, using low Frequency (< 1 MHz; usually from 100 to 500 kHz), only large discontinuities can be detected.

(e) Using high frequency (>1 MHz; usually from 1 to 25 MHz), the resolution is better and smaller discontinuities can be detected.

(e) The Size of the Ultrasonic Beam (a) The narrower the ultrasound beam, the better the resolution. (f) To reduce the diameter of the beam, focussed probes are sometimes used to concentrate the acoustic waves.

The wavelength of the ultrasound wave used has a significant consequence on the probability of detecting a flaw. Flaw must be larger than one-half the wavelength in order to have reasonable change to be detected. Two terms are usually used to describe NDT techniq‘s ability to detecte the flaws - sensitivity and resolution. Sensitivity is the ability to locate small discontinuities. Resolution is the ability of the system to locate discontinuities that are close together within the material or located near the part surface. Sensitivity and resolution quality increases with higher frequency (shorter waves) however consesus must be found between required sensitivity and resolution versus acoustic attenuation effects for composite materials frequency wise - high frequency wave front can be soon scattared within the specimen and wave wont reach its required target [6,46]

Detection capability and more precise damage size determination increases with frequency, however the attenuation as well. Hence, experimentally defined frequency should be chosen best suitable with inspection needs. Figure 2.20 shows different frequencies and defect resolution.

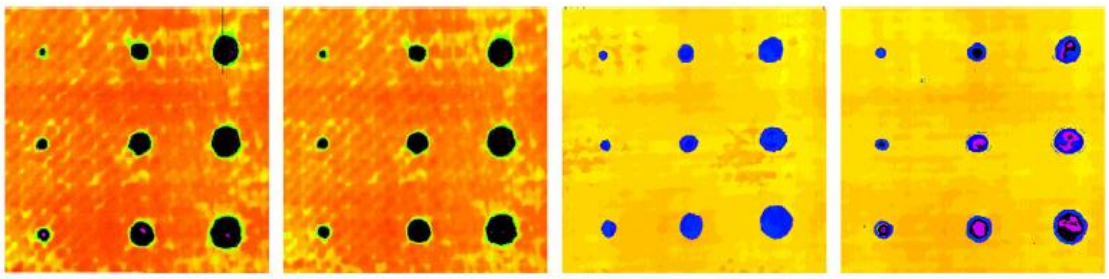

Figure 2-20. Damages C-scan comparison between different frequencies. a) detection at 2.25 MHz peak filtered pulse echo ; b) detection at 2.25 MHz threshold filtered pulse echo; c) detection at 5 MHz peak filtered pulse echo ; d) detection at 5 MHz threshold filtered pulse echo [44].

Probability of detection (POD) deals with reliable assessment of specimen. Many researches have been already done for different NDT technics and POD correlation. Its notable that phased arrays are considered one of the most reliable means to detect the defect [46].

Another phenomenon important for probability of detection is Near Field. When sound wave leaves the transducer a whole wave front is produced from multiple points along the face of the transducer. The cumulative effect of the wave front constructive and deconstructive interference of the individual waves is known as Near Field phenomena. It makes difficult to detect flaws which are located just below the surface. The size of the near field can be controlled by the probe frequency, transducer crystal diameter and material velocity [8] or by usage of the wedge. NZ can be found by using equation 2.2.

$$NZ = \frac{D^2 F}{4V} \qquad (2.2)$$

Where *NZ* is length of the near zone, *D* – diameter of the probe, *F* – frequency of the probe and *V* – sound velocity in the material.

2.6 ACOUSTIC ATTENUATION

As sound travels through materials sound wave is distorted, scattered or absorbed. Scattering phenomenon is caused by sound waves reflection, refraction or diffraction in each way that each sound particle becomes new sound wave source in all directions [15]. Sound attenuation is a measure for the sound loss in the material. Sound attenuation happens due to materials viscosity and sound pressure starts to diminish over the material. Sound attenuation is highly dependable of material matrix and type, whether it is solid or composite, non-homogenous materials. Different material matrix shape (refer to figure 2.21) and arrangement gives the most effect for absorption or scatter of ultrasonic wave. Sound attenuation can be used as ultrasonic spectroscopy tool for materials physical and chemical properties detection – material particles size and concentration [15].

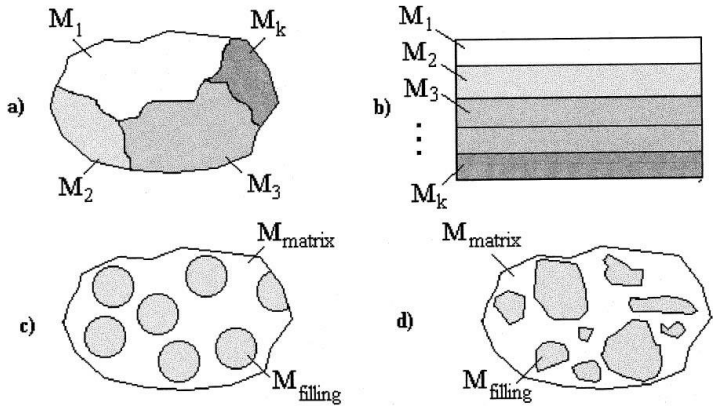

Figure 2-21. Molecular structure. (a) Multi-faced, (b) multi-layered, (c) two-component with regular filing, and (d) two-component with irregular filling [14]

Attenuation is highly dependable on sound frequency. Attenuation coefficient can be expressed in dB per cm and can be found from amplitude decay over distance made in material as in equation 2.3.

$$\alpha = -\frac{20}{x} log \frac{Ax}{Ao} \quad (2.3)$$

where, *x* – distance, *Ax*- amplitude at distance *x*, *Ao*- initial amplitude.

The amplitude change of a decaying plane wave can be expressed as equation 2.4

$$A = A_0 e^{-az} \quad (2.4)$$

In this expression $\mathbf{A_0}$ is the unattenuated amplitude of the propagating wave at some location. The amplitude **A** is the reduced amplitude after the wave has travelled a distance **z** from that initial location. The quantity α is the attenuation coefficient of the wave traveling in the z-direction. The dimensions of α are Nepers/length, where a Neper is a dimensionless quantity. The term **e** is the exponential (or Napier's constant) which is equal to approximately 2.71828 [7].

Composite materials attenuation as a phenomenon can be subdivided into the categories as viscoelastic attenuation, energy dissipation at the interface and scattering attenuation due to interface defects. However due to complex shaped wave forms, stress irregularities, wave scatter change there are still no well characterised model to define each attenuation component [16].

A good number of researchers have been already studying attenuation characteristics of fiber reinforced composite materials. Biwa [17-19] settled theoretical representation of viscoelastic composite material for investigating the scattering attenuation components and evaluate the effect of the ultrasonic wave propogation at fiber/matrix interface.

Determination of the size of defects in strongly attenuating materials still is needed to be performed expermentaly. Glass fiber which is used for propeller blade shell is considered to be highly attenuating material [20] .
Proportion of each attenuation subcomponent and frequency relation was established as showed in figure 2.22. With the increasing frequency scattering takes the most of the part in attenuation. With low frequency at which composites mostly are composites are being evaluated [21] energy dissipation at the interface is bigest additive to the attenuation.

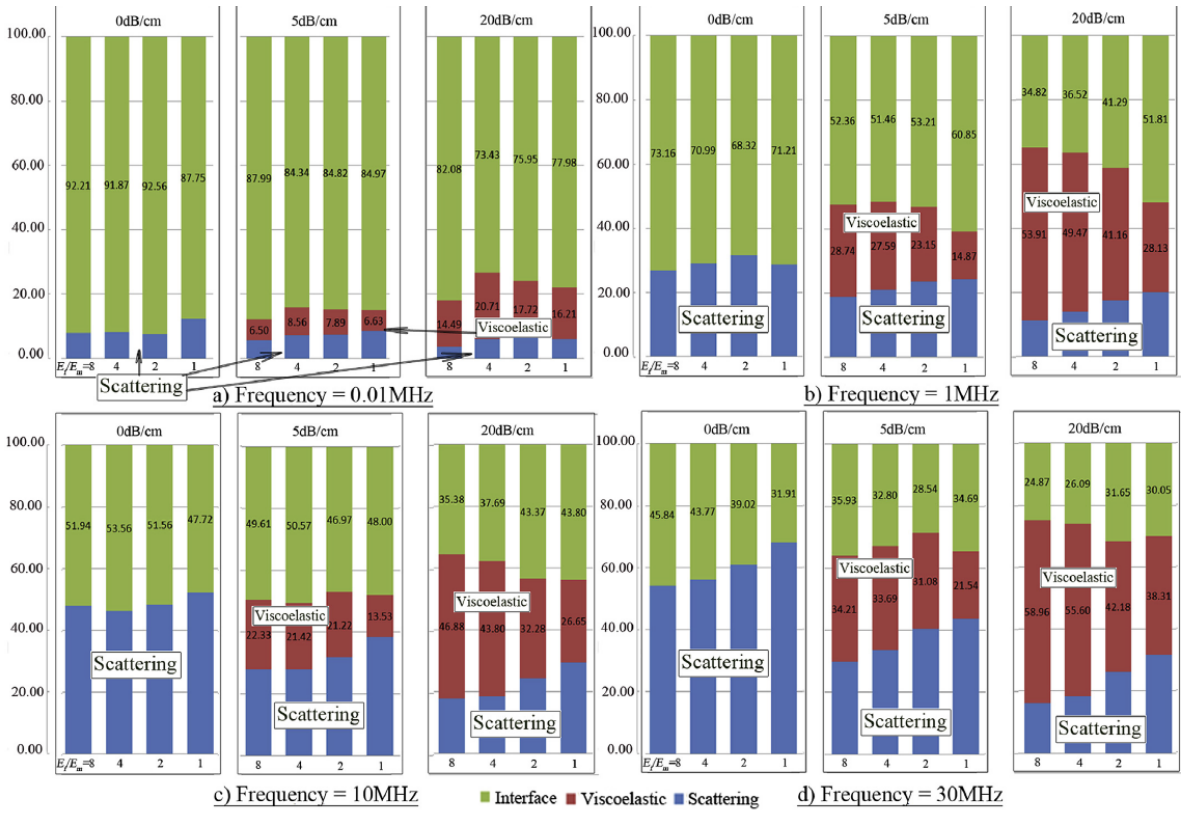

Figure 2-22. Proportion of each attenuation subcomponent and frequency relation [16]

Understanding the attenuation coefficients for each material of the propeller blade was one of the key element of this thesis. It was concluded that polyurthane foam has very high attenuation coefficient and ultrasound is disspered immediatly. Frequency has been used as low as 1 MHz due to available ultrasound generator/detector Omniscan capabilities. However electron microscopy images performed on polyurethane foam composites shows the complex shape of molecural structure , refer to figure 2.23 [39].

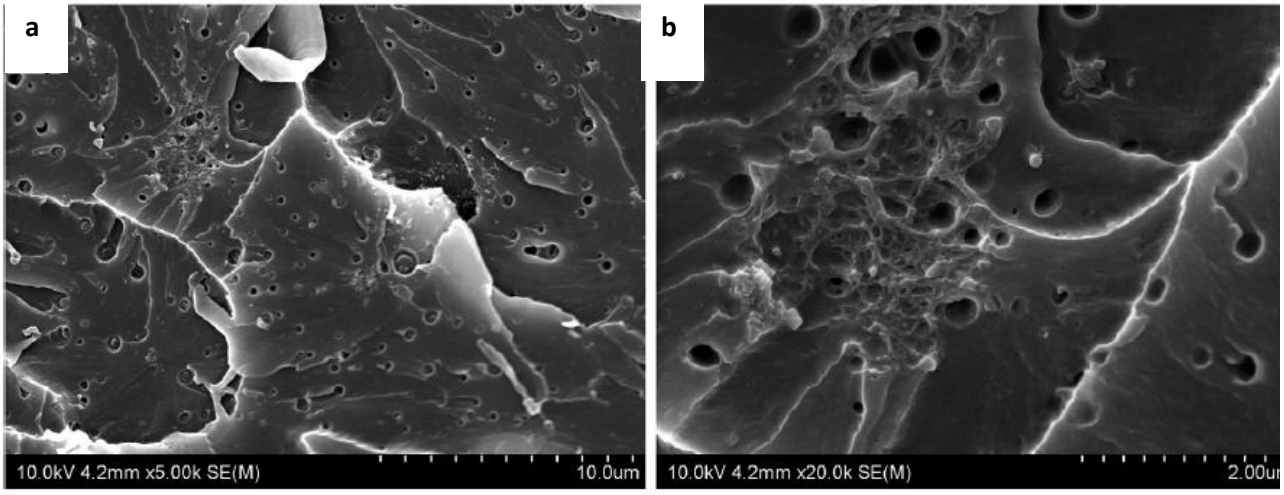

Figure 2-23. Scanning electron microscopy images of polyurethane foam with a) zoom at 5000 times b) zoom at 20000 times [39]

Predictive attenuation models are sometimes useful to be used. There are computing models for predictive attenuation which counts in particle size, porosity. In order to compute the predictive

attenuation coefficient material structure at molecular level must be known so it is not appropriate for reversed engineering projects. Furthermore, predictive models do not take into account intersection of the particles meaning there will always be small difference between real value [48].

From the research done regarding possible NDT methods to be used for propeller blade examination ultrasonic phased array technique is considered most suitable. Phased array gives ability to scan wide area at same time, technique uses same ultrasonic transceiver /receiver as contact probe which reduces the cost of the inspection, equipment is small and mobile and can be used outside when aircraft is standing in line station. Phased array inspection also gives high precision and able to detect the flaws in all layers of the blade, inspection duration is not time consuming, equipment preparation does not take long.

3. PROPELLER BLADE MODELLING IN CIVA SOFTWARE

During final thesis project we have been analysing theory of NDT inspections, their types and usage limits. Propeller blade design and materials which it's made of were evaluated using technical documentation available. Propeller blades inspection techniques which are used in service and in approved maintenance shop were described. Analysis on the physical real propeller blade and it is computer inspection model via CIVA NDT software performed. For this reason, real and beyond economical repair propeller blade used from ATR42-300.The main purpose to have the real blade was to cut it in two pieces in order to find out precise profile dimensions and materials distribution, which was important for making a computer model.

Propeller blade was 3D scanned to get precise dimensions for CIVA NDT modelling

CIVA NDT model has been established for correct probe shape, dimensions, type. Physical propeller blade has been examined physically.

Modelling tools allows to predict ultrasonic sound path, echoes, performance of phased array and optimise its performance. However, there will always be some inaccuracy of echoes positioning and as a consequence bad positioning of defects if complete propagation path cannot be precisely recreated in model or there are complex shape materials [12].

CIVA was created by EXTENDE software manufacture and gives wide variety of NDT techniques to be modelled on various shapes objects

- Eddy current
- Ultrasound
- Radiography
- Guided Wave Testing
- Computed Tomography

Ultrasound software gives the ability to simulate the inspection process with a wide range of transducers (conventional, Phased-arrays), specimens (from simple shapes to complex 3D CAD imported geometry), and defects (volume flaws, inclusions, delamination , cracks) The component can be homogeneous or composite with several layers . Materials for inspection can be metallic, fiber composites or granular composites [3,12]

Main features of the software [3,12]

- Specimen parametric geometries (planar, cylindrical, spherical, conical), 2D CAD editor or 3D CAD import
- Attenuation laws and database of isotropic materials
- Library build in for industrial probes
- Conventional UT probes (contact, angle beam, immersion, linear and annular phased arrays) with various shapes like rectangular, cylindrical, elliptical.
- Different wave computations for shear or longitudinal waves
- Multi layered structures and heterogeneous

3.1 PROPELLER BLADE MATERIALS AND GEOMETRY BACKGROUND

Blade which was previously rejected by manufacture due to erosion and delamination which caused too deep blend out of fiberglass shell. Below figure 3.1 represents the profile:

Figure 3-1. Blade profile section

Blade is composed of the following materials mentioned in table 3.1:

Table 3-1. Propeller Blade structure

1	Aluminium spar	70 mm wide, 19.6 mm thick
2	Polyurethane leading edge shape filling	Max thickness 18 mm
3	Polyurethane trailing edge shape filling	Max thickness 19.5 mm
4	Glass fiber composite shell / air foil	Thickness 2 mm
5	Adhesive at composite/metal and composite /composite joints	

Propeller shape is unique across its stations (refer to figure 2.3), it has turning fixture and its profile air foil and its dimensions are constantly changing as well.

3.2 SIMPLIFIED PROPELLER MODEL IN CIVA

3.2.1 Model drawing, materials parameters and probe type

CIVA software Ultrasonic module has special section for composite meterials testing and allows to create simple 3D shape specimen . It is also available to import Solid works/ CAD files for more complex shapes. Files after that must be reworked in CIVA in order to identify the interactions between layers - back wall, front wall, seperation between materials. Simple segment was created of the propeller blade theoretical inspection model keeping that it's profile does not change in geometry, however keeping the the fibre glass composite laminate, aluminum spar and poliurethane foam at its original dimmensions and maximum thickness . Detailed view can be seen in figure 3.2. Table 3.2 defines its visible layers which are numbered 1 to 4.

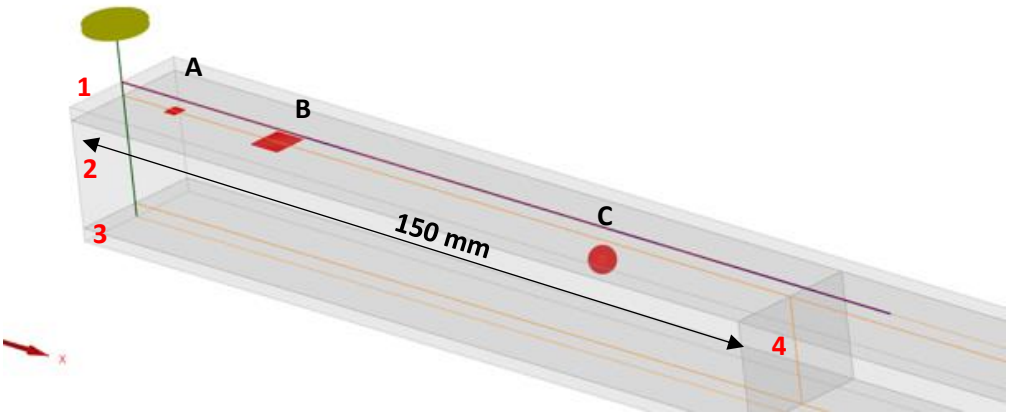

Figure 3-2. 3D model detailed view

Table 3-2. Sound velocity in layers

	Material	Thickness, mm	Density, g/cm³	Sound speed, m/s
1	Glass Fiber laminate layer (top wall)	2	1.85	2400
2	Polyurethane foam layer	19.5	0.48	1900
3	Glass Fiber laminate layer (back wall)	2	1.85	2400
4	Aluminium spar layer	19.5	2.7	6300

As per figure 3.2, 3 flaws has been placed in the specimen. Delamination type flaw at fiberglass layer and foam intersection with dimmensions 1x1mm (refer to A) , delamination type flaw with dimmensions 4x4 mm at fiberglass and foam intersection (refer to B) and water inclusion (void) in foam layer with diameter of 4mm (refer to C) .

It can be seen walls in between the different materials which acts like interactions which are predefined in CIVA during 3D model drawing. Main ultrasound parameters were set for each volume (1,2,3,4). Glass fiber laminate and aluminium spar volume parameters were taken from CIVA database (density, longitudinal wave velocity, transverse wave velocity). Table 2 listed parameters will be more specified/proved in master thesis after materials analysis/ physical tests performed. Ultrasound velocity shows relationship between the propagating velocity and the content of glass in the form of woven fabrics. The content of glass in a composite material causes an increase of the velocity with which waves propagate through the material [9]. Parameters taken as average for polyurethane material. Attenuation / structural noise type was set to modal for all volumes however this will be more specified in master thesis as polyurethane foam do have high sound attenuation. The amplitude change of a decaying plane wave can be expressed as showed in equation 2.3.

In order to set the computer model more realistic in CIVA, probe parameters have been selected to be same as could be used experimentally contact probe CX545 model used in laboratory was chosen for modelling with following parameters: 3.5 MHz and 12.7 mm diameter.

It was determined to use contact type and position the probe at height of ultrasound near zone (NZ), other sources call this Near Field. Using equation 2.3 and entering the numbers we get NZ:

$NZ = ((0.00925)^2 * (3.5 * 〚10〛 \text{^}6))/(4 * 1498) = 0.0321\text{m} = 32.1\text{ mm}$

Having this, probe was positioned in 32.1 mm height above the sample.

3.2.2 Defects positioning

CIVA gives opportunity to place defects at various shapes and dimensions across the scanning profile. Defect can be delamination at the joint, water inclusion or other type. By placing defects at various sections results at A scan can show amplitude changes versus time. By comparing the defects dimensions and amplitudes got via A-scans, physical scanning can be performed to verify. In total 3 delamination's and one water inclusion were set in the model with different dimensions and locations.

3.3 SIMPLIFIED PROPELLER BLADE PULSE ECHO ANALYSIS

As identified in figure 3.2 simplified propeller blade segment has been modelled in CIVA software.

This paragraph identifies the capability of this probe to detect the flaws in various sections of the simplified propeller blade segment. Probe has been positioned 3.21 cm above the specimen to avoid the Near Zone. Probe scanning was set to number of 6 steps along X axis, each step 10mm apart along X axis and number of 1 step was set on Y axis. This was chosen in order to save time on computation time.

3.3.1 Flawless view analysis

We can see that interface at front wall amplitude is much higher than backwall amplitude. This might be caused by acoustic impedance differences between water and material specimen as attunuation is not evaluated now. 4 amplitude points can be observed and do meet 4 intersections between different materials . From below figure 3.3 we can summarise 4 points:

A – peak at entry to glassfiber laminate volume; B – entry to poliurethane foam volume; C – entry to back wall glass fiber laminate volume; D – back wall echo. No other signals detected;

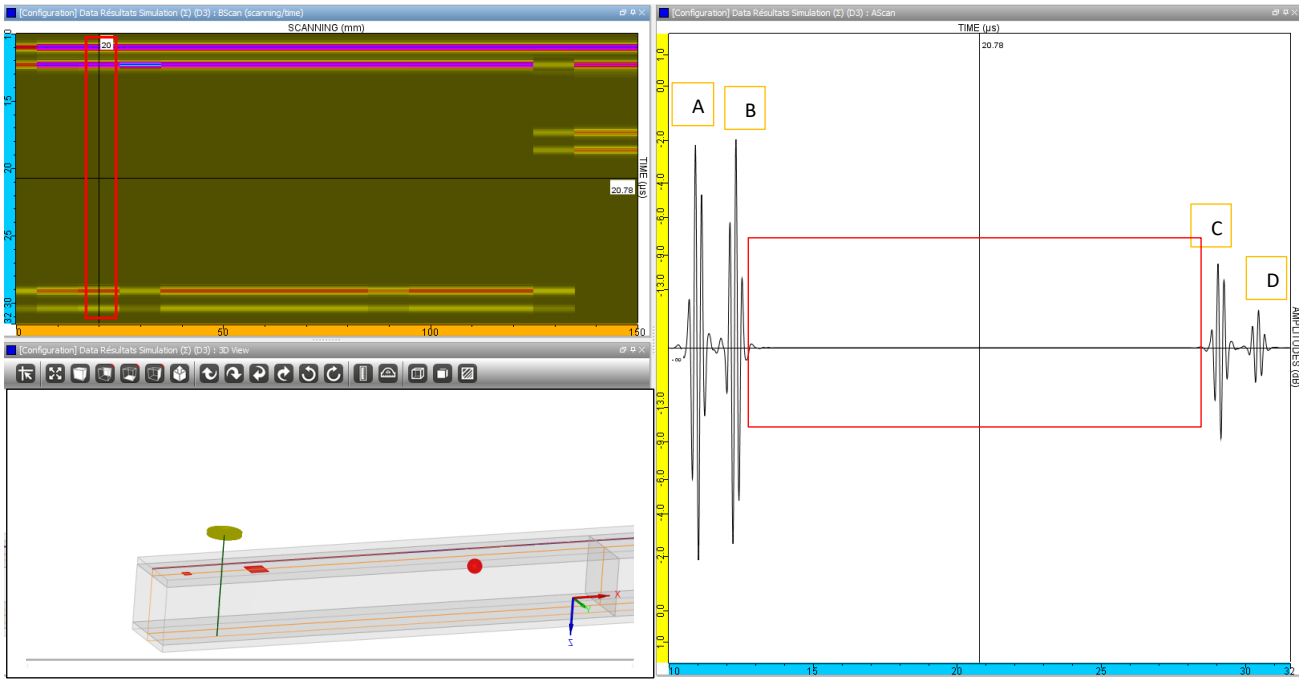

Figure 3-3. No defects A-scan / B-scan

Red rectangular shows the probe scanning location in the 3D model - between two delamination's - small and bigger. This region between was modelled without a defect and as such this is plotted in A-scan and B-scan. A-scan does not give any echo back in the region between points B and C - locations where material change.

3.3.2 Flaws detection

Delamination size that was tried to be detected was 1mm x 1mm . Frequency of 3.5 MHz was enough to detect the flaw and it can be seen in figure 3.4 A-scan on second peak, point A , which is higher than comparing to normal. Back echo from foam – glass fiber interaction was received weaker at point B . This signaled , that sound path was abnormaly distorted.

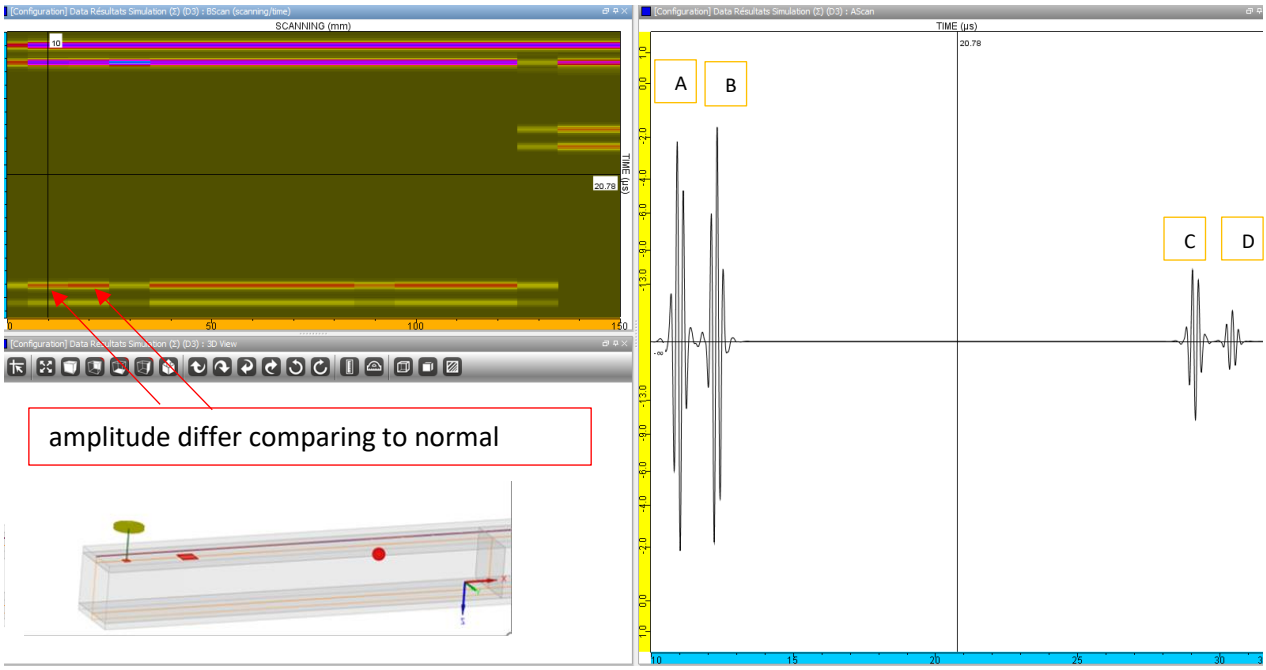

Figure 3-4. Small delamination detection A-scan/B-scan

Comparing to figure 3.4 (small delamination) larger delamination size of 4 x 4 mm was detected as well in between two layers – foam and fiberglass laminate. A-scan returned even higher peak at point A in figure 10 than in 4.1.2 and even weaker back echo at point B. Entry peak does not change in 4.1.2 nor in 4.1.3 nor in 4.1.1.

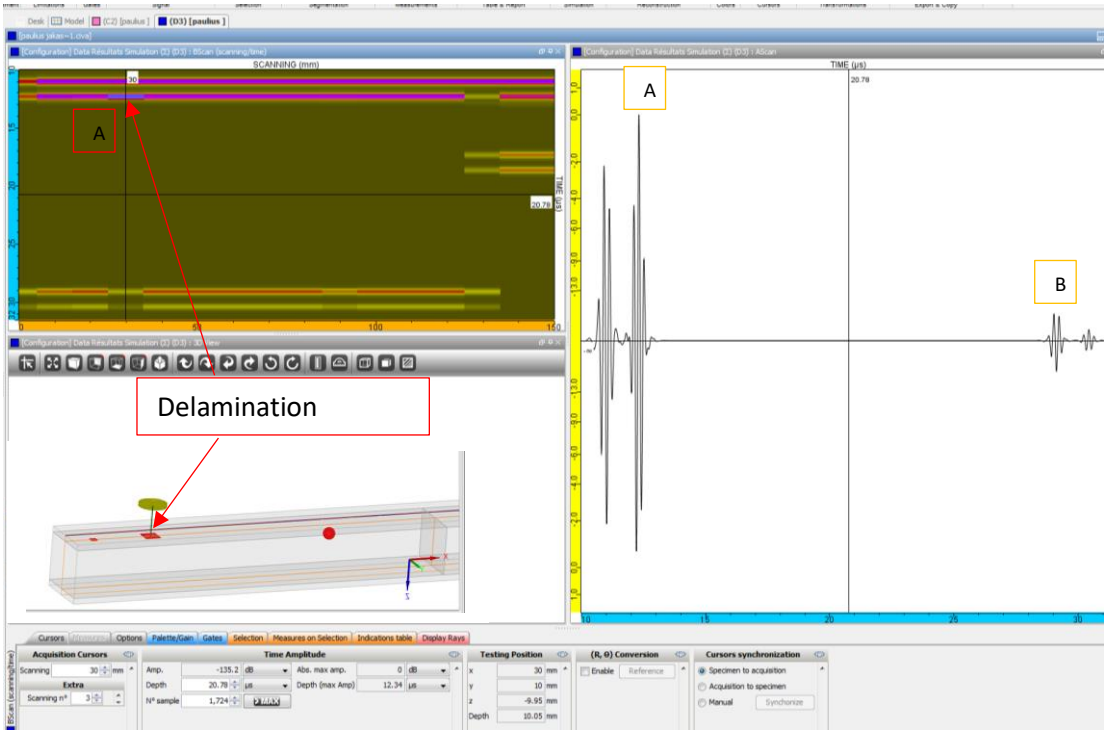

Figure 3-5. Big delamination detection A-scan/B-scan

As mentioned in beginning of section 3.1 scanning was done at increments of 6 steps with 10 mm apart to each other . Therefore water inclusion was not detected (did not returned any specific echo in A scan), however it showed its presence in another way in figure 3.6. Due to part of the sound wave hidden back echo which came back from 3rd layer is weaker than normal (refer to 4.1.1).B scan showed weaker signal comparing to no-flaws zone.

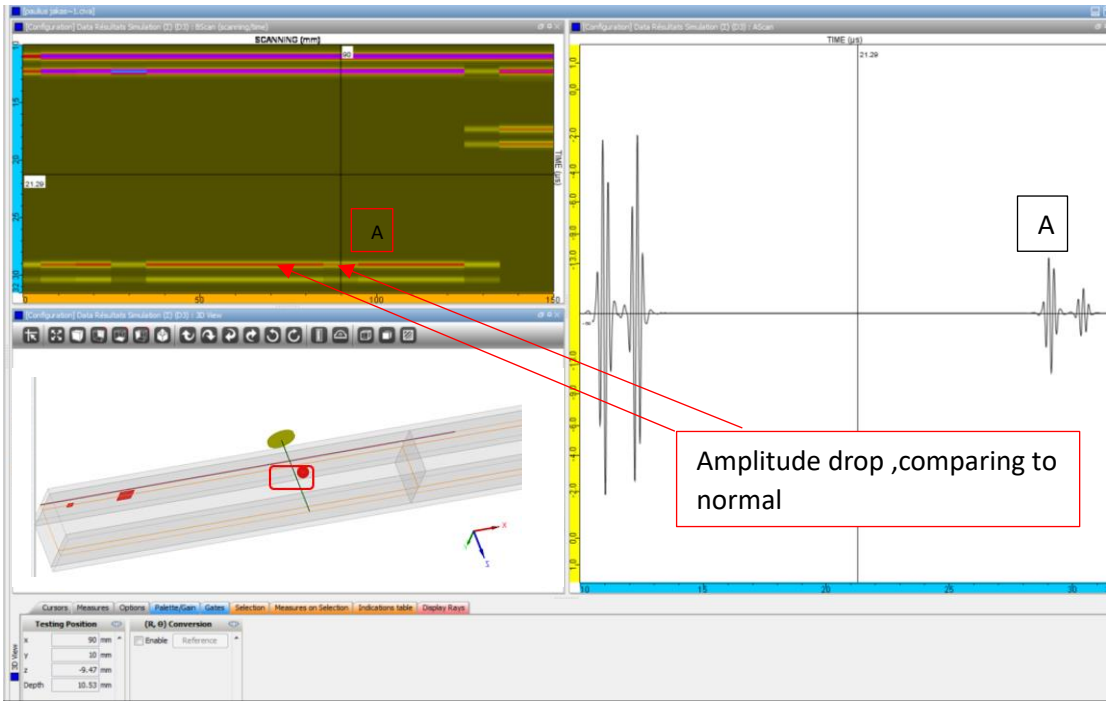

Figure 3-6. Water inclusion detection A-scan/ B-scan

If we compare amplitude of the back-echo graphs in figure 3.7 to determine values, we can see weaker signal strength partly hidden by inclusion - back wall echo at -12.3 dB, which is 2.1 dB lower than normal zone peak at -10.2 dB.

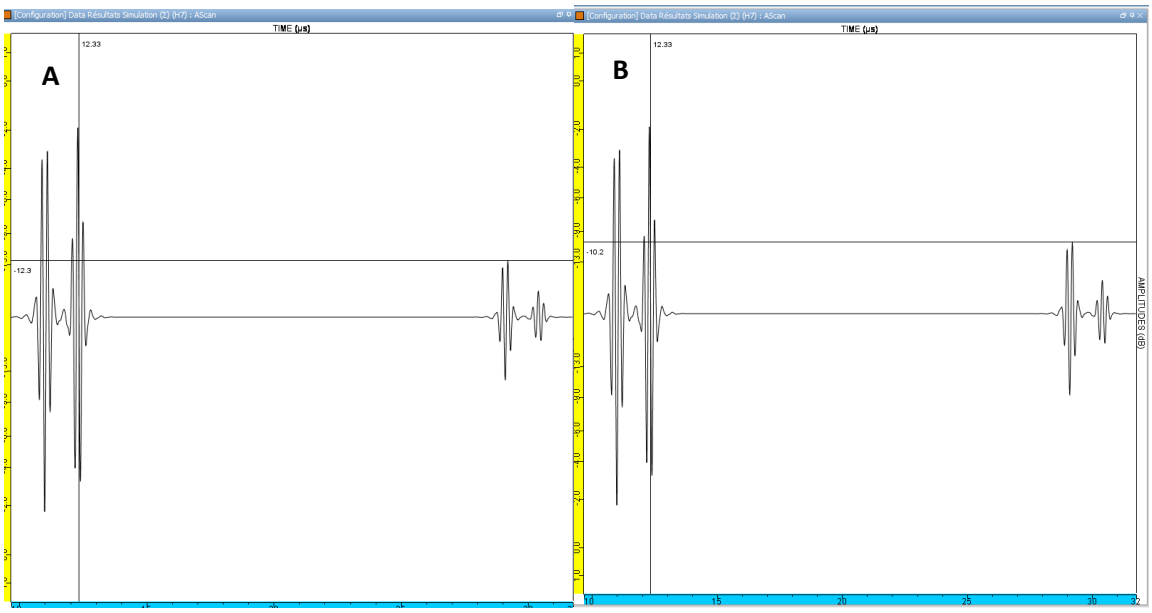

Figure 3-7. Amplitudes comparison. A- back echo amplitude with water inclusion; B- back echo for zone without flaws.

Another test was conducted with delamination deeper than interlayer and positioned specifically in foam volume. Delamination echo amplitude can bee seen in figure 3.8 point A. From echo time in A-scan its possible to to presume the depth – lower than centre and having true time its posible to calculate precise depth .

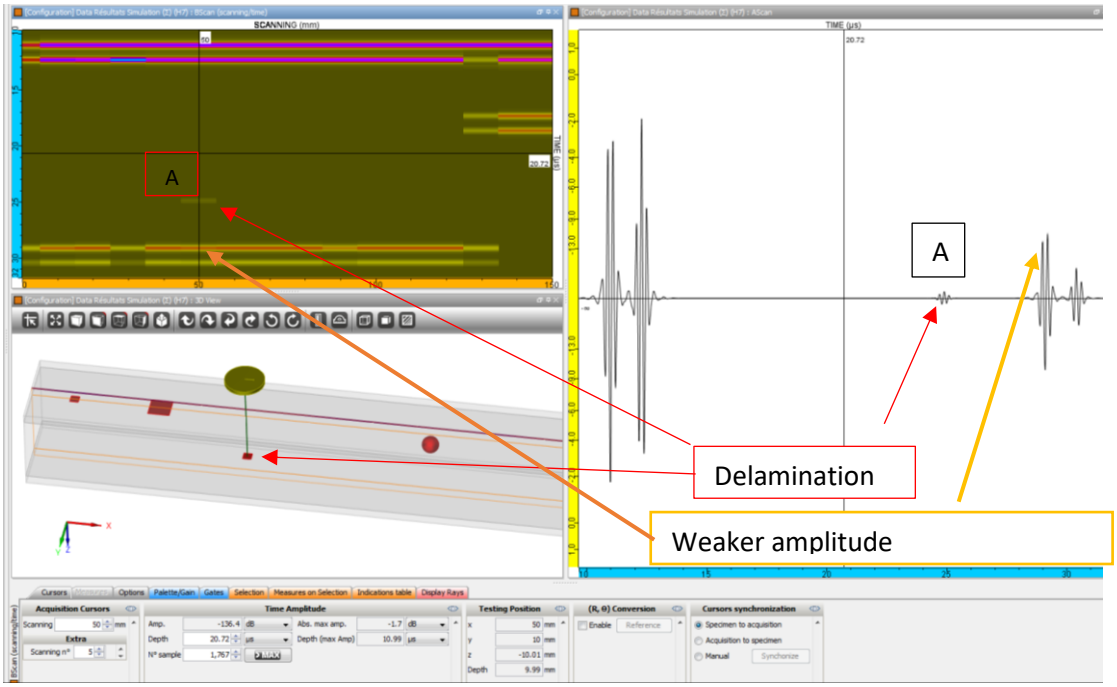

Figure 3-8. A-scan / B-scan for deep delamination

At the intersection with aluminum spar volume (reffering to figure 3.9 volume 1 – aluminium , volume 2 foam) we can observe 6 amplitude peaks , named points A , B, C , D , E, F in figure 3.9. A – initial peak at the entry - does not change comparing to other tests ; B - we can see signal devided between aluminum and foam volumes which gives back two echoes C /D and E/F. Due to devided signal between to layers , amplitudes are smaller, due to sound wave velocity C/D are returned faster than E/F back echo.

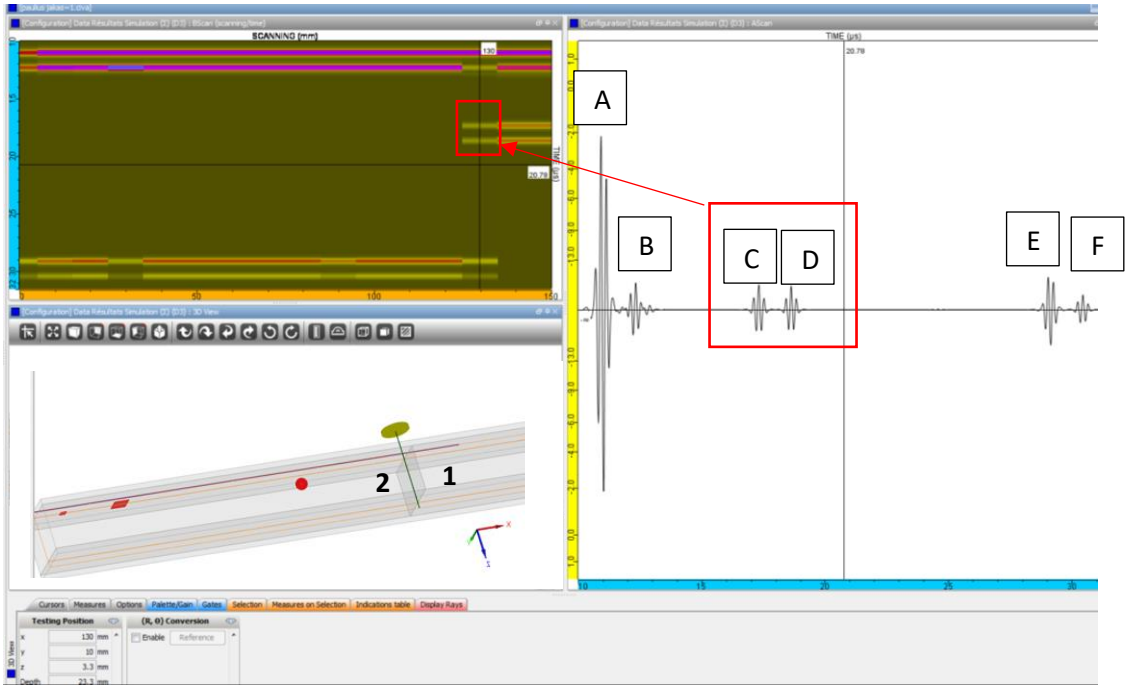

Figure 3-9. A-scan/ B-scan graphs at aluminium and foam intersection

We can observe one distingtive difference comparing to only composite path – back echoes returned much faster due to sound velocity increase in aluminum and due to signal is going throught aluminum and glass fiber interaction signal amplitude peaks at A scan is higher – refer to figure 3.10.

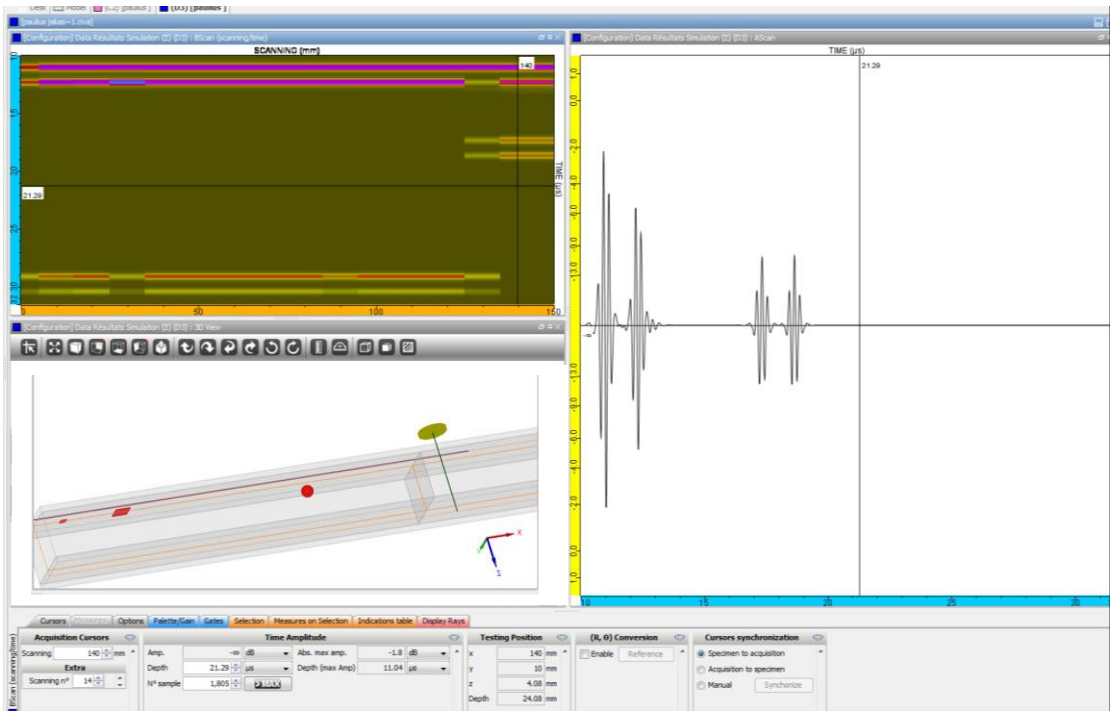

Figure 3-10. A-scan / B-scan in aluminium

3.4 SIMPLIFIED MODEL GRAPHS COMPARISON

Graphs comparison was done on A-scan view and comparing their amplitudes. Using peaks, it can used couple of methods in order to determine the flaw location. Analysis by peak amplitude or arrival time can be utilised [11] as showed in table 3.3.

Table 3-3. Amplitudes analysis methods [11]

Analysis	Technique
Peak AMPLITUDE	Artificial defect echo comparison; Backwall echo comparison; Decibel Drop;
FREQUENCY content	Deconvolution; Frequency response
Arrival Time	Impulse response; Delay time

Referring to figure 3.11, 5 distinctive points can be analysed when comparing only aluminium path (red) and fiberglass – aluminium – fiber glass path (black).

A – entry point in front wall fiber glass peak does not change ;

B – aluminum returned smaller peak ;

C- due to small sound attunuation in alluminum back echoes are more or less at same amplitude;

D – echo returned slower for signal which went thought composite;

E- smaller amplitude than D shows glassfiber laminate sound attenuation properties;

Basically this A-scan shows differences between aliuminum and composite laminates sound waves penetrability features.

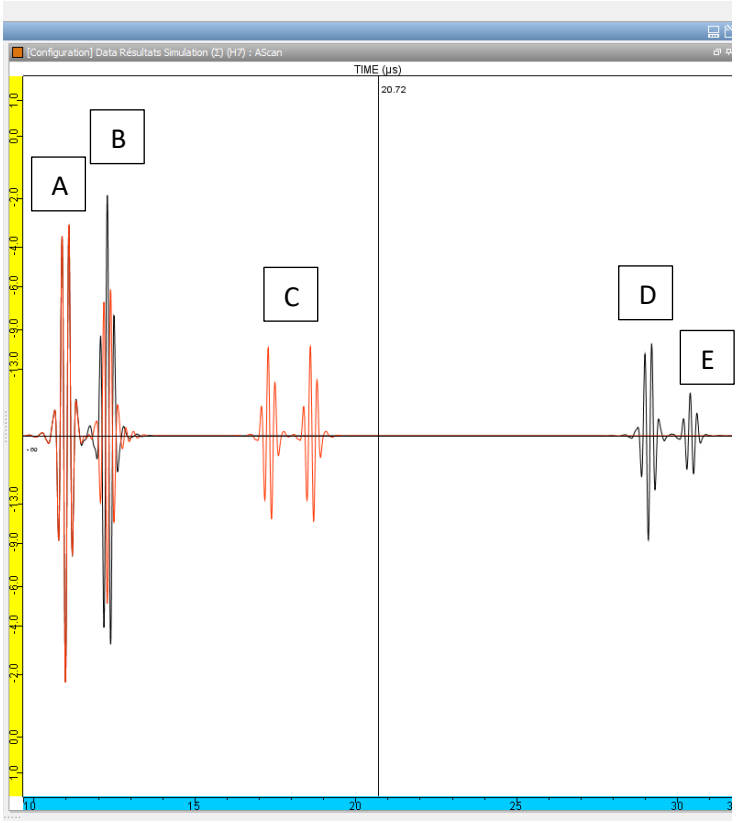

Figure 3-11. Aluminium path versus composite path comparison

Different size delaminations can be compared with no flaw zone. Figure 3.12 shows yellow A-scan representing big delamination and black A-scan representing small delamination. This was plotted for comparison on the amplitude peaks in order to show amplitude and delamination size connection. A point has the same peak in dB, as there is nothing different at this point – same front wall entry pattern. At point B due to different size of delamination's, amplitude peak is 1,5 dB higher for yellow delamination.

Figure 3.12 shows comparison between big delamination and no flaw zone peak amplitudes. Red is for big delamination, black is for no flow zone at point B (intersection).

It can clearly seen in figure 3.12 that amplitude peak comparing small and bigger delamination is higher and that back echo is weaker due to sound wave attenuation. Bigger delamination zone gives +1.9 dB stronger amplitude comparing to no flaw zone amplitude at points B - at two layers intersection and small delamination gives +0,4 dB stronger amplitude comparing to no flaw zone at point B. Having this information, we could determine, that flaw/delamination could be suspected if

signal amplitude is higher than -1,9db on the A-scan at point B. its most often that delamination's form in the two layer intersection, therefore point B normal amplitude value is important to get.

Summarising figure 3.12 we can make a table 3.4 listed dB values at certain points:

Table 3-4. Amplitudes comparison between A-scans

Location	**Point**	**Amplitude, dB**	**Amplitude, dB**	**Amplitude, dB**
Front wall intersection	A	-3	-3	-3
Intersection btw two materials	B	0	-1,5	-1,9
Intersection btw two materials	C	Not measured	Not measured	-10,2
Back wall echo	D	Not measured	Not measured	Not measured

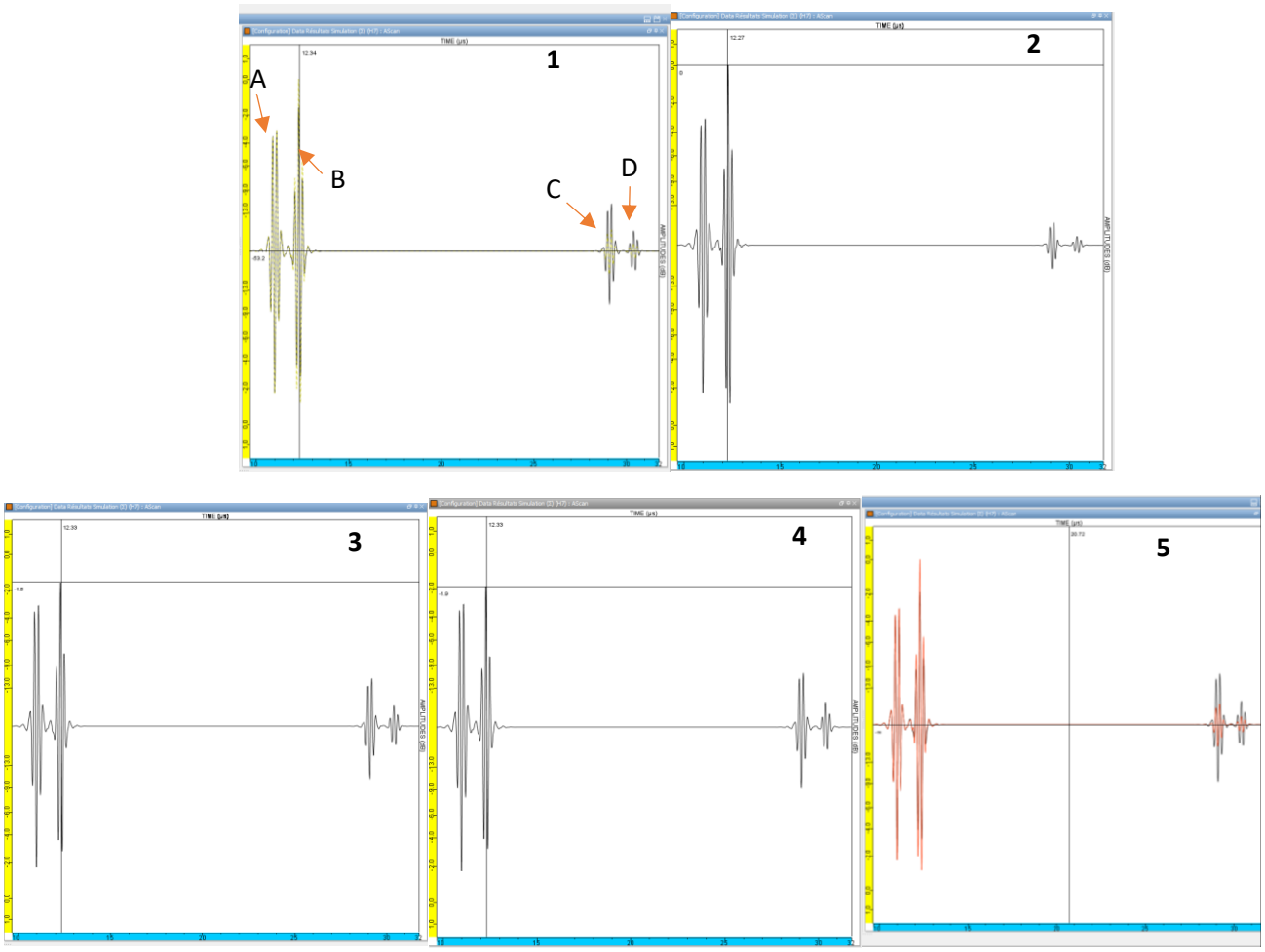

Figure 3-12. A scans comparison when transducers are positioned over different size delaminations. 1 – different sizes delaminations peak amplitudes comparison, 2. larger delamination amplitude peak; 3 – minor delamination amplitude peak, 4 – no defect zone amplitude peak; 5 – big delamination versus no flaw zone

3.5 PROPELLER BLADE ANALYSIS IN CIVA WITH 1:1 GEOMETRY

In order to obtain precise theoretical modelling results and do cross-sectional inspection of the blade, precise geometry of the air foil, different materials volumes distribution and dimensions had to be found and transferred into computerised model in CIVA.

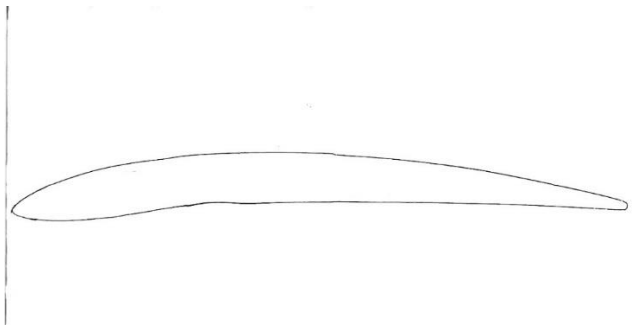

Figure 3-13. Propeller blade air foil scanned profile with natural flaws at the composite shell

In order to have precise geometry in CIVA blade model, propeller blade has been cut twice and than geometry scanned with 3D scanner – referring to figure 2.2 blade has been cut from STA 64 till STA 77 (blade tip) as showed in figure 3.14 and propeller blade portion STA 60-64 as showed in figure 3.15. Using this cut portion of the propeller blade tip (figure 3.15) air foil 2D view has been generated as showed in figure 3.13. Time of flight 3D laser scanner has been used which uses light beam to scrutiny the specimen geometry. 3D scanner had built in laser range finder which computes pulse of light and the amount of time before its reflected. The laser range finder uses one light pulse at a time, so 3D scanner moved 360° around the specimen before all the points where calculated. 3D scanner precision was 0.01 mm which produced high resolution image of the propeller blade tip with all the natural flaws within the fiberglass layer.

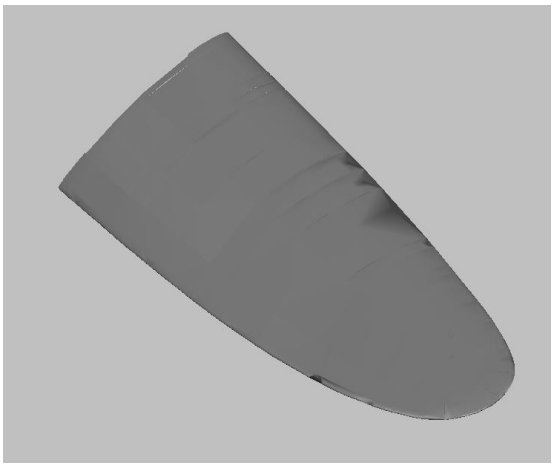

Figure 3-14. 3D scanned propeller blade tip, Blade stations 64-77

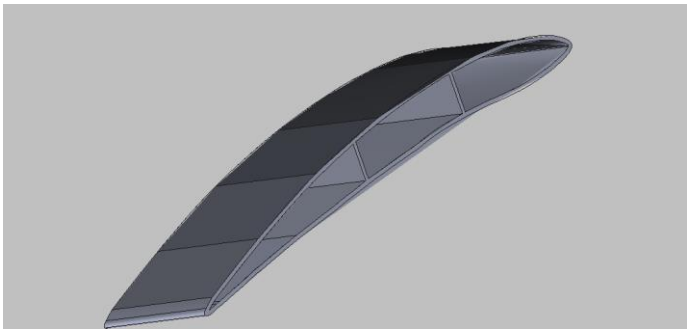

Figure 3-15. Propeller blade portion scanned, stations 60-64

Using scanned profile, 3D CAD IGS file created which would be recognised by CIVA. Propeller blade model has been imported to CIVA with precise geometry. Different materials volumes as showed in figure 3.16 had been assigned in CIVA using specimen's materials window.

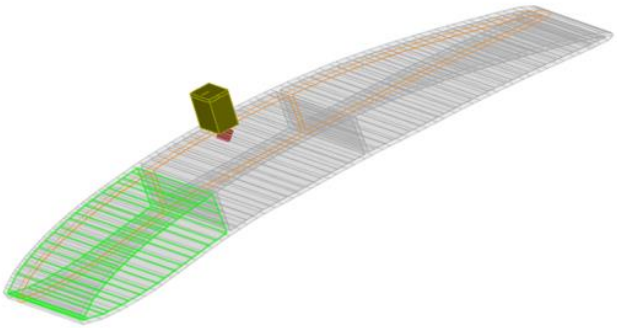

Figure 3-16. CIVA blade model

Using data acquired from paragraph 4 and using tables 4.6, 4.9, 4.16 , CIVA model has been set using ultrasound speed in the specific materials and sound attenuation coefficient. Than contact probe CX545 with frequency 3.5 MHz has been used to get A scan for fiberglass – aluminium – fiberglass layers. Refer to figure 3.17 ant items 1 and 5.

Figure 3-17. Section inspection where 1 - Aluminium spar; 5 – Glass fiber composite shell

In order to understand any differences from theoretical and experimental results A-scans are presented in figures 3.18 for theoretical and 3.19 for experimental inspection.

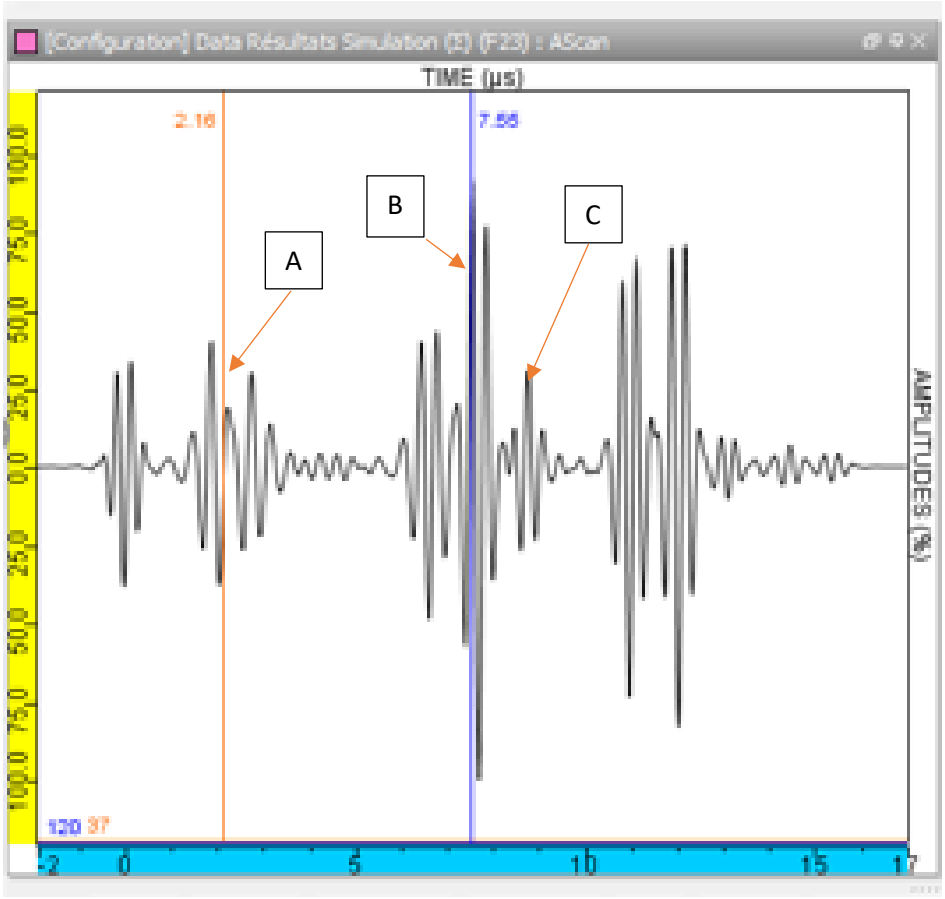

Figure 3-18. Theoretical A scan for cross sectional scanning

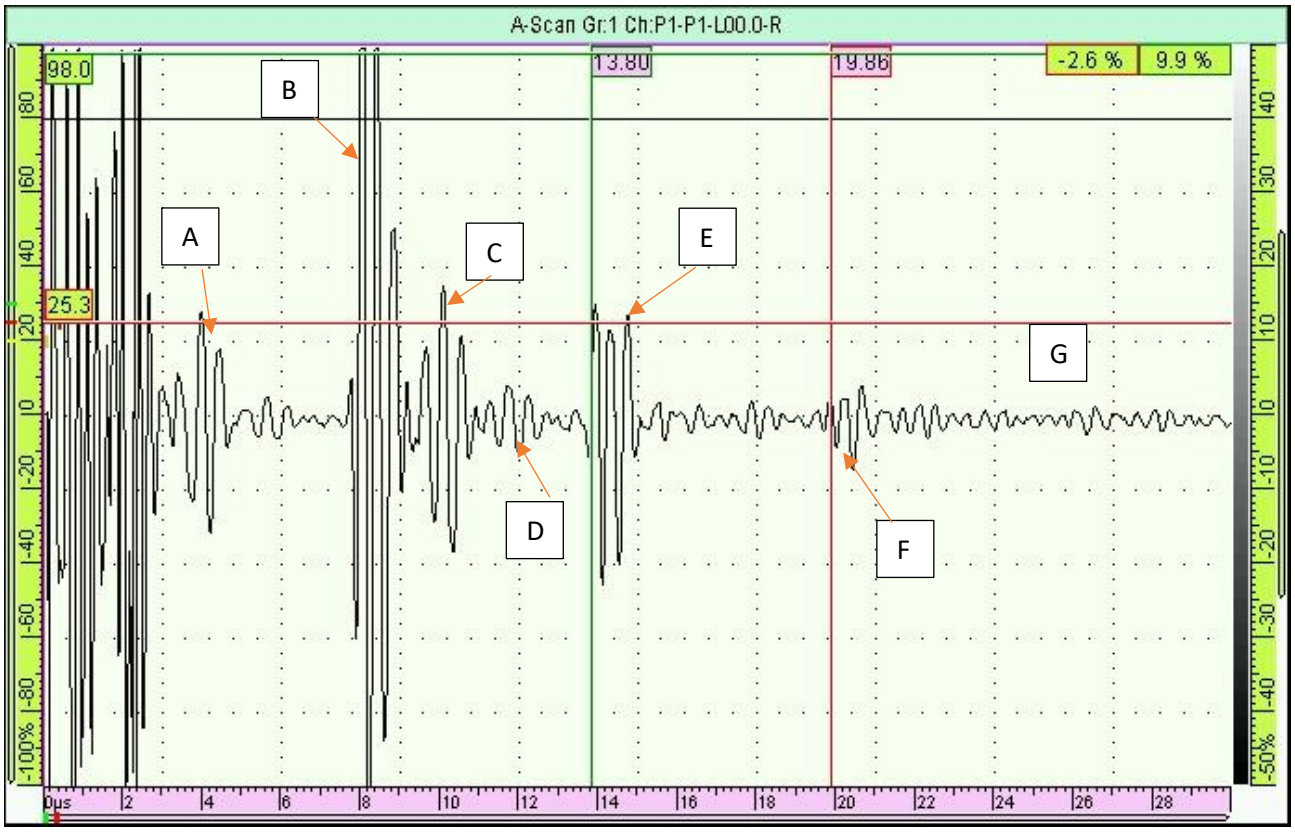

Figure 3-19.Expermental A scan for cross sectional scanning

Results have been compared in table 3.5.

Table 3-5. Experimental and Theoretical results comparison

Echo	Description	Differences
A	Echo from top fiber glass	Signal amplitude difference between experimental and theoretical is 5 %
B	Echo from aluminium	Signal amplitude difference between experimental and theoretical is 5 %
C	Echo from bottom fiber glass layer	Signal amplitude difference between experimental and theoretical is 5 %
D	2nd echo from top fiber glass	Echo is missing in theoretical model
E	2nd echo from aluminium back wall	Theoretical is higher than experimental. This is because of sound dissemination which can't be theoretically described.
F	3rd echo from aluminium backwall	Not examined in theoretical model

Glass fiber layer A-scans have been examined experimentally and theoretically in order to determine if experimentally retrieved in paragraph 4.5 gives appropriate results in CIVA. Same 3.5 MHz probe model CX545 has been used. RF signals chosen for evaluation. For experimental A scan glass fiber sample with dimensions 2.34mm x 19 mm x 28mm has been used with set up showed in figure 3.20.

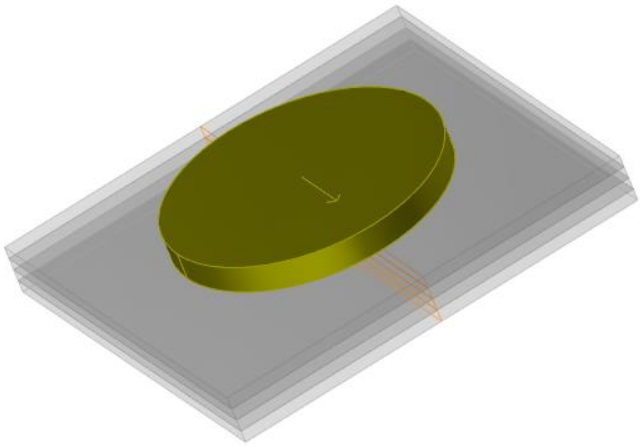

Figure 3-20. Glass fiber composite sample inspection cross section view

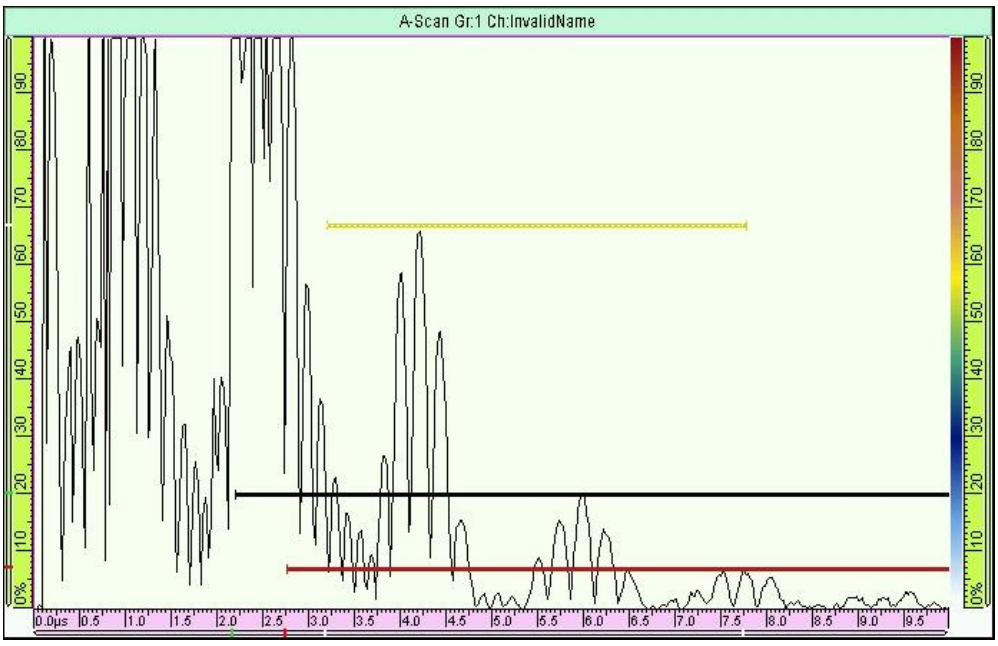

Figure 3-21. Experimental A scan of glass fiber

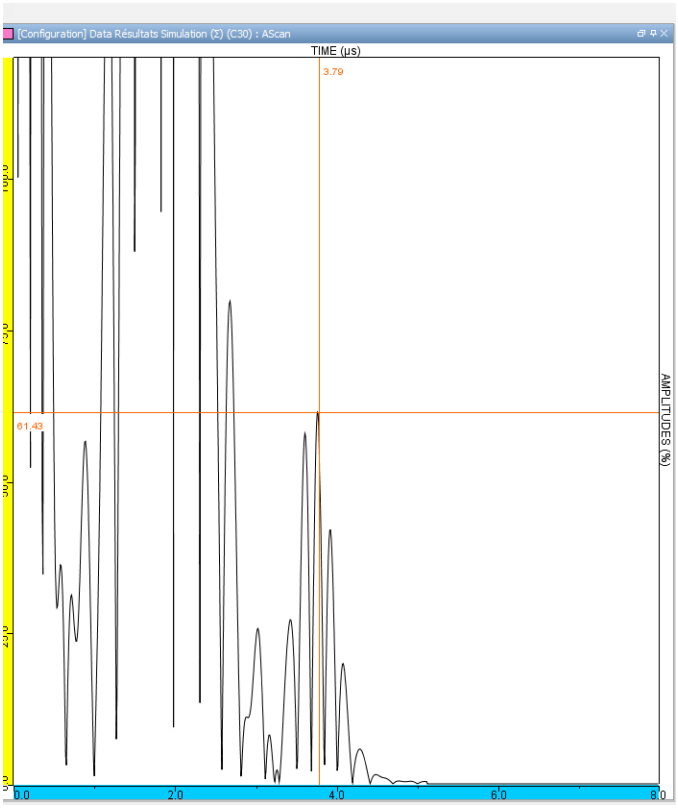

Figure 3-22. Theoretical A scan of glass fiber utilising attenuation laws

Experimental amplitude – 66 % showed in figure 3.21 and theoretical amplitude received in figure 3.22 was 61,43 % which gives difference of 8 %. Considering the complex attenuation phenomena results considered as satisfying. Time of backwall echo theoretically received 3.79 µs and experimentally 4.1 µs which gives 7.5 % difference.

Phased array inspection has been set up in CIVA as showed in figure 3.23 for flaws detection and inspection of fiberglass-aluminium-fiberglass layers. Linear 3.5 MHz Phased array has been used with 64 elements , active aperture of 64mm , pitch 1mm , elevation 7mm mated with wedge with refraction angle 0 , height 20mm , plexiglass material . Interlayer delamination flaw of 15mm x 10 mm has been placed in top fiberglass layer above the aluminium spar as showed in figure 3.23.

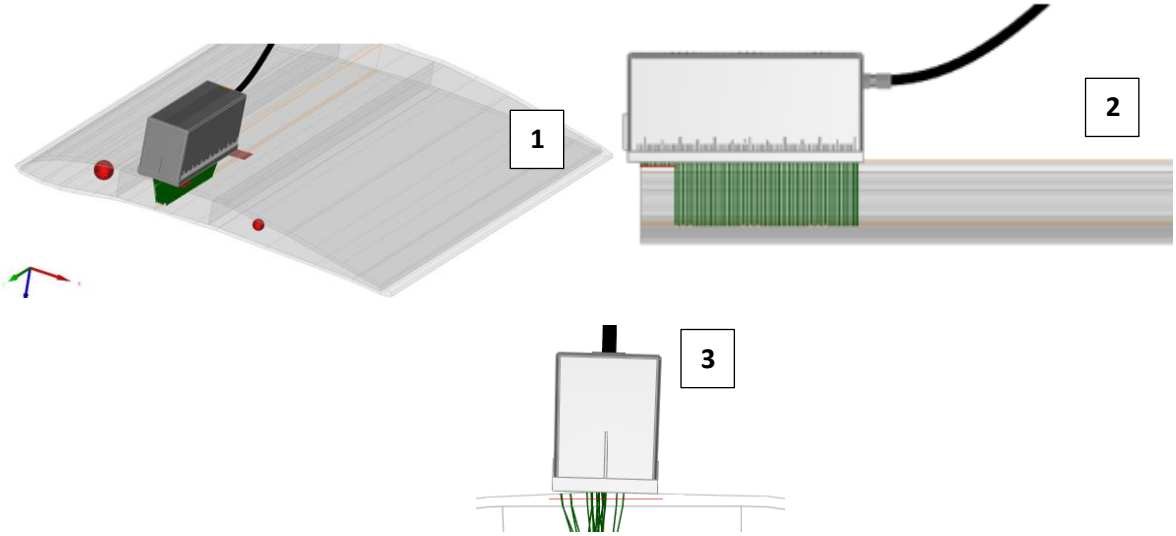

Figure 3-23. Phased array (3.5MHz) set up in CIVA for flaw detection. 1 – general view of the position and propeller blade volumes. 2 – phased array side view during inspection . 3 - flaw position in the fiberglass layer

Figure 3-24 shows the linear electronical scanning result of the interlayer delamination of the top fiberglass layer with aperture of 64 elements.

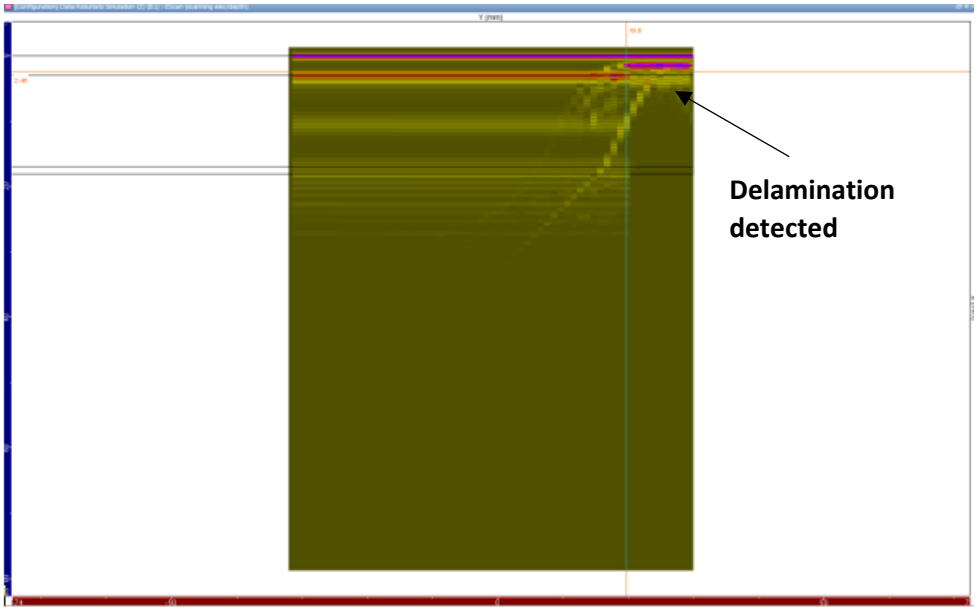

Figure 3-24. Top fiberglass laminate interlayer delamination detection in CIVA .

Inspection of the fiberglass-aluminium-fiberglass layer has been set in order to check the echoes and compare with experimental results. Electronical scanning and A scan result is presented in figure 3.25.

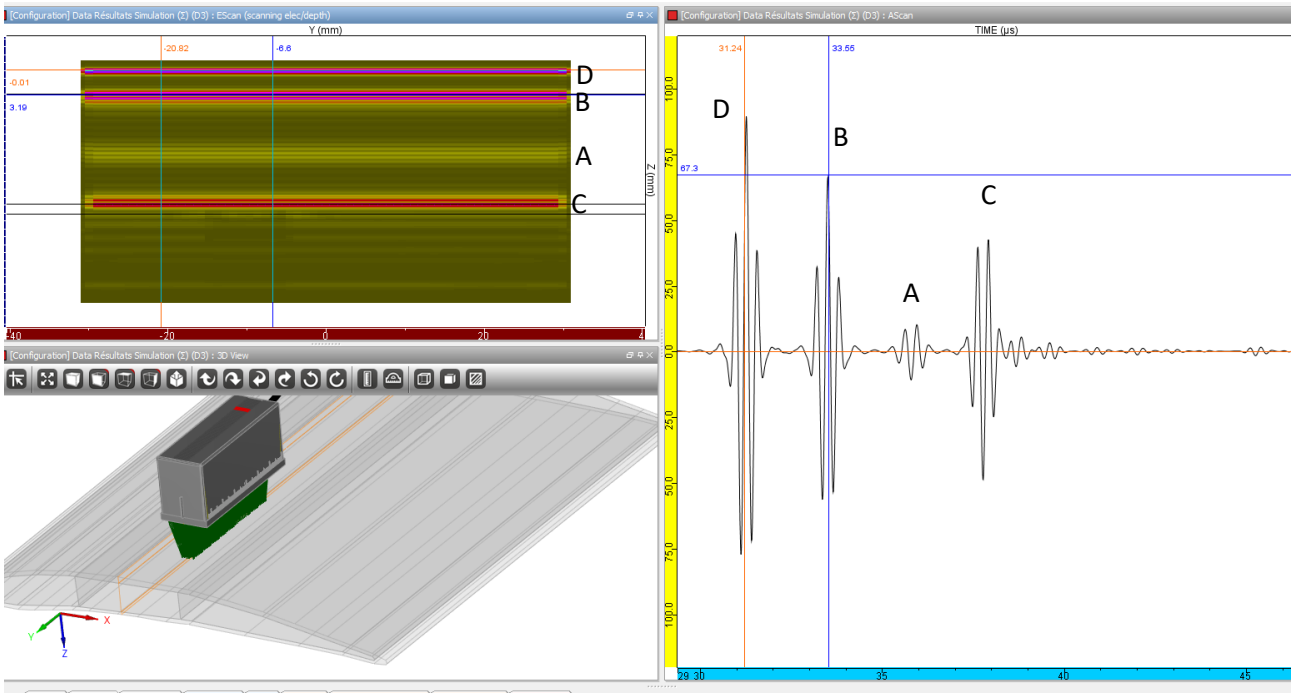

Figure 3-25. Electronic scanning Echoes analysis in CIVA (3.5 MHz PA)

Time between wedge back echo and top fiber glass layer was received 2.31µs which is same time interval as received experimentally. Referring to figure 3.24 echo A Is from aluminium spar, B from top fiberglass layer, D from the wedge and C from bottom fiberglass layer. Figure 3.24 which is theoretical scanning can be compared to experimental scanning results presented in figure 5.11 (5 MHz PA) and figure 5.20 (3.5 MHz PA).

From theoretical analysis we can see that phased array with frequency 3.5 MHz is most suitable NDT method giving linear S-scan result of 64mm inspection zone. Flaws can be detected in aluminium, fiberglass layers and their intersections except foam and this inspection method saves time considering all propeller blade inspection. Phased array can be used also for local propeller blade area inspection.

4. PROPELLER BLADE MATERIALS EXPERIMENTAL EVALUATION

4.1 PROPELLER MATERIALS ANALYSIS

In order to determine each propeller blade material characteristics, blade has been cut and separate layers opened. Various probes have been utilised to choose the most appropriate one for the result. Ultrasonic pulse-echo NDT has been used for each material. Contact type probes used can be seen in figure 4.1 and their description in table 4.1

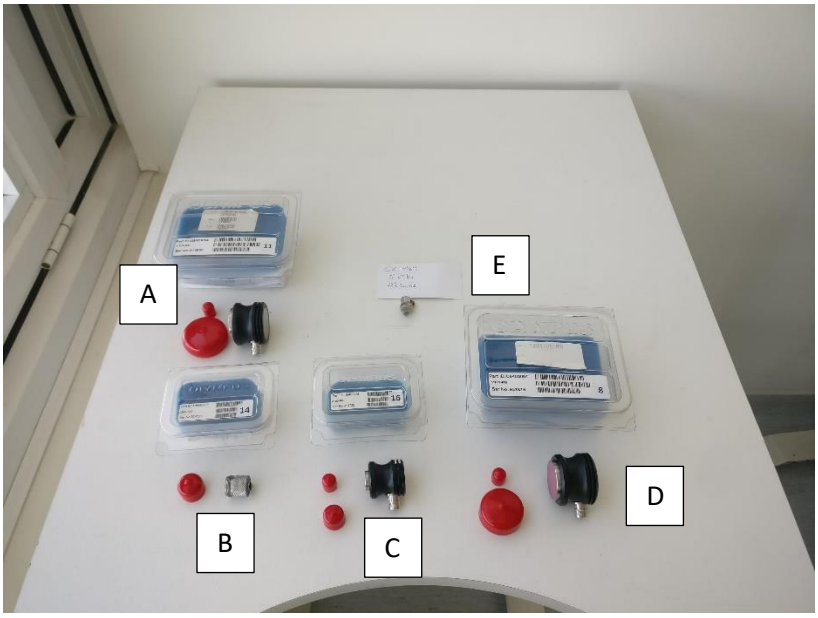

Figure 4-1. Probes used

Table 4-1. Ultrasonic transducers used for materials characteristics visual presentation

Probe	Type
A	Type V102, 1 MHz, Normal incidence longitudinal wave, 25.4 mm diameter
B	Type C545, 3.5 MHz, Normal incidence longitudinal wave, 12.7 mm diameter
C	Type V109, 5 MHz, Normal incidence longitudinal wave, 12.7 mm diameter
D	Type V101, 0.5 MHz, Normal incidence longitudinal wave, 25.4 mm diameter
E	Type CX-164, 5 MHz, Normal incidence longitudinal wave, 6.35 mm diameter , plexiglass delay line

4.1 INSPECTION SETUP

In order to get proper materials properties assigned into CIVA model propeller blade has been inspected via OLYMPUS OMNISCAN MX portable device for Ultrasonic and Eddy current analysis. Setup is showed in figure 4.2.

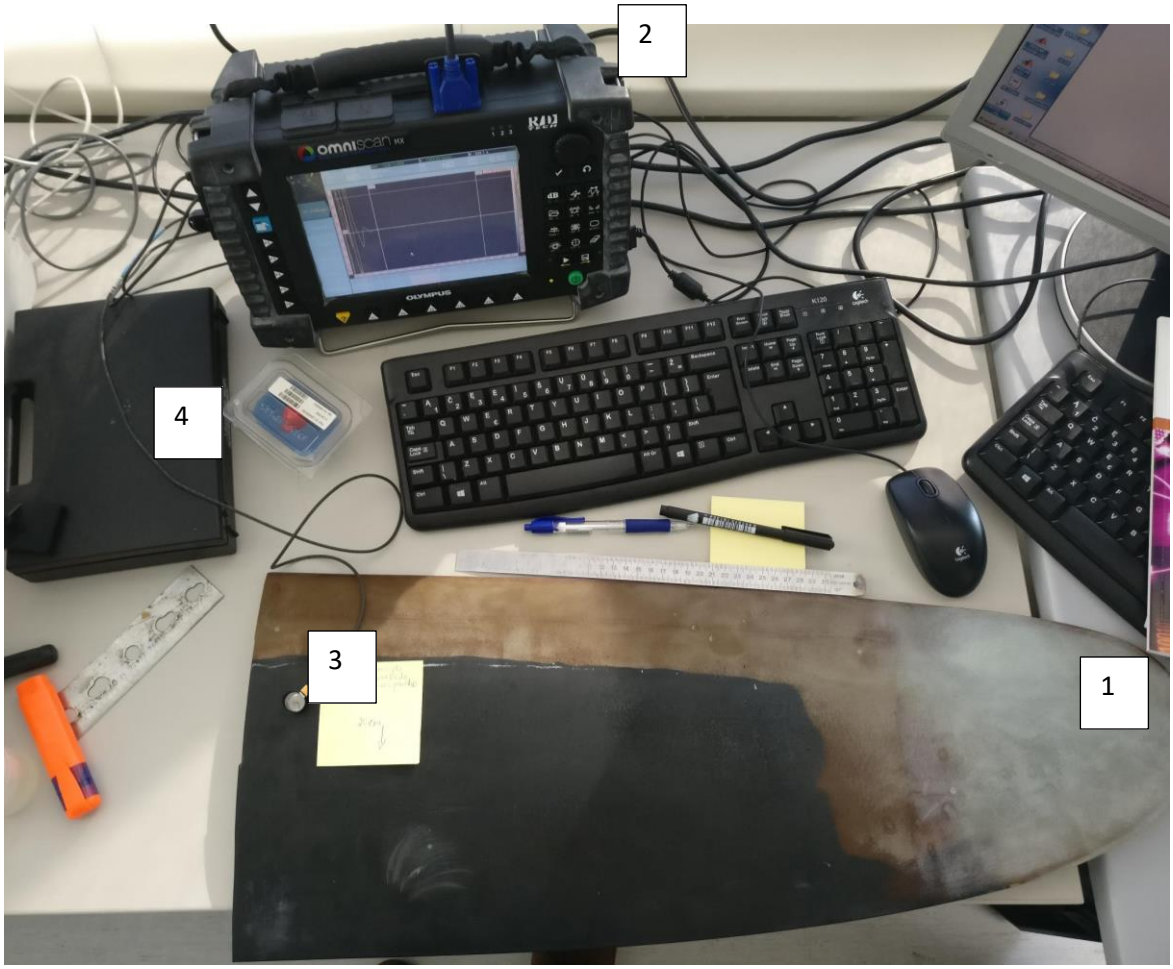

Figure 4-2. Propeller inspection set-up

Referring to figure 4.2, Point 1 is the cut specimen – propeller blade tip which will be examined , blade station 64-77 (refer to figure 2.2), point 2 is ultrasonic pulse transceiver /receiver (Olympus OmniScan), with probe (point 3) connected via wire (point 4) . Wire can be reused with various same type transducers.

9 points were selected across blade with listed locations in table 4.2.

Table 4-2. Inspection points distribution across the blade air foil

Zone	Point number	LOCATION		
		From T/E	From L/E	From edge
Alumiunum spar fiberglass shell	1	183 mm	110 mm	35 mm
Alumiunum spar fiberglass shell	2	163 mm	135 mm	17 mm
Alumiunum spar fiberglass shell	3	198 mm	100 mm	13 mm
Alumiunum spar fiberglass shell	4	175 mm	120 mm	105 mm
Alumiunum spar fiberglass shell	5	155 mm	140 mm	10 mm
Foam and fiberglass sheel	6	110 mm	185 mm	20 mm
Foam Foam and fiberglass sheel	7	83 mm	210 mm	22 mm
Foam Foam and fiberglass sheel	8	115mm	180mm	65mm
Foam without fiberglass antierrorion paint	9	245mm	40mm	170mm

Locations on blade showed in figure 4.3.

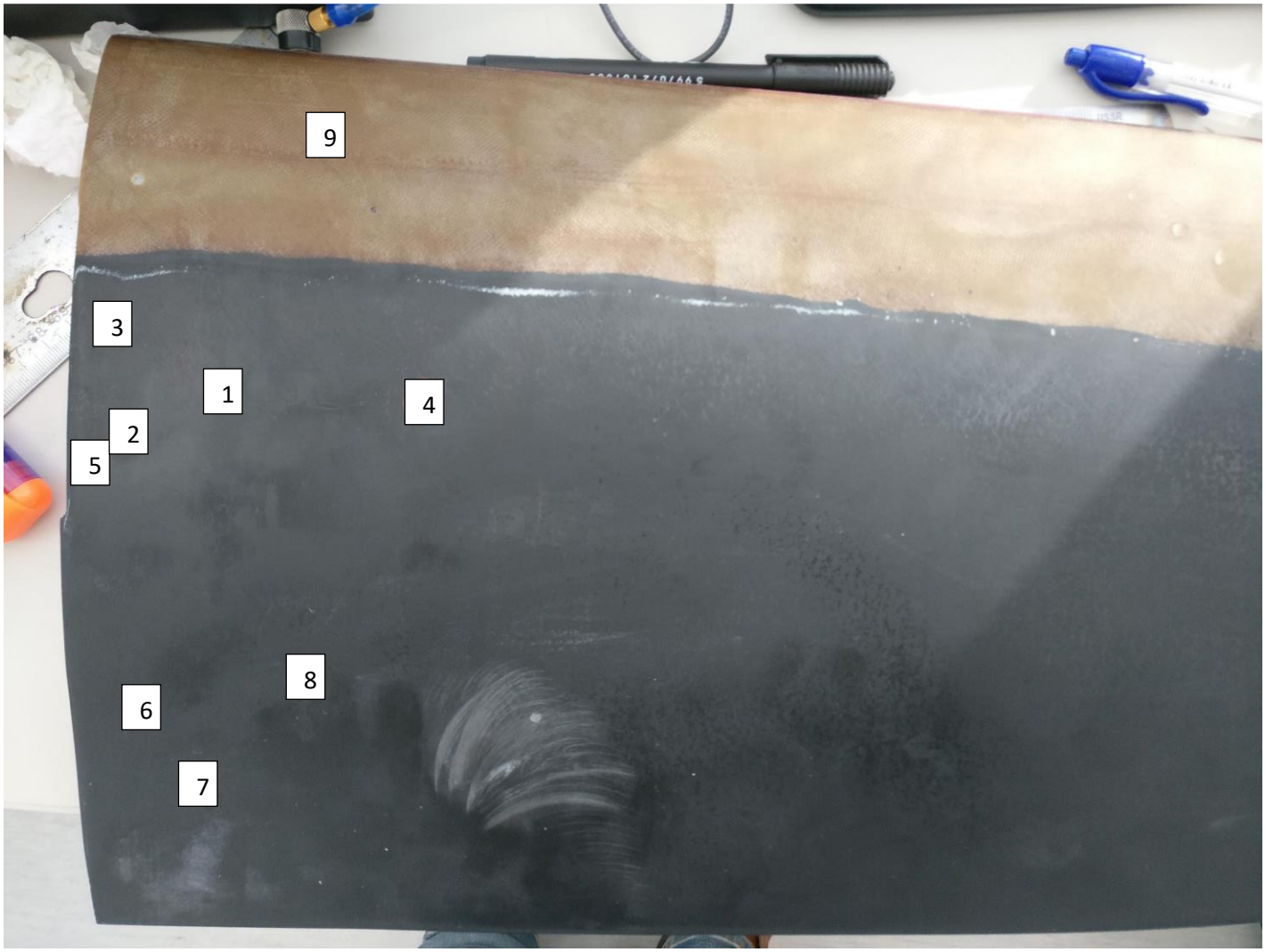

Figure 4-3. Blade inspection points

4.2 ALUMINIUM ALLOY CORE WITH GLASS FIBRE SHELL

Aluminium and fiber glass shell combined properties have been received with following equipment in table 4.3.

Table 4-3. Aluminium and glass fiber layers combined inspection equipment

Probe	Olympus V109, 5 MHz, 9.52 mm diameter, Contact type
Gain	0-40 dB
Wire	Olympus BCM74-3
Coupler	Water

Inspection results as per setup as identified are given in table 4.4 and retrieved using A-scans presented in figure 4.4.

Table 4-4. Speed of sound of Aluminium layer and glass fiber shell combined

Point	Time 1st peak, µs	Time 2nd peak , µs	Wave distance, mm	Avarage time, µs	Sound velocity, m/s
1	5,99	6,19	22	5,95	6655
2	5,85	6,07	22		
3	6,31	6,26	21,5		
4	5,71	5,58	22		
5	5,88	6,01	22		

Sound velocity through glass fibre and aluminium core combined received was 6655 m/s, comparing to normal sound velocity 6400m/s. Sound velocity is found from equation 4.1.

$$V = 2H/t \qquad (4.1)$$

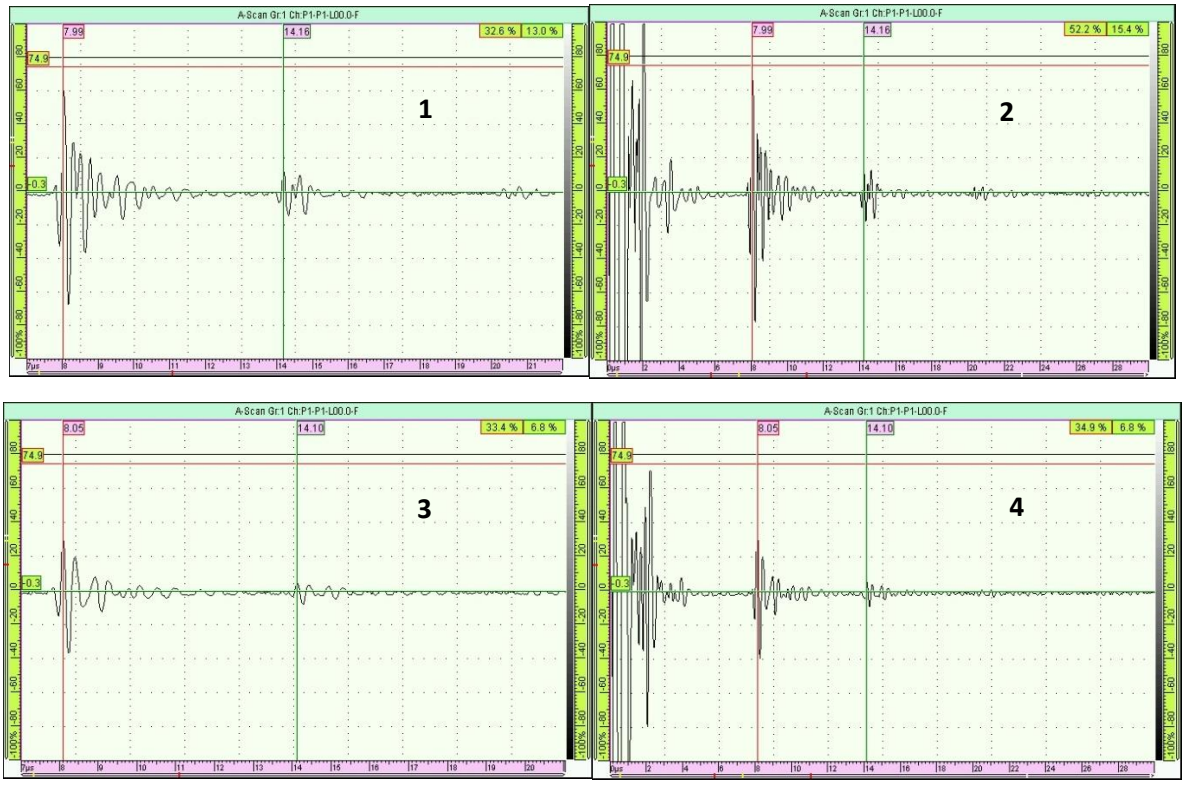

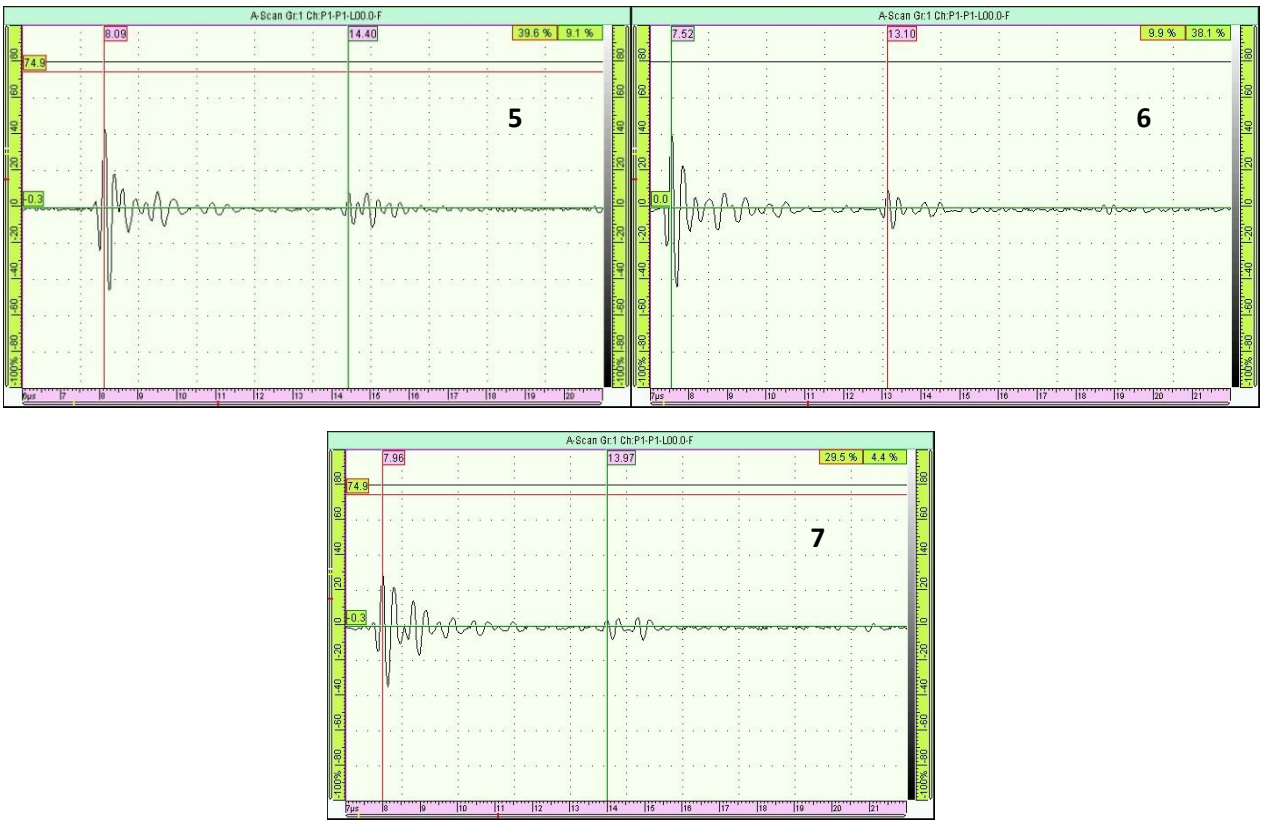

Figure 4-4. A scan of the multiple points. 1- Point 1 A scan signal echo (Aluminium alloy core) ; 2- Point 1 global A scan view; 3- Point 2 A scan signal echo (Aluminium alloy core); 4- point 2 A scan global view ; 5 - point 3 A scan signal echo (Aluminium alloy core); 6 - point 4 A scan signal echo (Aluminium alloy core); 7 - point 5 A scan signal echo (Aluminium alloy core)

4.3 ALUMINIUM ALLOY CORE WITHOUT FIBERGLASS COMPOSITE SHELL

Fiberglass layers has been removed and Aluminium has been inspected. Layer thickness is 20.55mm. Olympus contact type C545 probe with frequency 3.5 MHz and 12.5 mm diameter used and following backwall echoes has been received as identified in figure 4.5 and table 4.5.

Table 4-5. Aluminium layer backwall echoes time

Time 1st peak , µs	Time 2nd peak , µs	Wave distance, mm	Wave travel time , µs	Sound velocity m/s
13.47	19.95	20.55	6.48	6342
19.95	26.10	20.55	6.15	6682

Using equation 4.1, average sound velocity for aluminium layer received - 6512 m/s. 1.72% difference is received comparing to standard Aluminium speed of sound – 6400m/s.

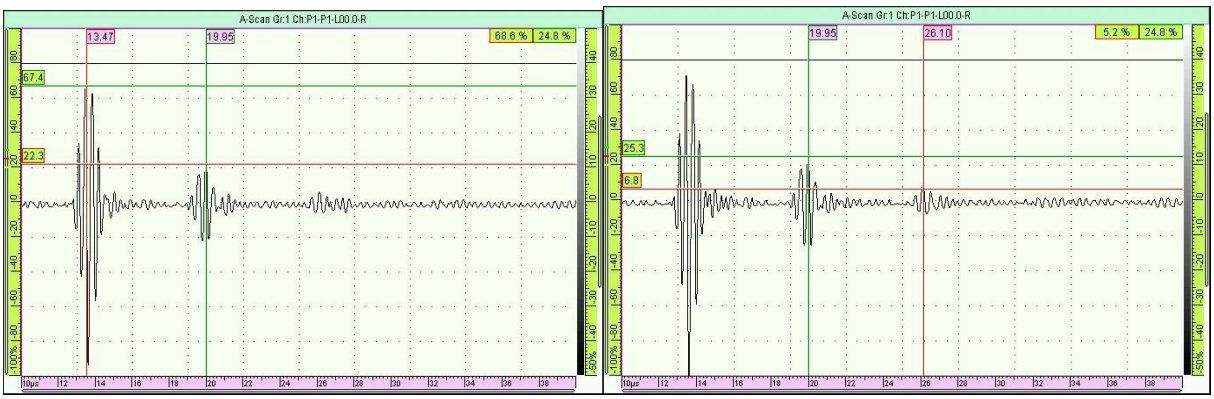

Figure 4-5. A scan for aluminium core only

4.4 PROPELLER BLADE FOAM ANALYSIS

4.4.1 Foam properties analysis

It was not possible to determine sound velocity at points 6,7,8,9 where glass fibre and polyurethane foam are bonded. Due to sound attenuation there was no back echo with various time and gain selections

Various probes used as listed in table 4.6.

Table 4-6. Ultrasonic transducers list used for polyurethane foam inspection

Probe	Type
Probe 1	Olympus model V126-RM, 5 MHz, 9.52mm diameter, Contact type
Probe 2	Olympus V102-RB, 1 MHz, 25mm diameter, Contact type
Probe 3	Olympus V104-RB, 2.25 MHz, 25mm diameter, Contact type
Probe 4	Olympus CX-164, 5 MHz, 0.25 in diameter with delay line
Probe 5	Olympus C545-SM, 3.5 MHz, 0.5 in diameter with no delay line
Probe 6	Olympus DHC703, dual line, 1 MHz, 0.5 in diameter, no delay line
Coupler	Water

Figure 4.6 represents of the A scan results for the polyurethane foam.

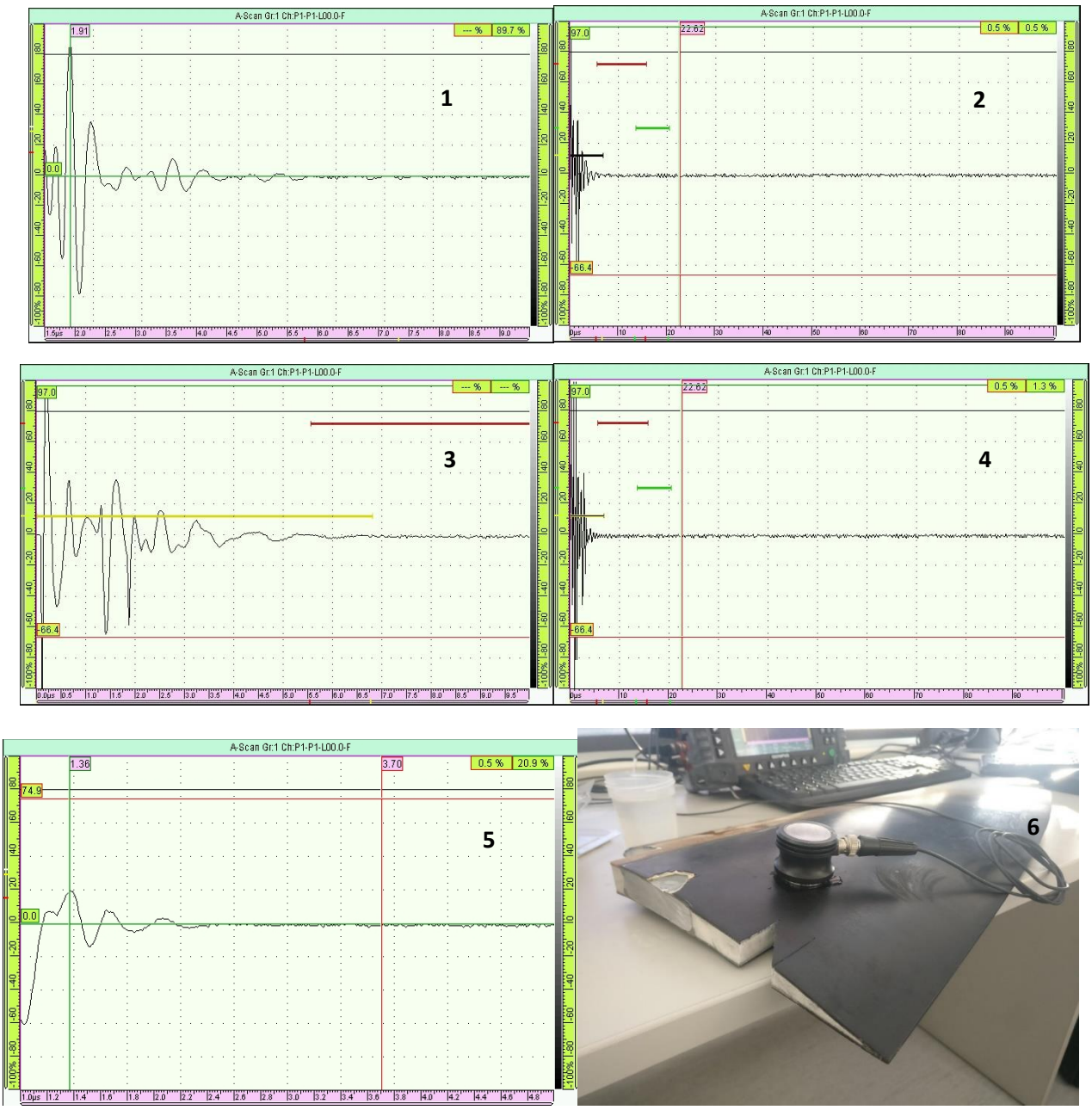

Figure 4-6. Polyurethane foam inspection. 1- point 6 , V126-RM probe, 5 MHz; 2- point 6 V-102 Probe 1Mhz; 3 - point 6 , V-102 probe, 1 MHz; 4- point 8, V104BR probe, 2.25 MHz global view; 5- point 9, 5MHz, probe V126 (no erosion paint); 6 – UT transducer location visual representation at point 8.

4.4.2 Foam sample analysis and ultrasound continuity check into stainless steel

2 Foam samples has been cut from propeller blade and blended to form equal rectangle shape. Dimensions 1mm x 15 mm x 40 mm and dimensions 8 mm x 25 mm x 37 mm. Samples are presented in figure 4.7.

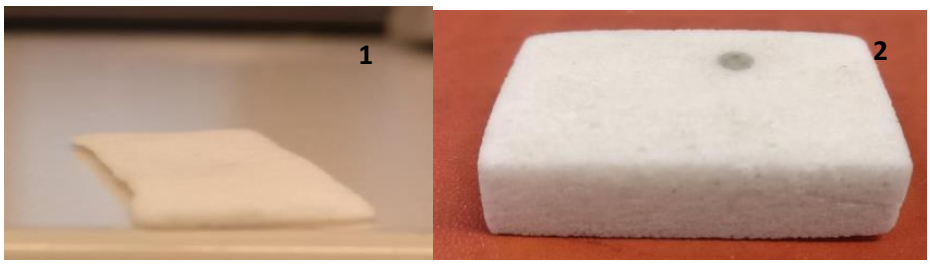

Figure 4-7. 2 Polyurethane foam samples; 1 – height 1mm; 2 – height 8mm

No signal went through the 8mm height sample, hence 1mm sample was cut in order to check if the attenuation is this high not to pass 1mm as well. Check was performed as be per figure 4.8 with no signal went through the foam into the metal as can be observed in figure 4.9. It can be compared with glass fiber acoustic continuity in 4.9.

Figure 4-8. Transducer positioning for foam continuity check

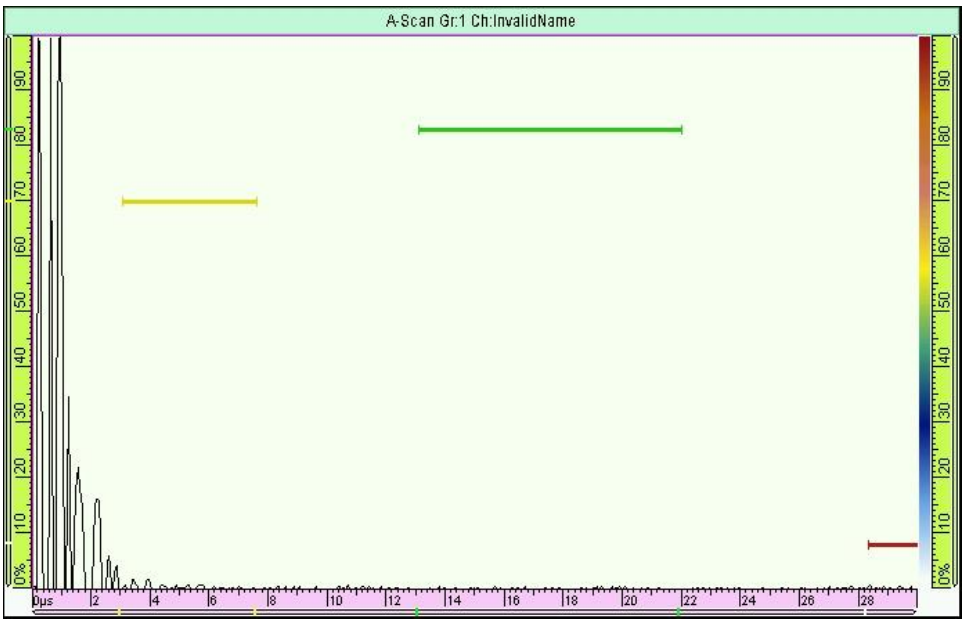

Figure 4-9. 1mm Polyurethane foam height sample's A-scan

By using foam dimensions and sample weight (2.02g) it was determined that foam density is 0.17g/cm³.

Foam has very high ultrasound attenuation and dispersion properties. It was not possible to have any frequency passed. Olympus OmniScan is working at the 1MHz frequency and higher, so lower frequencies could not be used.

4.5 FIBER GLASS MATERIAL EVALUATION

4.5.1 Fiber glass material characteristics

Various types and frequencies have been used for fiberglass inspection as identified in table 4.7

Table 4-7. Transducers used for fiberglass inspection

Model	Properties	Results
CX-164	5 MHz, 0.25 in diameter, delay line	Frequency was too high to precisely see back echo
C545-SM	3.5 MHz, 0.5 in diameter, no delay line	3.5 MHz frequency was good to see the backwall echo
DHC703	1 MHz, 0.5 in diameter, no delay line, dual line	Frequency was too low

Fiber glass sample has been cut from propeller blade showed in figure 4.10 with dimensions 2.34 mm x 19 mm x 28mm.

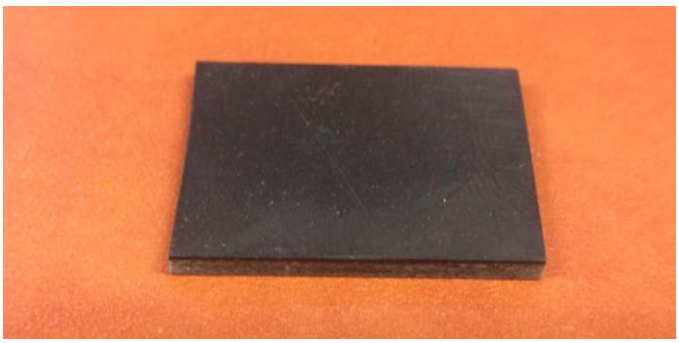

Figure 4-10. Fiber glass composite sample

Using Probe C545, 3.5 MHz it was retrieved good back echo signal via A scan showed in figure. Using this ultrasound speed in the fiber layer and fiber glass attenuation could have been compiled using equation 2.3 and results presented in figure 4.8 . A-scans are presented in figure 4.11 and 4.12 with description in table 4.9.

Table 4-8. Fiberglass layer speed of sound

Amplitude A(o), %	**Amplitude A(x), %**	**Distance, mm**	**Time,1st peak, µs**	**Time 2nd peak µs**	**Attenuation coefficient, α**	**Attenuation coefficient, α**	**Frequency**
71,9	23,1	2,34	4.08µs	5.81	493 N/m	4287 dB/m, or 4.287 dB/mm	3.5 MHz

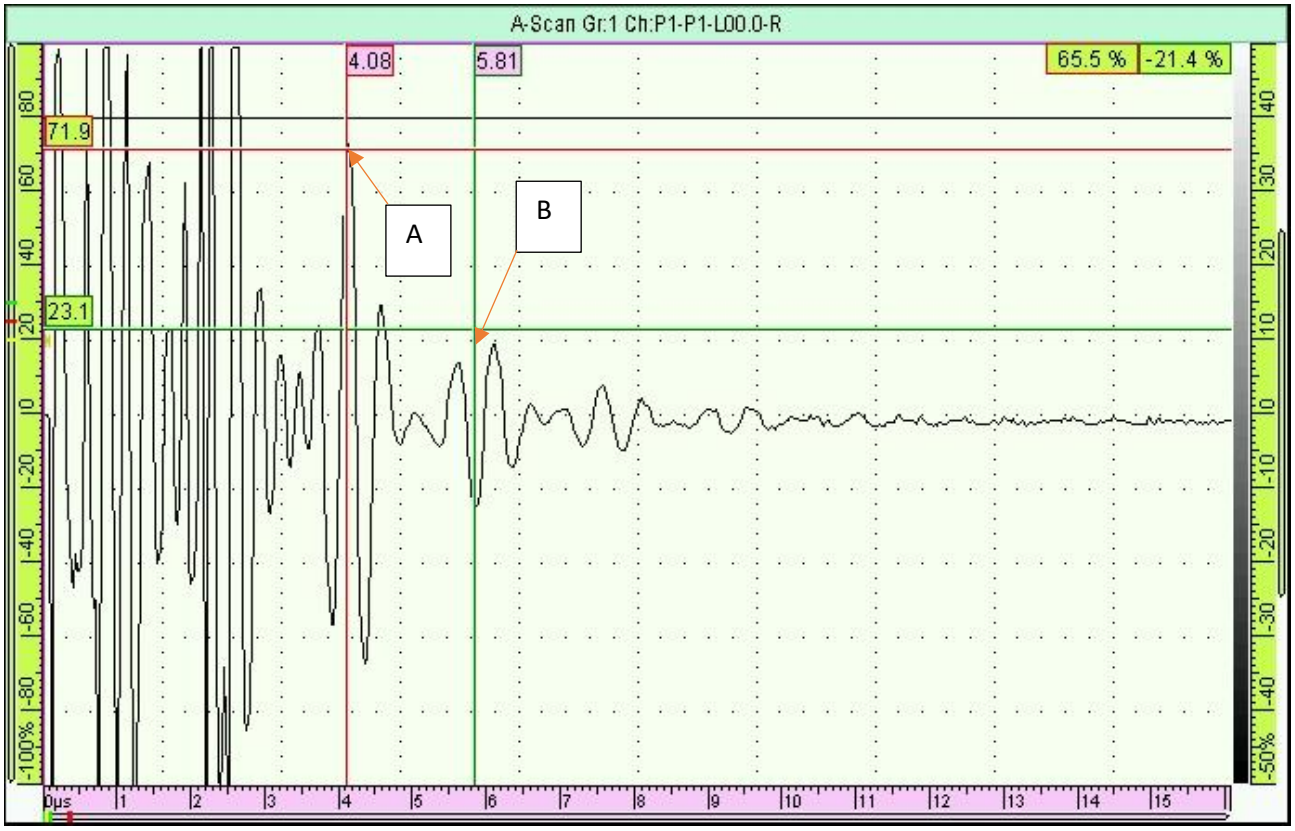

Figure 4-11. Fiber glass sample A scan

It was later on checked via Phased array using same frequency – 3.5 MHz – in order to cross check the first back echo signal timing. Time is the same as it can be seen in figure 4.12.

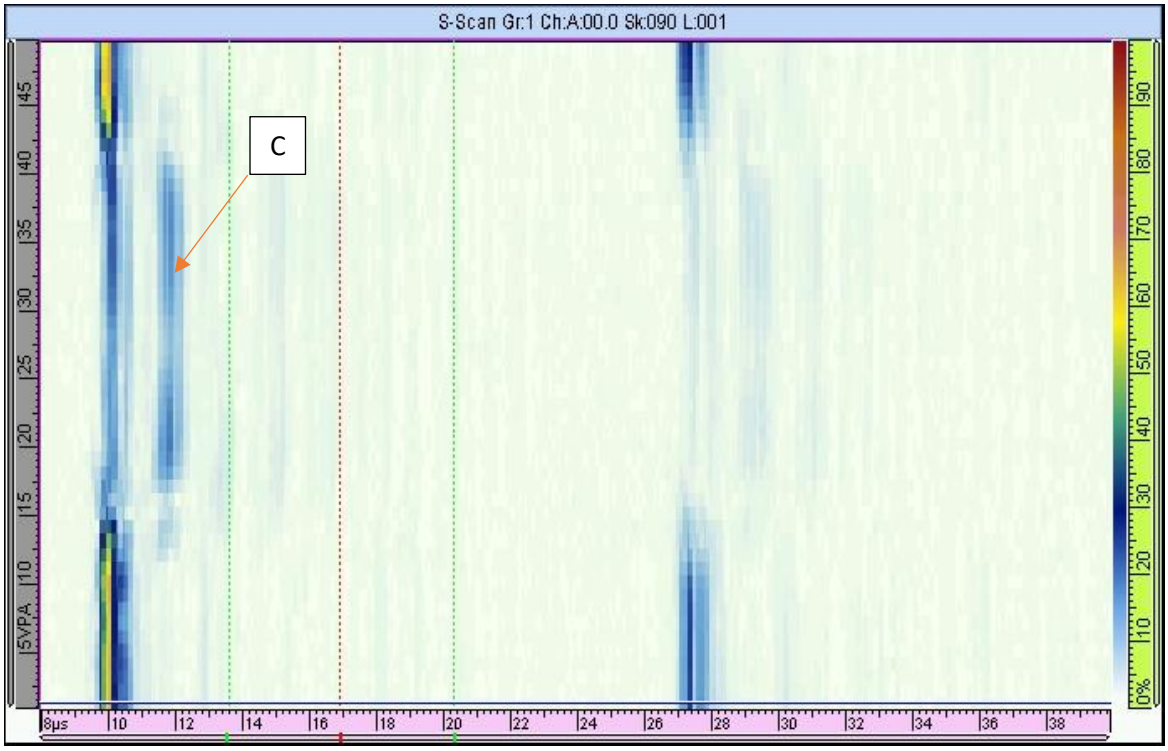

Figure 4-12. S-scan of glass fiber laminate sample

Table 4-9. Electronic scanning 4.11 and 4.12 results description

Echo	DESCRIPTION
A	1ST back wall echo from sample backwall
B	2nd back wall echo from sample backwall
C	Echo from glass fiber backwall in S-scan.

Using the equation 4.1 fiberglass laminate acoustic characteristics are found and listed in table 4.10

Table 4-10. Experimentally retrieved glass fiber composite acoustic characteristics

Material characteristics table	
Density	1.55 g/cm³
Ultrasound velocity	2705 m/s
Attenuation	4.287 dB/mm

4.5.2 Fiber glass sample ultrasound continuity check into stainless steel

Comparing to foam sample, glass fiber is much better ultrasound conductor. It was checked with stainless steel with set up in 4.13 and results in figure 4.14.

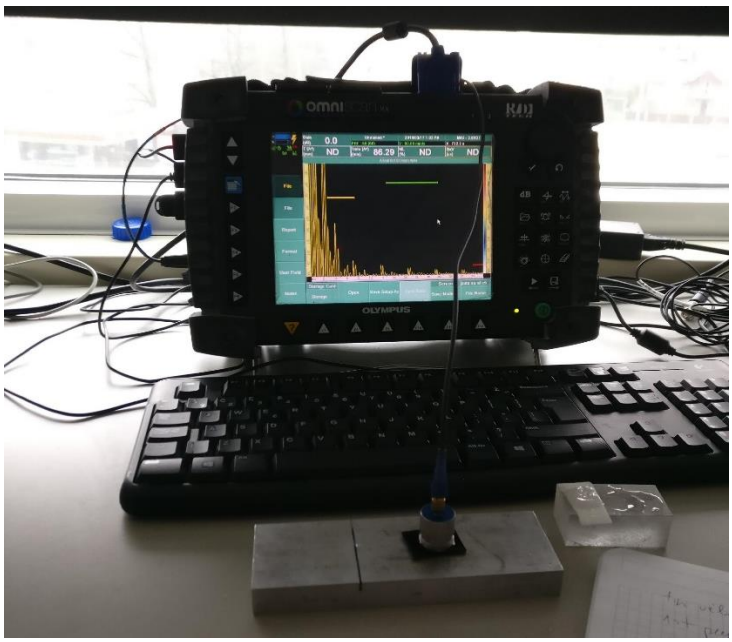

Figure 4-13. Glass fiber acoustic continuity check setup

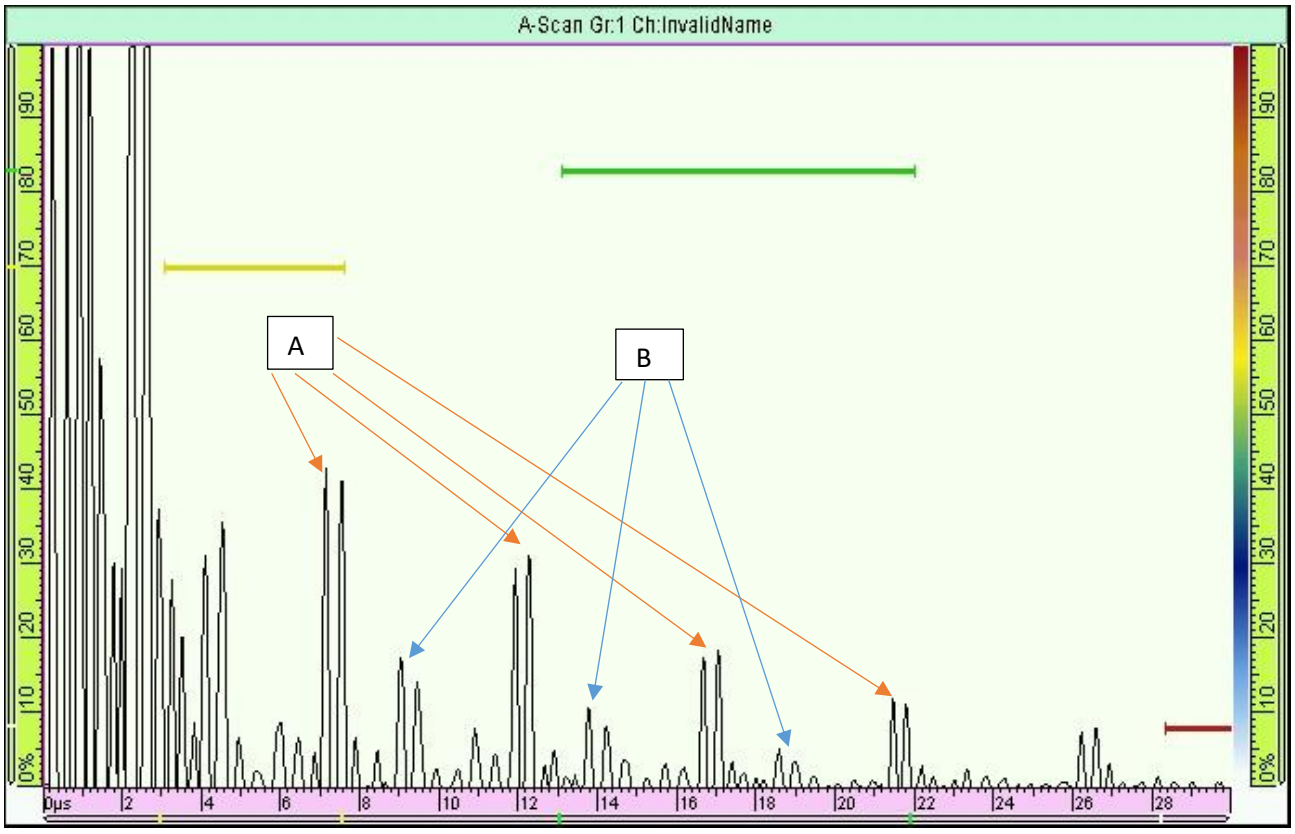

Figure 4-14. A scan of glass fiber composite acoustic continuity. A – metal backwall echo and B – Fiber glass composite backwall echo

4.6 ALUMINIUM LAYER SOUND ATTENUATION

All materials give some level of sound distortion within distance and sound intensity is diminished. Natural materials produce sound scattering and absorption and this combined loss of energy of scattering and absorption is called attenuation. Attenuation can be expressed by decay rate of the wave. Sound attenuation is required parameter in CIVA modelling. Probe used was Olympus V109, 5 MHz with 12.7mm diameter. Using equation 2.3 it was calculated sound attenuation coefficient in aluminium core and results presented in table 4.11. A-scan of Aluminium echoes are presented in figure 4.15.

Table 4-11. Aluminium acoustic attenuation

Amplitude A(o), %	Amplitude A(x), %	Distance X,mm	Attenuation coefficient , α	Attenuation coefficient, α	Frequency
76.4	28.8	20.23	48 N/m	418 dB/m;	3.5 MHz
31.3	10.8	20.23	52 N/m	456 dB/m	
Average			50 N/m	437 dB/m; 0.437 dB/mm	

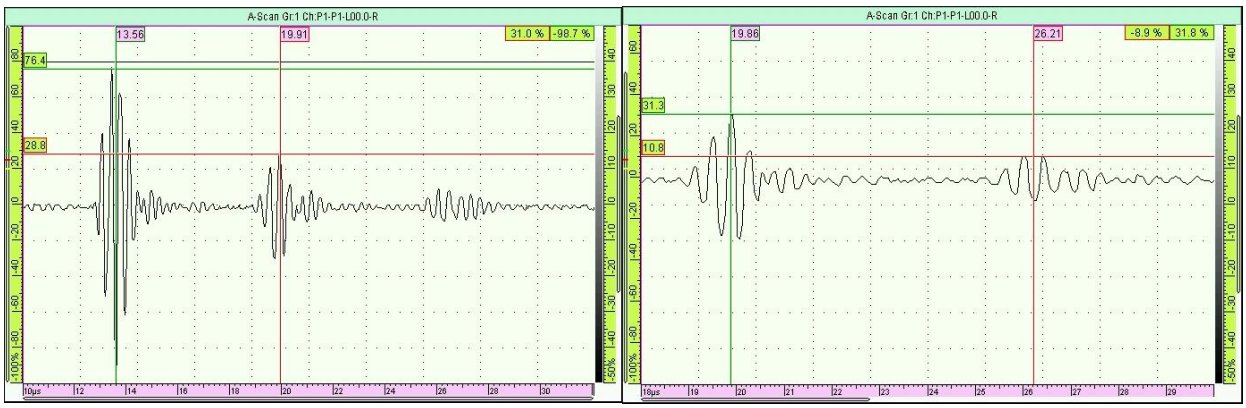

Figure 4-15. Amplitude decay due to attenuation, Aluminium at 3.5MHz

5.1 EVALUATION WITHOUT WEDGE

As first inspection and to determine the near field phenomena for phased array, inspection without the wedge has been chosen with linear, near wall type, 5 MHz frequency phased array. Model Olympus 5L128-NW3, 128 elements, active aperture 128 mm, pitch 1 mm, elevation 7 mm, dimensions 130 mm x 21 mm x 35mm.

5.1.1. Phased array 5 MHz without wedge - inspection of fiber glass – Aluminium - fiber glass layers

Phased array probe with 128 elements has been placed above fiber glass composite shell and aluminium spar as showed in cross-sectional view figure 5.1.

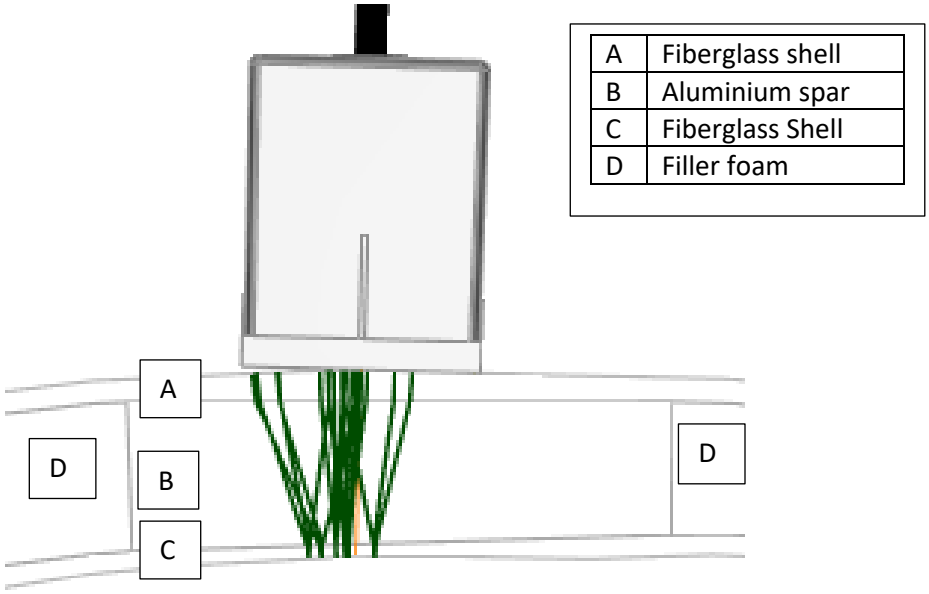

Figure 5-1. Inspection cross-sectional view with PA without wedge

Phased array has been placed 30 mm from the edge as showed in figure 5.2. Scans presented in figure 5.3. A point represents Near Field phenomena for phased array while point B shows backwall echo from the top fiberglass layer. Aluminium spar backwall echo is point C and backwall echo from bottom fiberglass layer while D represents back wall echo from bottom fiber glass layer.

Figure 5-2. Location of the PA during inspection

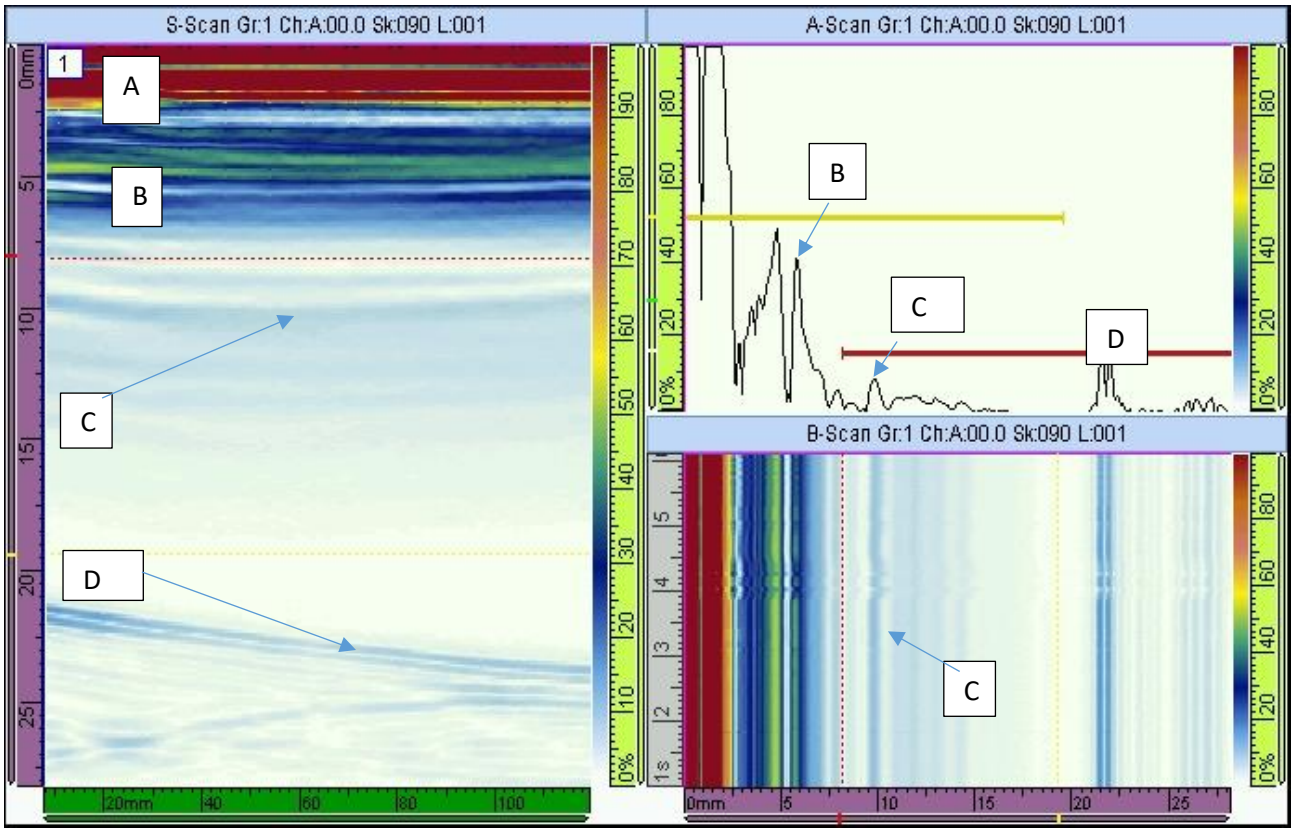

Figure 5-3. A/B/S scans of Linear phased array above the fiber glass-Aluminium- fiber glass layers.

It can be noticed from figure 5.3 that using phased array without a wedge causes difficulty to clearly see sound path and echo signal from top fiberglass layer backwall, it's not possible to determine the small defects in fiberglass layer and within the fiberglass layer. However, it was possible to detect obvious voids from the aluminium spar even without the wedge. Refer to figure 5.4.

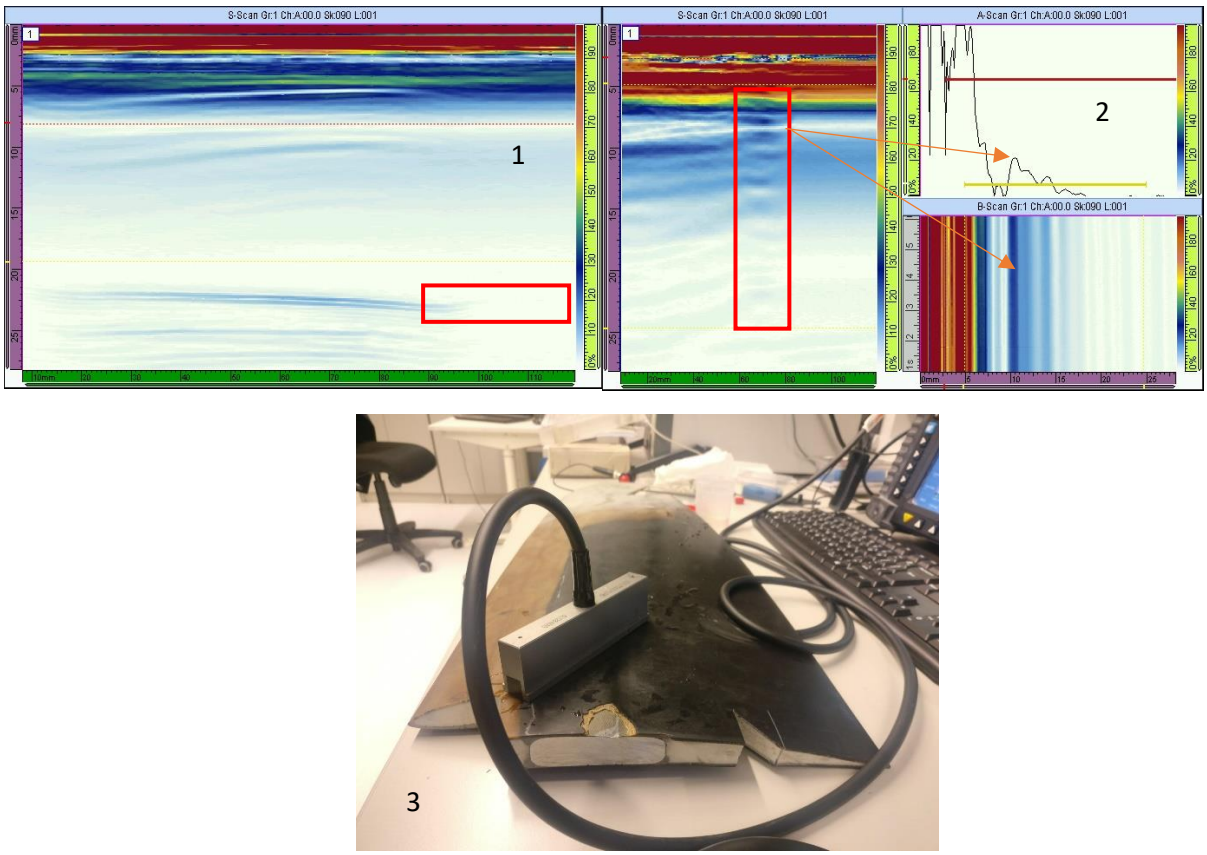

Figure 5-4. Fiberglass void detection without a wedge

In the figure 5.4 item 1 we can see no backwall echo from aluminium spar and bottom fiberglass layer. This is because phased array is turned as showed in figure 3 and signal is dispersed by foam layer. Figure 5.4 item 2 shows multiple echoes starting from top fiberglass layer caused by delamination between fiber glass and metal spar.

5.2 PROPELLER BLADE ANALYSIS USING PHASED ARRAY WITH WEDGE

In order to better understand effects of the phased array used without wedge and make a comparison judgment which technique is better, phased array has been mated with wedge. Also, in paragraph 5.2 sample has been tested with two frequencies – 5 MHz and 3.5 MHz in order to obtain the resolution differences and determine better frequency. From the paragraph 2.6 it was determined that acoustic attenuation is highly dependent on frequency, hence it is necessary to find the middle point between resolution, detectable flaws and acoustic attenuation effects.

5.2.1 Phased Array 5 MHz – description and properties

Phased array type Olympus 5L128-NW3 has been used which is linear , near wall type, has 128 elements with each element width of 1mm. Wedge has been selected to be Olympus SNW3-OL-IHC-C made of Plexiglass with height of 20mm. Speed of sound in the plexiglass is 1280 m/s as per wedge characteristics table. This wedge was selected due to perfect fit with phased array 5L128. There are 4 tightening screws to make sure that phased array does not move during inspection. Water as coupler has been used between phased array and the wedge. Wedge height is visually showed in figure 5.5. It also very important to understand the echoes coming from the bottom of the wedge - at which time

period they come and what is the amplitude of the signal when there is no test sample beneath. This is important to test the wedge without the sample in order not to mix up the echoes coming from the wedge and sample materials intersections later during the inspection.

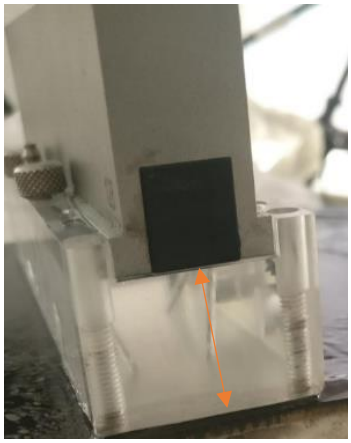

Figure 5-5. Wedge's height visual identification

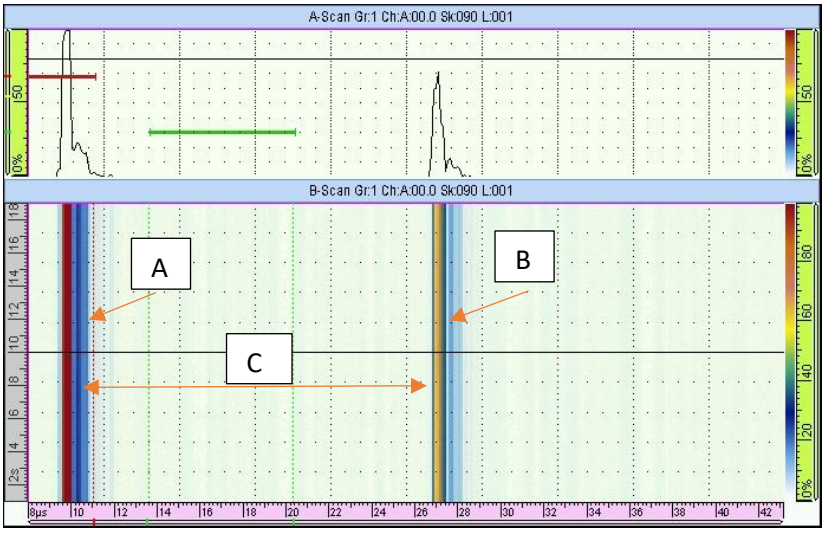

Figure 5-6. Wedge's own echoes distribution

From the figure 5.6 it can be determined 3 points to describe. A echo is the first echo from the wedge bottom. Second echo from the wedge comes at point B. Area between two echoes is area C where the specimen will be analysed and all the flaws would be showed. 1st echo is coming at 10µs and is dependent on the material of the wedge (in this case plexiglass) and height of the wedge. Usage of the wedge assures that Near Field effects do not contribute the results.

5.2.2 Inspection of fiber glass – Foam – fiber glass layers

Inspection of the specimen was started with fiberglass and foam intersections. Figures 5.7 and 5.8 represents to cross-sectional view for the leading and trailing edges of the propeller blade.

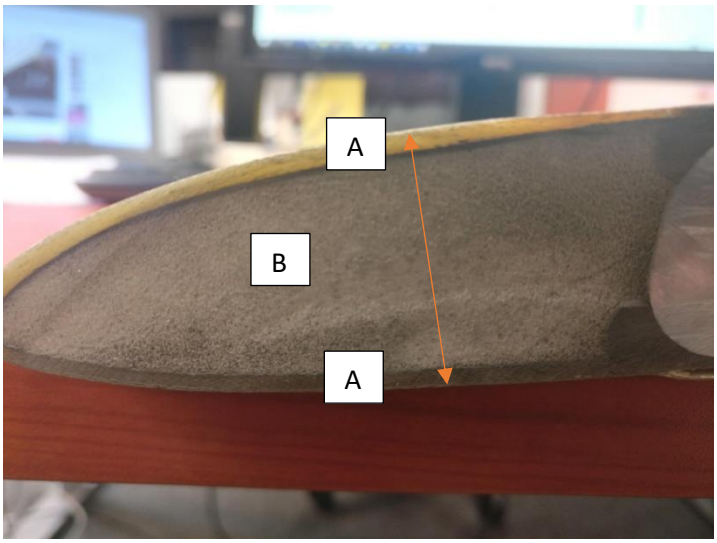

Figure 5-7. Inspection cross-sectional view, blade leading edge. A- fiberglass shell; B – polyurethane foam.

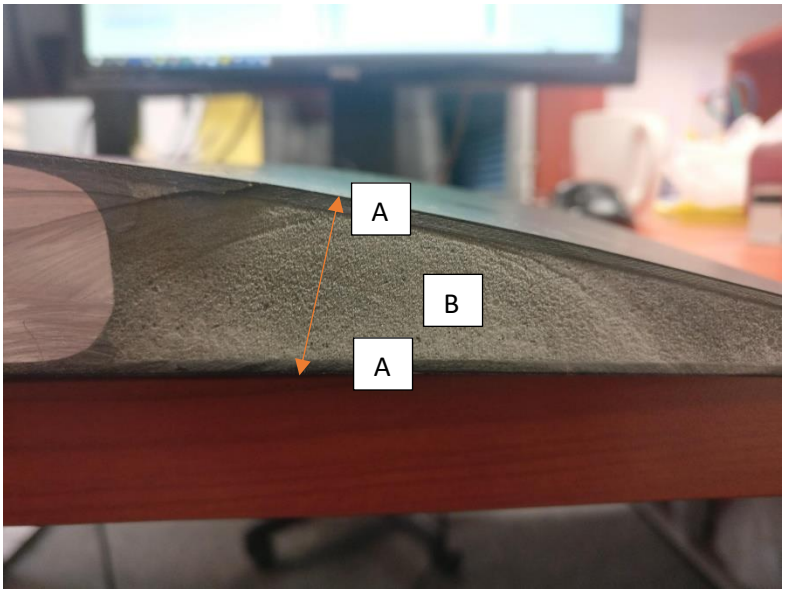

Figure 5-8. Inspection cross-sectional view, blade trailing edge. A- fiberglass shell; B – polyurethane foam.

From figures 5.7 and 5.8 2 unique zones could be identified which all come with their own attenuation coefficients as described and found in paragraphs 4.4 and 4.5. Layer A is fiberglass and standard height is 2mm. Zone B is Polyurethane foam which does not have fixed height and is following their air-foil of the blade. For simplicity reasons height showed in figure 5.7 and 5.8 was selected to be the same – 16 mm. Inspection with phased array 5 MHz was conducted and results showed in figure 5.9 (B-scan).

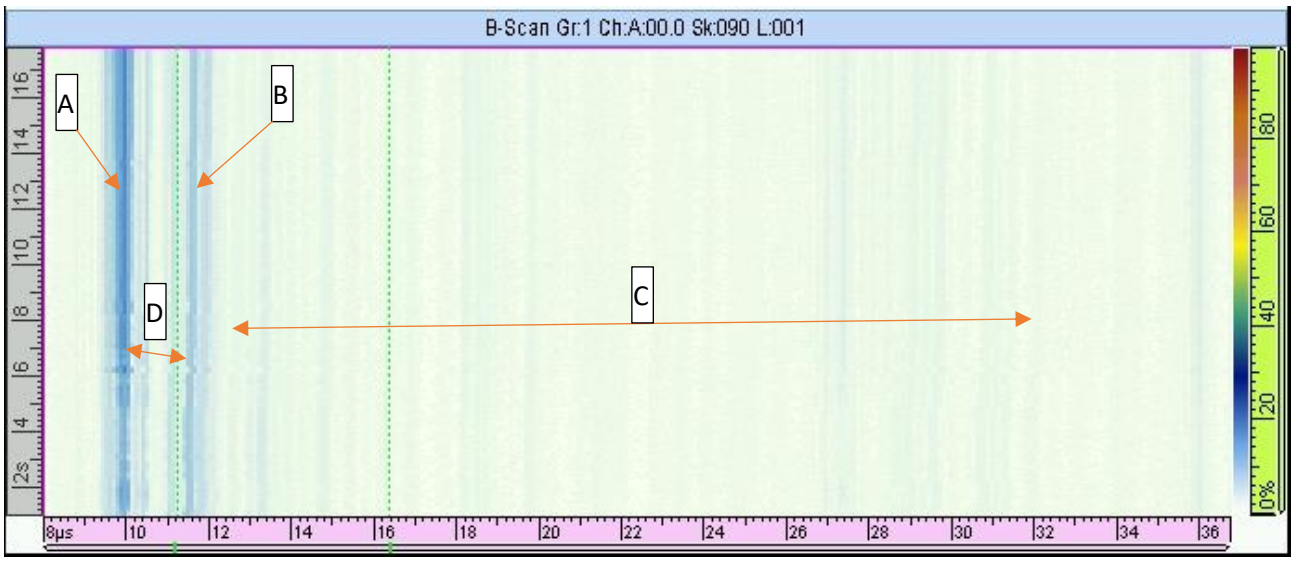

Figure 5-9. 5 MHz PA inspection for fiberglass-foam-fiberglass layers

Referring to figure 5.9 A point is 1st echo from the wedge backwall. Where point B is top fiberglass backwall echo. After the fiberglass layer there are no echoes received back as ultrasound wave is shattered by foam layer as showed in area C. There is no second echo from wedge backwall and there is no echo from bottom fiberglass layer. However, Area D is indeed showing the flawless top fiberglass condition.

5.2.3 Inspection of Fiberglass – Aluminium – Fiberglass layers

Second inspection has been conducted for Aluminium spar and cross-sectional view is showed in figure 5.10.

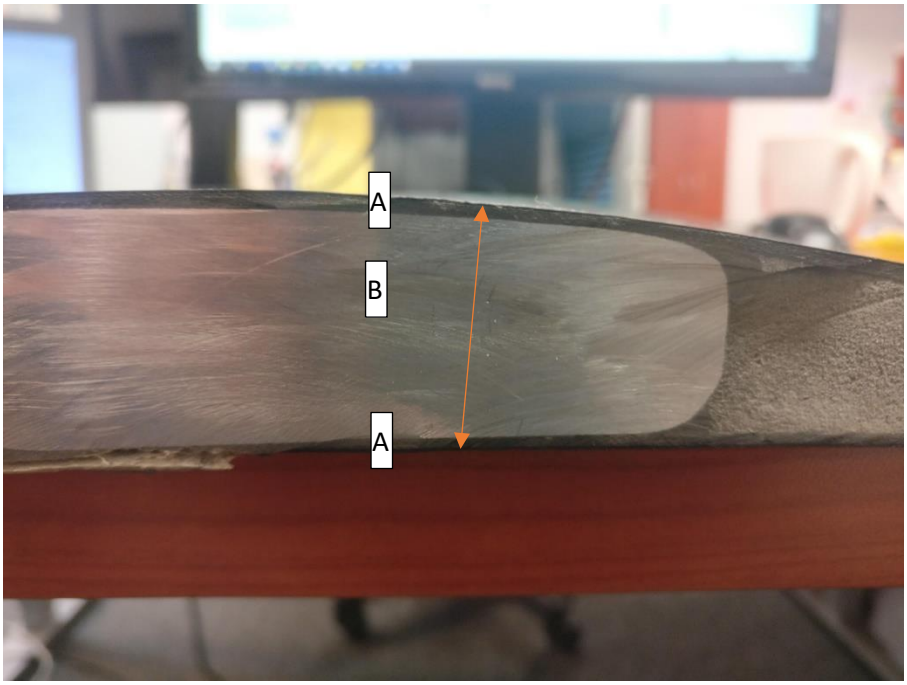

Figure 5-10. Cross-sectional inspection view. A- fiber glass shell; B – Aluminium spar

Aluminium spar which is represented as B in figure 5.10 has height of 20 mm and fiberglass shell which is presented as area A has height of 2 mm. Inspection with PA of 5 MHz has been done and S

scan view is presented in figure 5.11. B scan has been recorded as well with elevated gain to 26 dB in order to show the standard flawless bond in between the fiberglass shell.

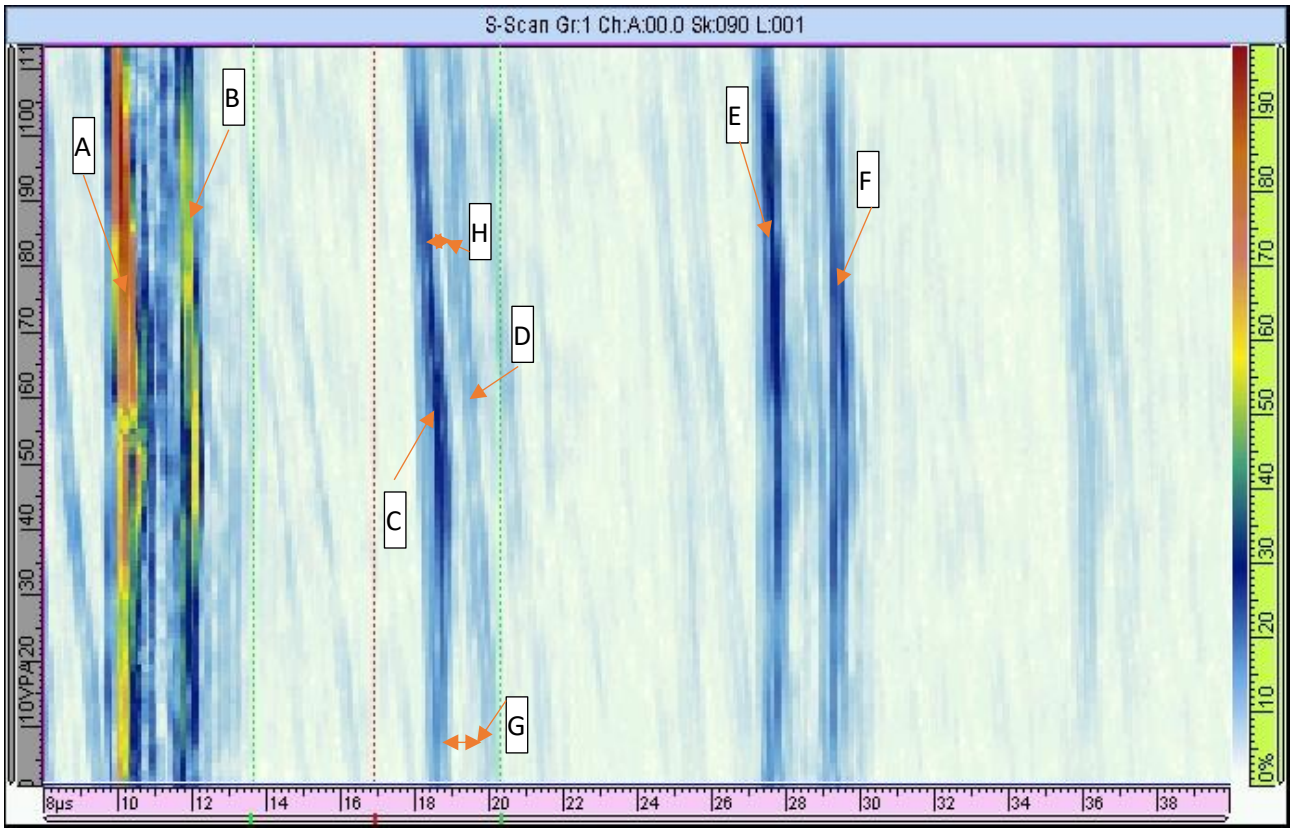

Figure 5-11. 5 MHz PA inspection of Fiberglass - Aluminium - Fiberglass layers

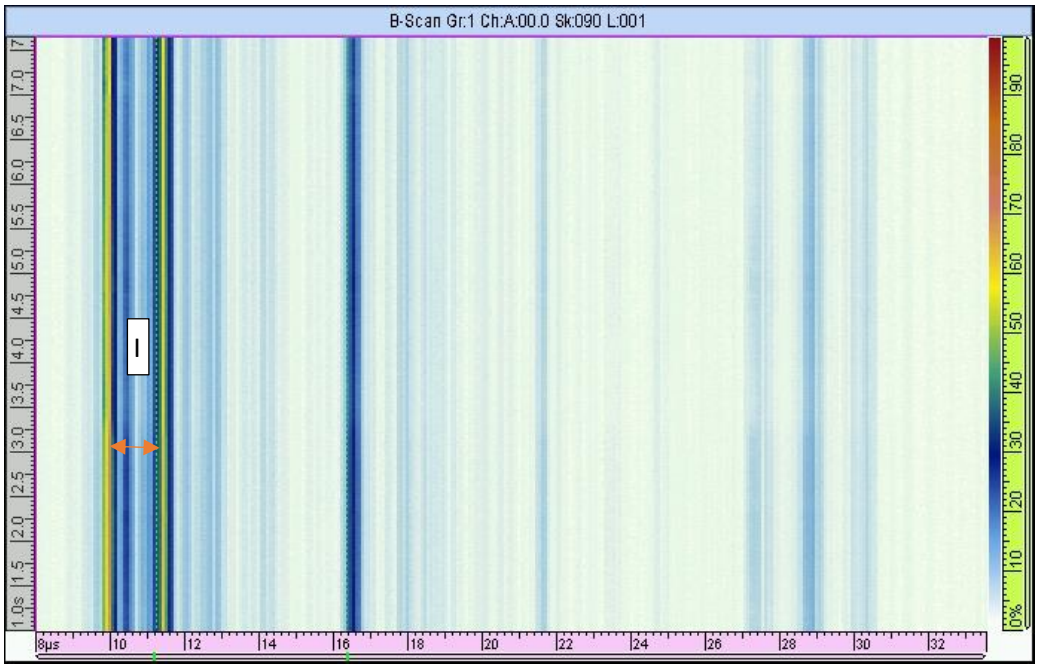

Figure 5-12. B scan of figure 5.11

From figures 5.11 and 5.12 there are various points to be described. A echo is a 1st echo from the wedge back wall. Top fiberglass layer backwall echo is presented in B echo. Echo C is aluminium layer backwall echo and D echo is bottom fiberglass layer backwall echo. Echo E is 2nd echo from wedge backwall while F is second echo from top fiberglass layer. Points G and H represents different timing in echoes from bottom fiberglass layer. Such difference is received due to rework of fiberglass layer in some of the locations of propeller blade. Where layer thickness is reduced due to rework ultrasound wave travel faster. Point I in the B-scan was presented to better understand any flaws within the fiberglass layer. It can be seen that echo is strong and stable which lets to make a conclusion that fiberglass layer in figure 5.12 does not have any flaws. It is also clear that resolution given by 5MHz PA is enough to determine any deficiencies in the layer's intersections and within the layers. From points C and D is it interesting to see how good S scan represents the changing air foil of the propeller blade – echo line is following the aluminium spar curvature within the phased array detection zone as it starts just before 18μs and ends up after 18μs.

5.2.4 Flaws detection Phased Array 5 MHz

In paragraph it was started with S scans of the cross-sectional profiles of the propeller blade - leading edge, trailing edge and middle section. However, it is also important to understand if phased array can detect the flaws in different areas and what are expected echoes to be seen.

5.2.4.1 Fiber glass delamination within the fiber layers

Artificial defect has been done in top fiber glass layer just above the aluminium spar as showed in figure 5.13. Defect has been done to simulate the interlayer delamination of the fiberglass shell with length of 16mm. PA inspection has been conducted with S scan result in figure 5.14.

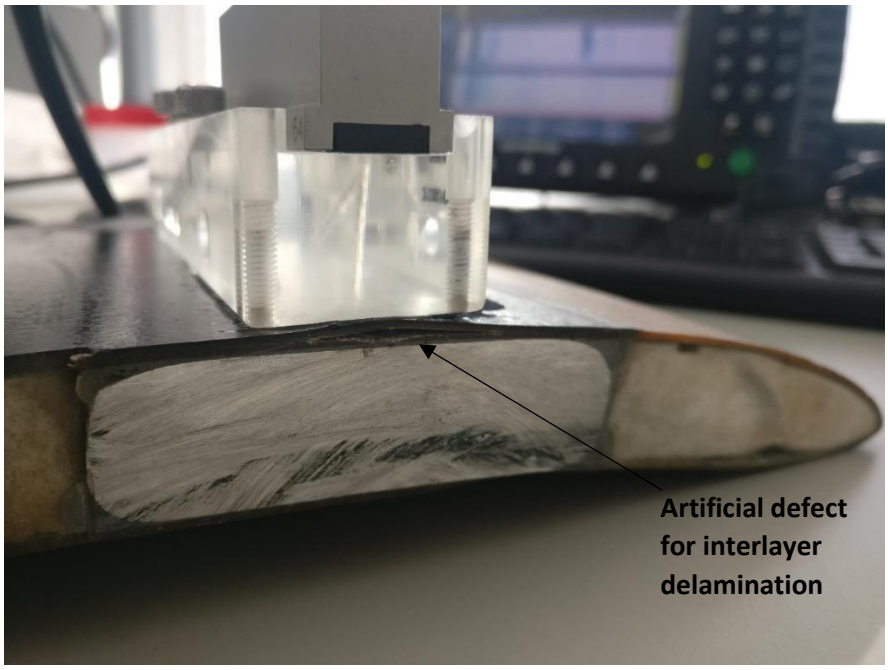

Figure 5-13. Top Fiberglass defect and PA cross-sectional view

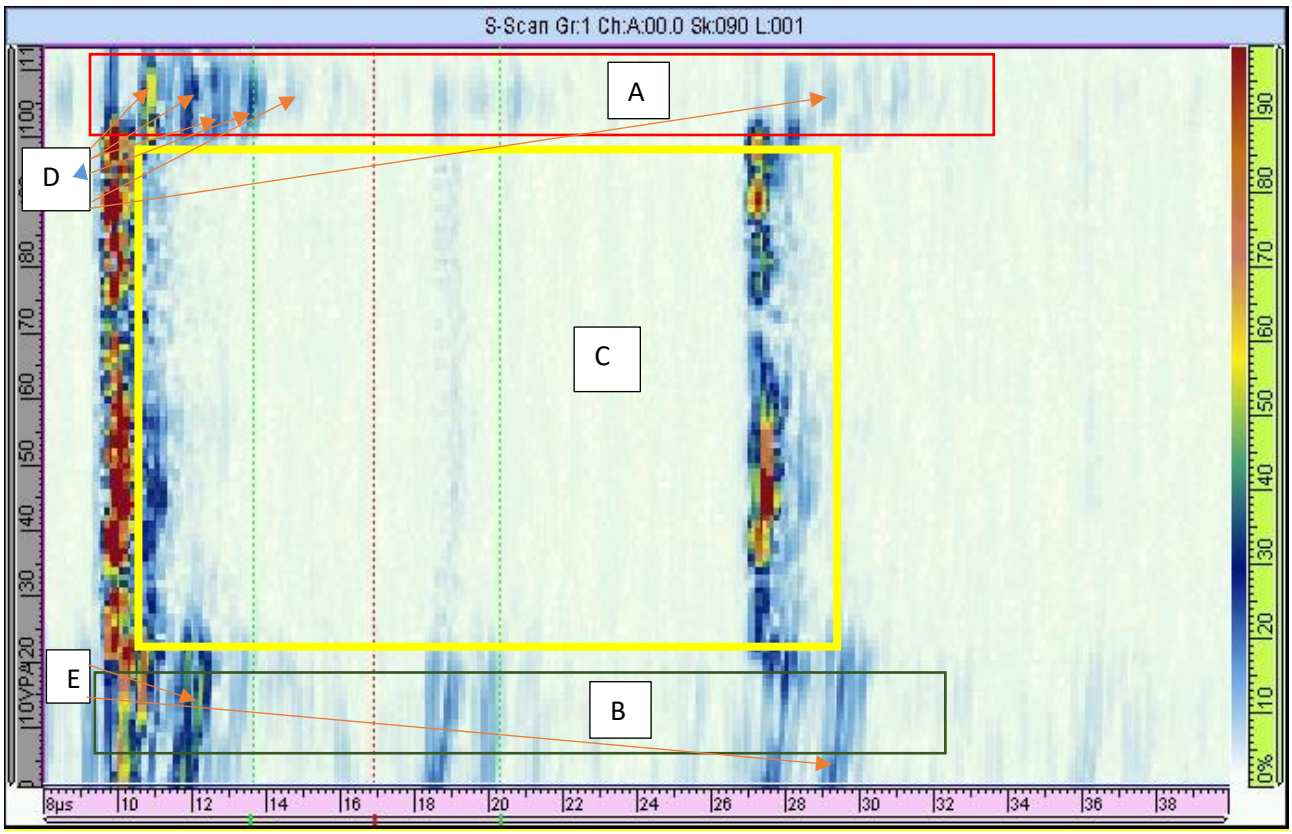

Figure 5-14. Interlayer delamination in top fiberglass (PA 5 MHz)

It can be noticed in the area A within figure 5.14 multiple echoes comparing to zone B which is flawless. Point E represents flawless fiberglass backwall echoes. Zone C shows that phased array wedge was not in proper contact with the specimen during inspection as only wedge echoes can be observed.

5.2.4.2 Filler foam deficiencies

In order to analyse if the foam defects can be detected two artificial defects has been done in the foam layer. Figure 5.15 shows defect 1 and 2.

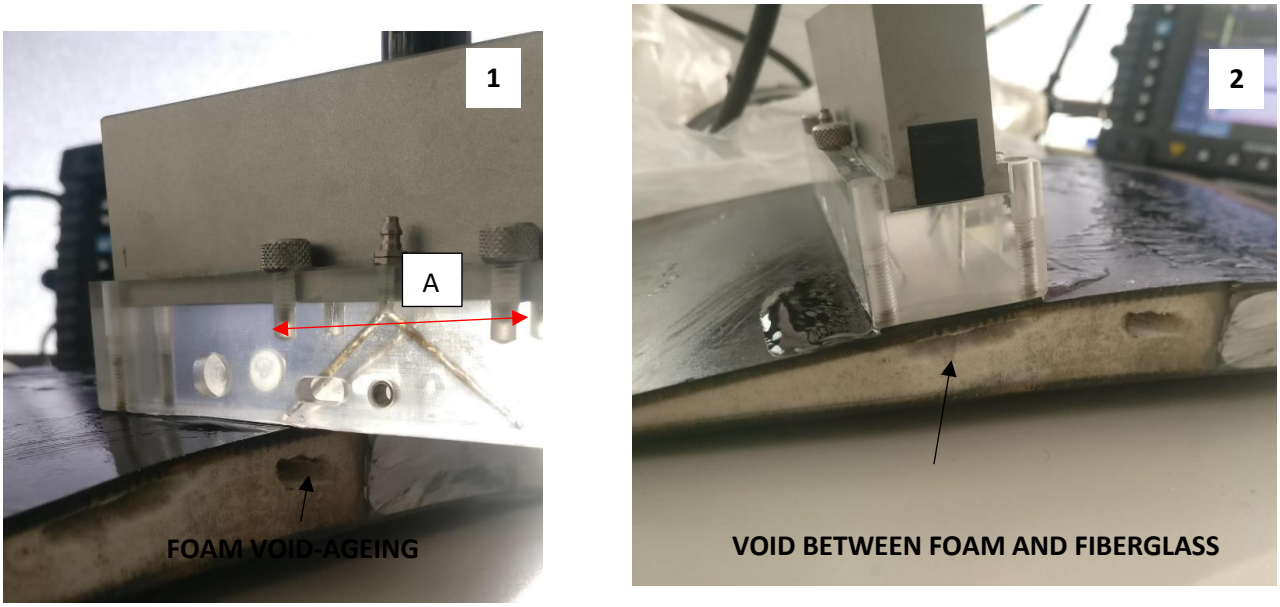

Figure 5-15. Foam artificial defects position and PA position

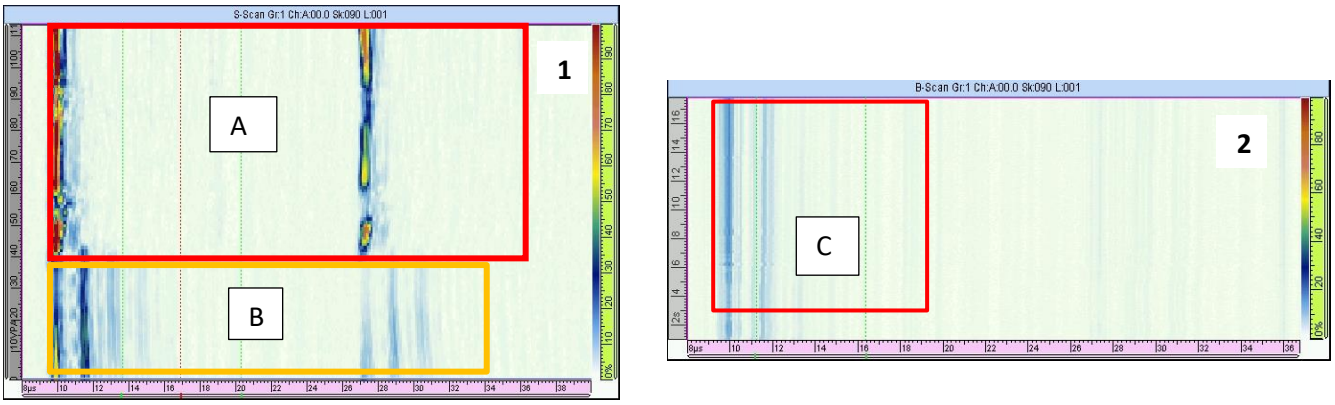

Figure 5-16. Foam defects S scans.

Figure 5.16 shows the scan for the defect 1 and 2. Area C shows no echo from the void after the fiberglass layer where point B shows only wedge and top fiberglass layer echoes. Area A is received as wedge is not in proper contact with propeller blade air foil - position of the PA is showed in figure 5.15 item 1. Due to very high polyurethane foam acoustic attenuation it is not possible to detect any defects within the foam layer. Inspection repeated with lower frequency 3.5 MHz in 5.3.3.4 paragraph in order to test if 3.5 MHz usage would enable to detect.

5.2.4.3 Detection capabilities of back wall shell deficiencies

In order to check Phased array 5 MHz resolution in S scan artificial defect has been done on the backwall of the propeller blade fiberglass shell. It was needed to know if the flaw can be detected if inspection is conducted from the top. Figure 5.17 represents the flaw and phased array positions during the inspection.

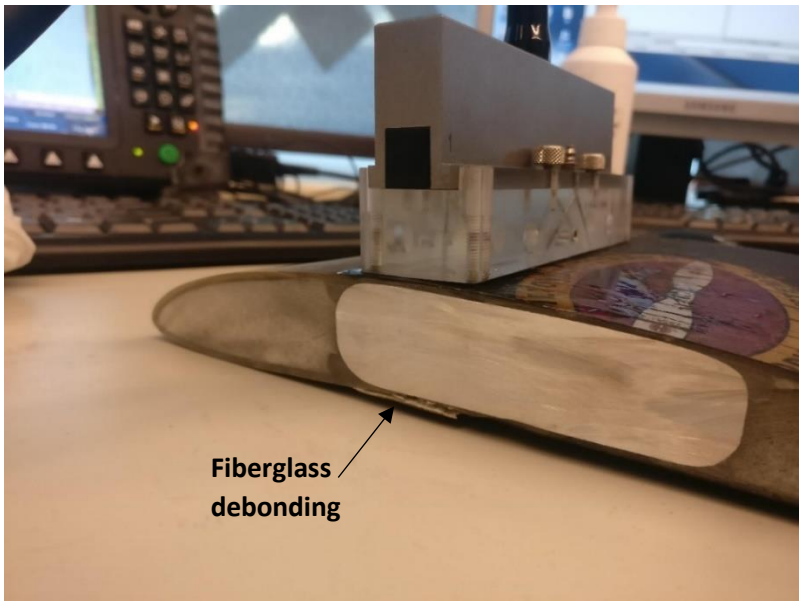

Figure 5-17. Bottom glass fiber composite shell debond and phased array set up during inspection

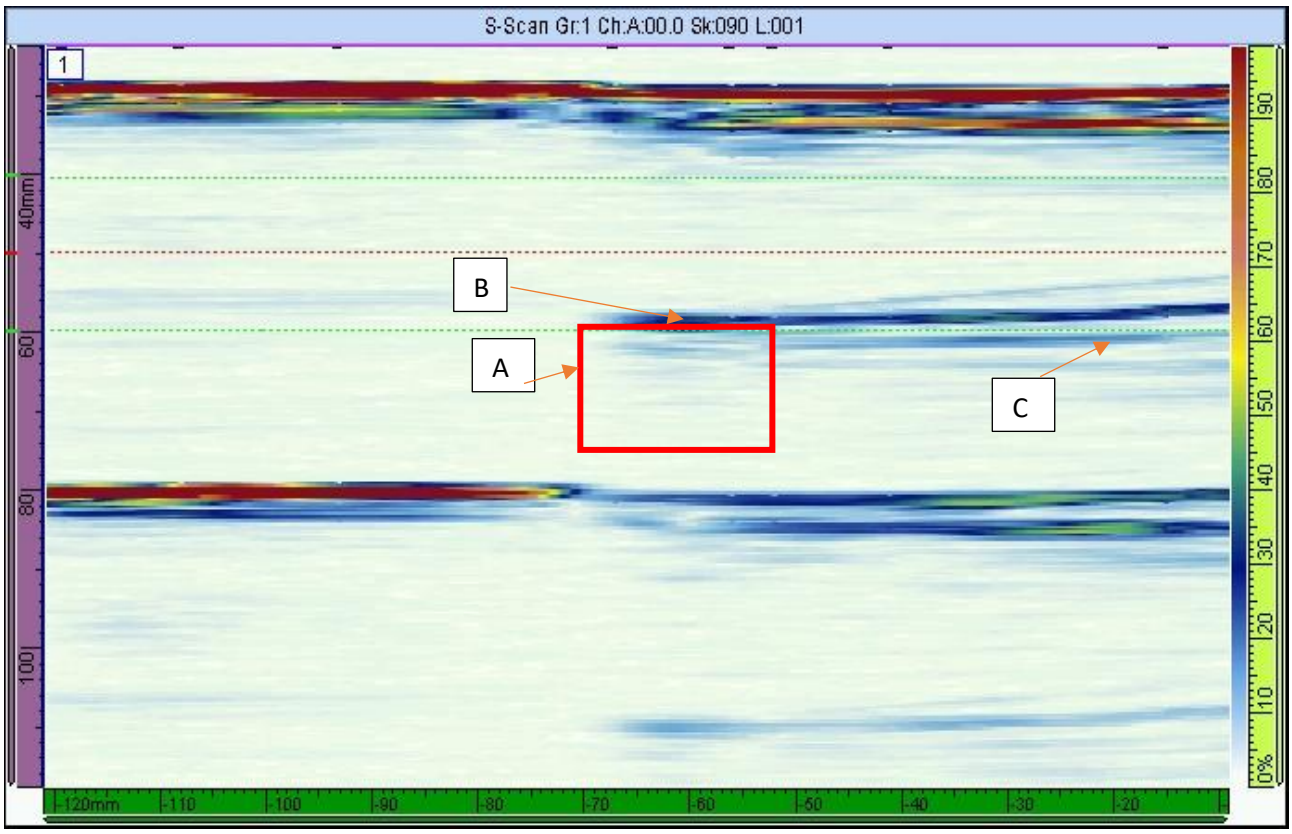

Figure 5-18. S scan of the backwall fiberglass flaw (PA 5 MHz)

Referring to figure 5.18 echo B shows the echo from aluminium backwall and A shows the flaw area. Debonding produces additional echoes as showed in area A and the echo line is disturbed. Normal echo would be as showed in C.

5.3 Analysis with Phased array 3.5 MHz

In order to compare the resolution, phased array of 3.5 MHz has been used, model selected Olympus 5L64-NW3 with active aperture 64 mm, elevation 7mm , pitch 1mm , and external dimensions 66 mm x 19 mm x 25 mm. Wedge has been selected same as used for Phased array of 5 MHz. Figure 5.19 shows the setup.

Figure 5-19. 3.5 MHz and wedge setup

5.3.1 Inspection of fiber glass – Aluminium – Fiber glass layers

Inspection has been started from the propeller middle section inspecting the fiberglass-Aluminium-fiberglass layers. S-scan and B-scan are presented in figure 5.20. Inspection cross-sectional view is identical to figure 5.10 view.

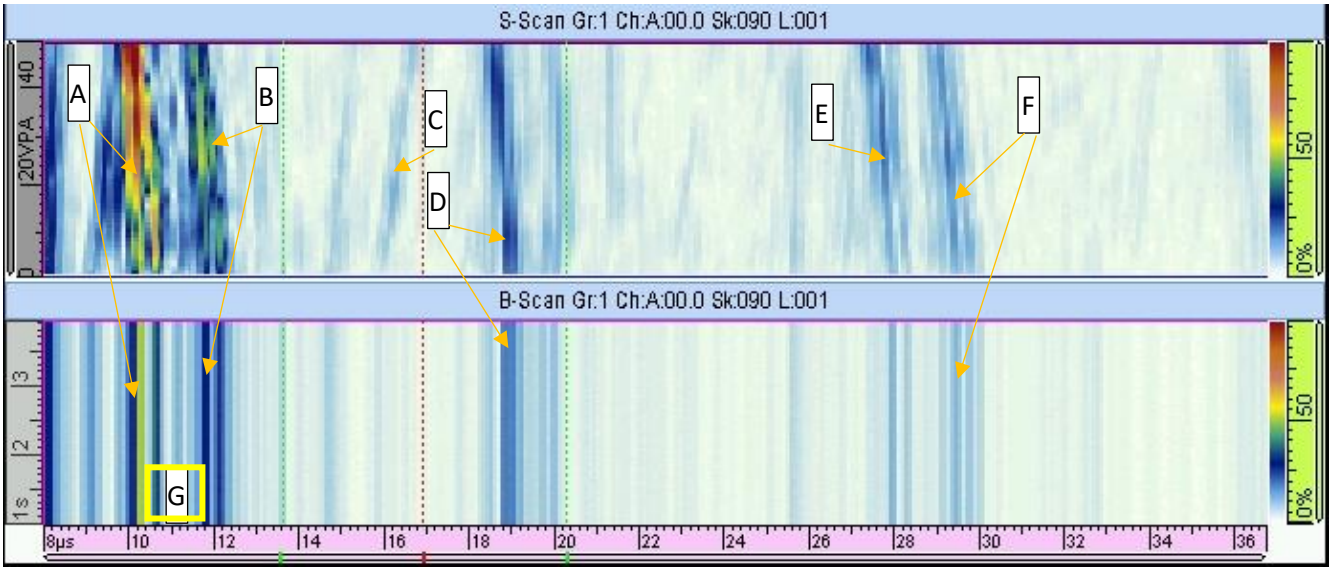

Figure 5-20. Fiberglass – Aluminium- Fiberglass layers inspection with Phased array 3.5 MHz at gain 23 dB

As of 5 MHz phased array point A echo is wedge 1st echo and B echo is fiberglass layer. It can be noticed that B echo is a bit steered following the air-foil of the propeller blade. As a difference from 5 MHz phased array S-scan echoes C is introduced in figure 5.20 which represents the repetitive echoes from the fiberglass layers. This is because 3.5 MHz wave is less attenuated than 5 MHz wave by fiberglass layer. Echo D represents aluminium spar backwall echo. S scan also shows that echo is following the air-foil of the propeller in same pattern as B echo. Echo E shows 2nd backwall echo from the wedge and echo F 2nd backwall echo from the fiberglass. Comparing to 5 MHz phased array inspection it can be observed more distinctive echoes within the fiberglass layer – in total 4. F echo is also steered in same pattern as echoes B and D following the air-foil. Observing G zone gives clear view on any defects within the fiberglass layer. In the provided figure 5.20 there are no defects. It can be also observed that visibility within the glassfiber layer is better with 3.5 MHz phased array.

5.3.2 Inspection of fiber glass – Foam – fiber glass

In paragraph 5.2.2 it was foam and fiberglass intersections has been already inspected with 5 MHz phased array and it was concluded that no backwall echo can be received from the foam layer nor the bottom fiberglass layer due to strong acoustic attenuation within the foam. It was tried with 3.5 MHz phased array to check if there is any difference and this frequency could go through the foam. The inspection setup is identical as showed in figures 5.7 and 5.8. S-scan and B-scan of the 3.5 MHz usage is showed in figure 5.21.

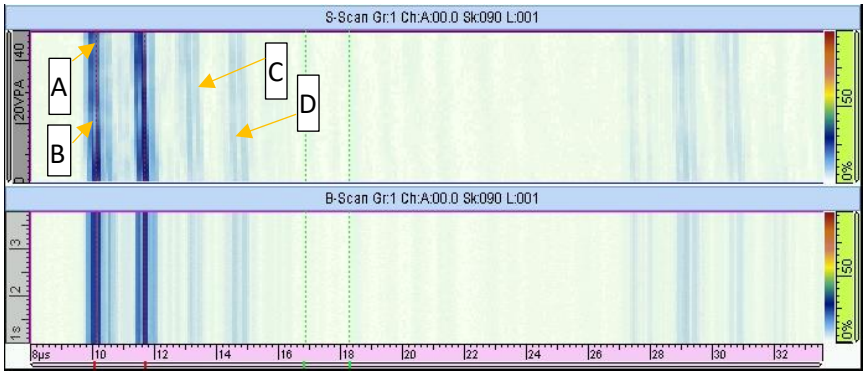

Figure 5-21. Inspection of Fiberglass- Foam - Fiberglass layers (PA 3.5 MHz)

The result received is identical to 5 MHz usage the echoes wise from bottom fiberglass layer. However, as it could have been observed in figure 5.20, same in figure 5.21 repetitive echoes can be received from top fiberglass and they are marked as C and D echoes. While A is 1st wedge backwall echo and B is 1st top fiberglass layer backwall echo. C is 2nd backwall echo from top fiber glass and D is 3rd backwall echo.

This inspection concludes that within the fiberglass layer there is no deficiencies.

5.3.3 Flaws detection Phased Array 3.5 MHz

Various flaws had been examined with phased array 5 MHz having 128 elements and it was concluded that the defects introduced in the propeller blade could have been detected. It is important to understand if usage of 3.5 MHz would detect the flaws more precisely or it would be visa versus and flaws would not be detected. As well it was important to conclude foam flaws cannot be detected by using lower frequency for better penetration.

5.3.3.1 Fiberglass delamination between the *layers*

The same artificial interlayer delamination which was examined in paragraph 5.2.4.1 has been tested with 3.5 MHz phased array. Refer to figure 5.13 for the delamination and phased array setup which was identical with 3.5MHz array as well. S-scan of this inspection is presented in figure 5.22.

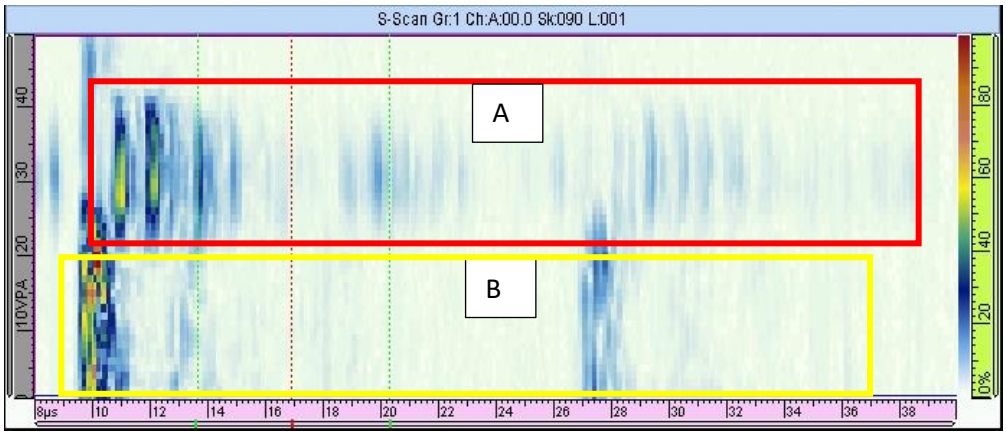

Figure 5-22. Interlayer delamination of top fiberglass (PA 3.5 MHz)

Due to the elements reduction of 3.5 MHz we got longer area A comparing to figure 5.14. However, it can be noticed that 3.5 MHz array delivered higher resolution. This is connected to better penetration capability of lower frequency array. It can be observed multiple echoes from delaminated layers within the fiberglass. Zone B represents the array part which was not fully engaged to propeller air foil. Comparing delaminated area, A view with figure 5.20 it can be noticed the differences between flawless and defected fiberglass layer.

5.3.3.2 Fiberglass delamination from foam (total)

In order to further examine and driven by the better resolution while using 3.5 MHz array zone of fiberglass composite with dimensions of 23mm x 20 mm has been cut away from foam filler. Figure 5.23 represents the cut area, foam exposure and the PA position during the inspection. S scan view is presented in figure 5.24.

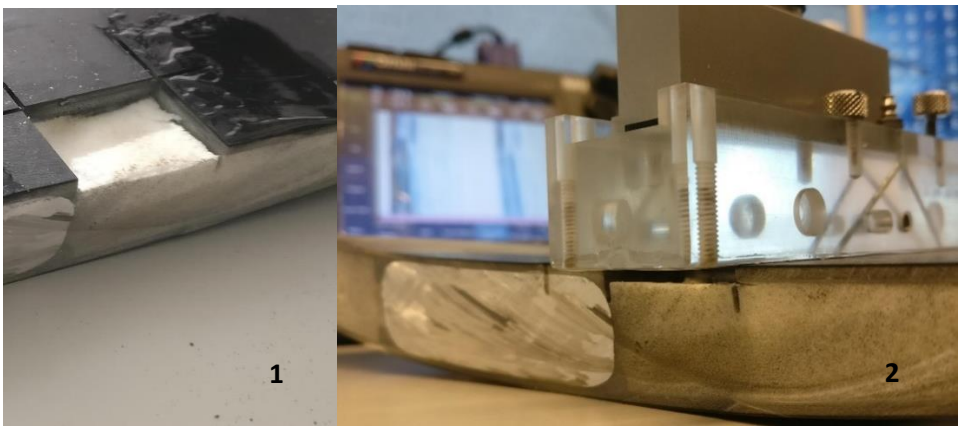

Figure 5-23. Total delamination set up (PA 3.5 MHz). 1 – artificial defect - glass fiber composite shell removed from foam filler; 2 – phased array set up during inspection

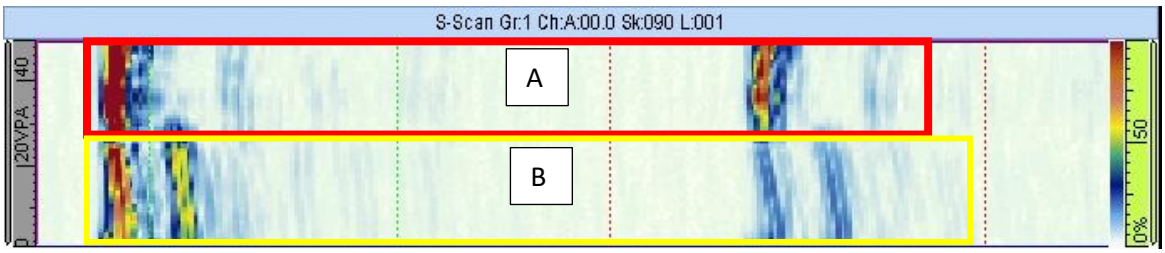

Figure 5-24. Fiber glass total delamination (PA 3.5 MHz)

Referring to figure 5.24 S-scan to distinctive zones can be seen – A and B. B zone represents flawless fiber glass layer and A represents totally delaminated fiberglass layer. Echo from the fiberglass backwall echo cannot be seen as there is no bond at all. It can be also examined that in case of total delamination the signal amplitude from the wedge backwall is stronger than comparing to no flaw zone B. In order to examine the area if cut fiberglass area would be glued back to the foam, fiberglass has been glued to foam filler and phased array inspection performed again. S-scan view is presented in figure 5.25.

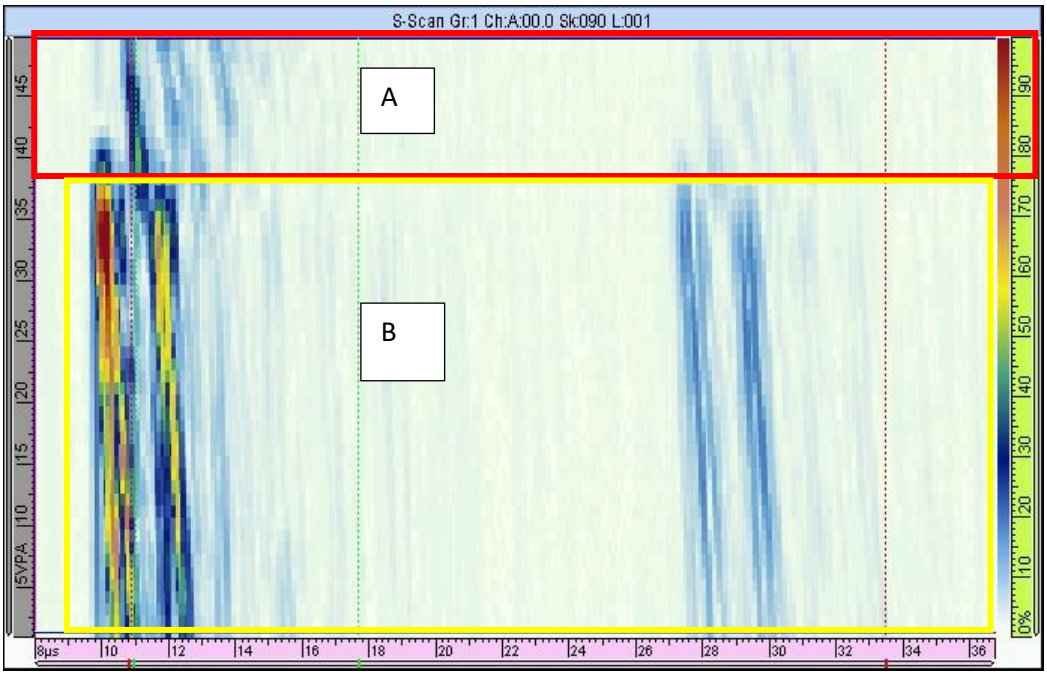

Figure 5-25. Fiberglass layer glued to foam (PA 3.5 MHz)

It can be observed in the area A that echo is received from the glassfiber, however its pattern is totally different than comparing to zone B which is flawless. This easily lets to detect repair zones which are done incorrectly, by comparing echo time at the repaired zone and unrepaired zone. It can be noticed that S-scan received is identical to theoretical S-scan delamination received with CIVA and presented in figure 3.23.

5.3.3.3 Fiber glass delamination from Aluminium (partial)

As it was inspected in paragraph 5.3.3.2 over the foam, same was applied for the glassfiber composite layer in the middle section of the propeller blade above the aluminium spar. Piece of composite has

been cut away from the spar and glued back into original position. The setup of the cutaway and phased array position during inspection can be observed in figure 5.26.

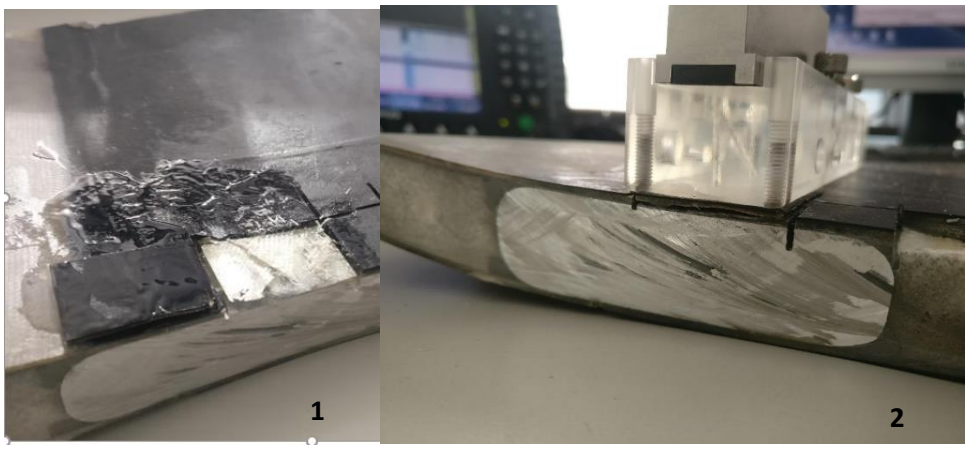

Figure 5-26. 1 - Fiberglass shell cut away from aluminium spar; 2 – phased array setup during inspection

Two S-scans are presented in figure 5-27 with zones A and B.

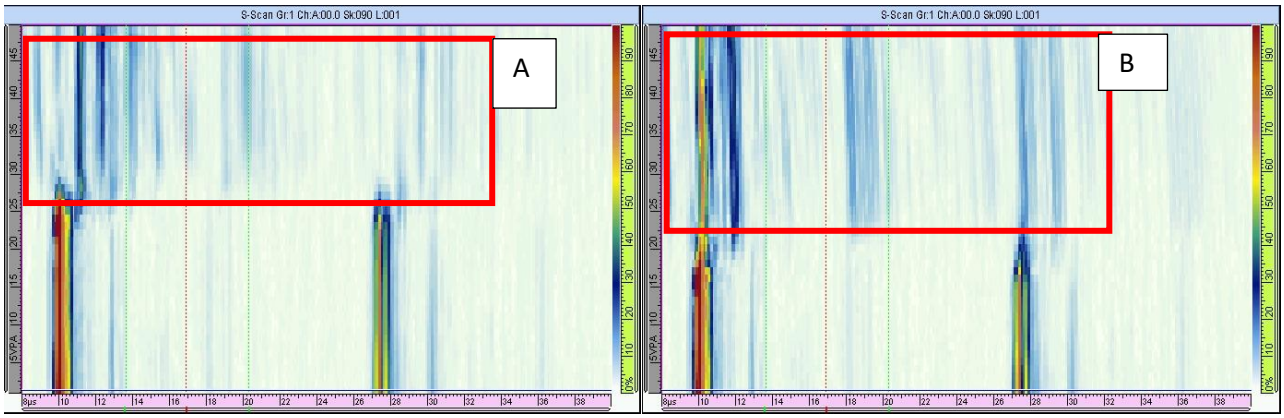

Figure 5-27. Fiberglass incorrect repair detection over the spar (PA 3.5 MHz)

S-scan area B is presented same location of propeller blade without any repairs to the fiberglass layer over the spar. Area A is representing artificial defect (repair) done as per figure 5.26. It can be observed that echo from aluminium spar is lost in the area A and incorrect repair is causing repetitive echoes showing the bond between fiberglass and aluminium spar is not good.

5.3.3.4 Filler foam defects

In order to prove that filler foam defects cannot be detected, 3.5 MHz array has been used. Set up is showed in figure 5.28.

Figure 5-28. Artificial polyurethane foam defects and phased array setup during inspection

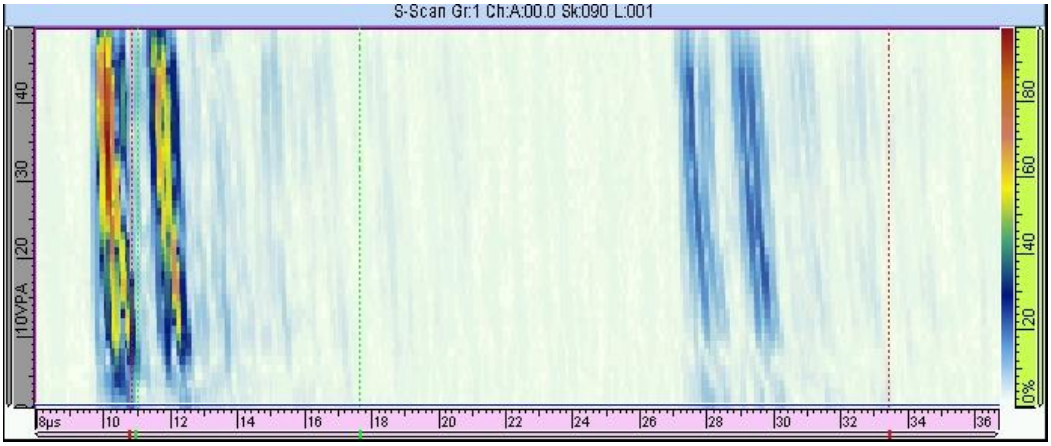

Figure 5-29. Filler foam defects (PA 3.5 MHz)

It can be observed from figure 5.29 that due to high foam attenuation defects within the foam are not detectable using phased array method even with lowering the frequency from 5 MHz to 3.5 MHz. Comparing to figure 5.16 we get the same result – no backwall echo from filler foam artificial defect.

5.3.3.5 Detection capabilities of back wall deficiencies in fiberglass layer

As similar inspection has been done with PA 5 MHz in paragraph 5.2.4.3 it was important to compare if 3.5 MHz is more suitable for backwall flaws detection due to better penetration capabilities through two composite layers. The same interlayer delamination has been used as showed in figure 5.13. Set up of phased array and a flaw has been done as showed in figure 5.30.

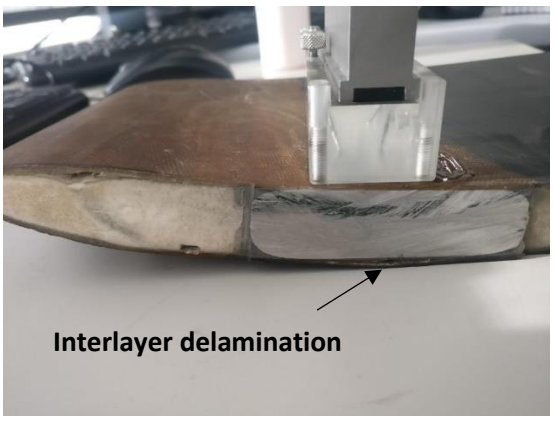

Figure 5-30. Artificial backwall flaw within the fiberglass

S-scan and B-scan are presented in figure 5.31.

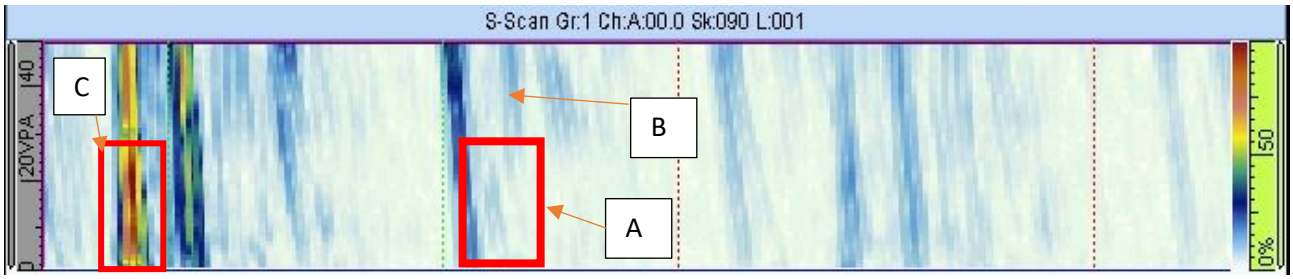

Figure 5-31. Backwall interlayer delamination (PA 3.5 MHz)

In case of this interlayer delamination phased array has been able to detect this as it can be showed in figure 5.31 area A comparing to normal echo as showed in B. Also, it can be observed that at the start of the delamination, wedge backwall echo is strengthened – ref to C.

Another analysis has been performed on the reworked fiberglass layer as showed in figure 5.32. It was important to test phased array resolution and sensitivity.

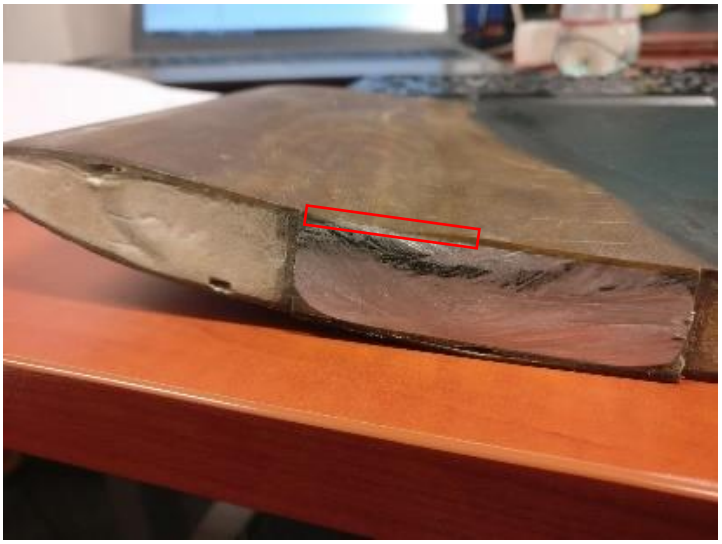

Figure 5-32 – Fiberglass shell blend-out performed to inspect the phased array resolution and sensitivity

S-scan which was received after the inspection of the blended fiberglass is presented in figure 5.33. Phased array 3.5 MHz was able to detect reduction of bottom side fiberglass layer thickness. Focal

law has been set in Omniscan to focus the beam at 30mm. Refer to the zone A in the figure 5.33. B-scan presented in figure 5.33 meanwhile shows no flaws within the inspection zone. Hence usage of phased array can detect the shell thickness reduction due to the repairs and the same time detect any flaws within such rework.

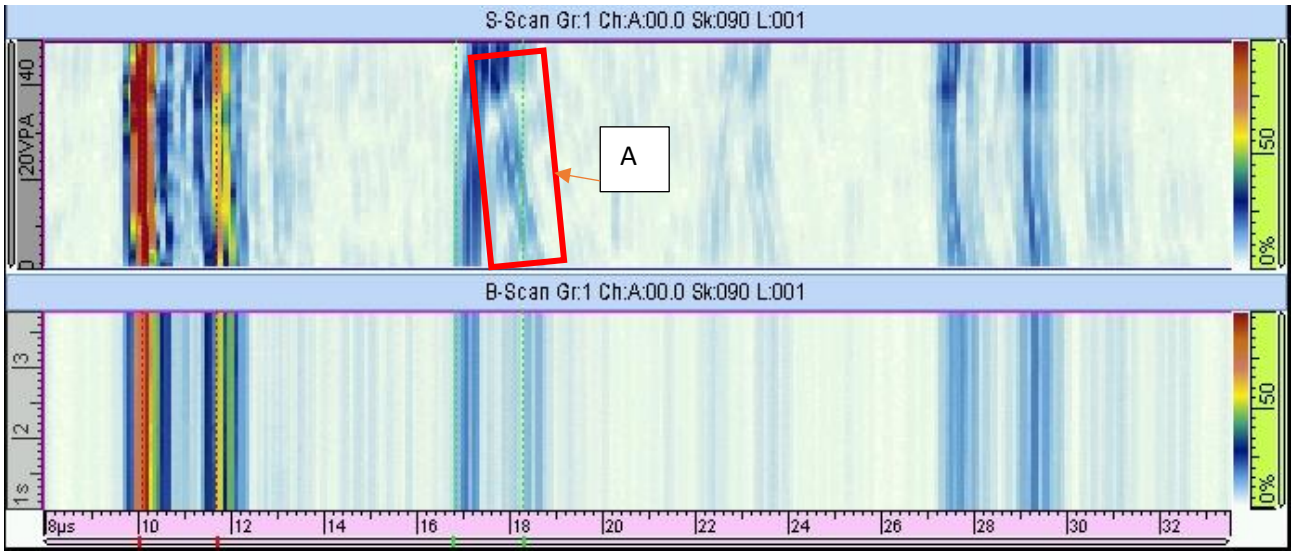

Figure 5-33. Fiberglass thickness reduction detection (PA 3.5 MHz) with focal law

In comparison to figure 5.33, 5 MHz array view of the reduced thickness fiberglass is provided in figure 5.34. It can be observed that resolution given by 3.5 MHz frequency is slightly better comparing to 5 MHz.

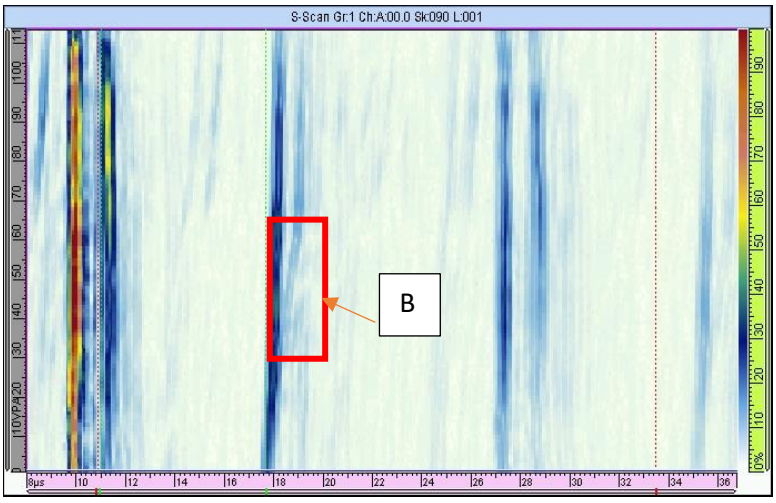

Figure 5-34. Fiberglass thickness reduction detection (PA 5 MHz)

5.3.3.6 Fiberglass shell mechanical impact damages

It is very common for propeller blade to suffer mechanical damages during the life span. This comes from various sources as hail damage, tooling damage, accidental damages. Thus, it was important to test if phased array has detected such defects within the fiberglass shell.

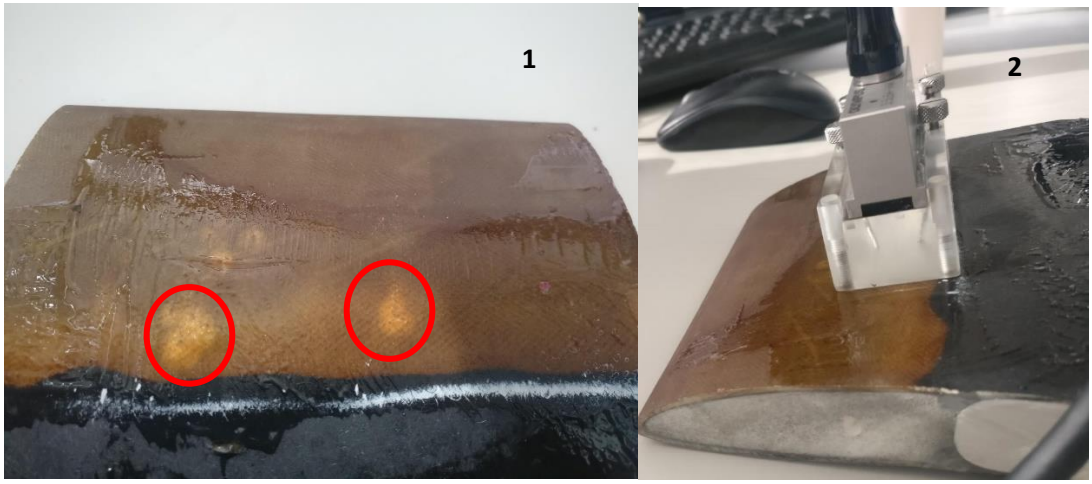

Figure 5-35. 1 -artificial mechanical impact damages done on glass fiber composite shell at the leading edge of the blade; 2 – phased array setup during inspection

Artificial impact zones have been done as showed and inspected with phased array as showed in figure 5.35. S-scan of the inspection is presented in figure 5.36. Due to the crushed fiberglass shell the echo received is different comparing to no flaw zone figure.

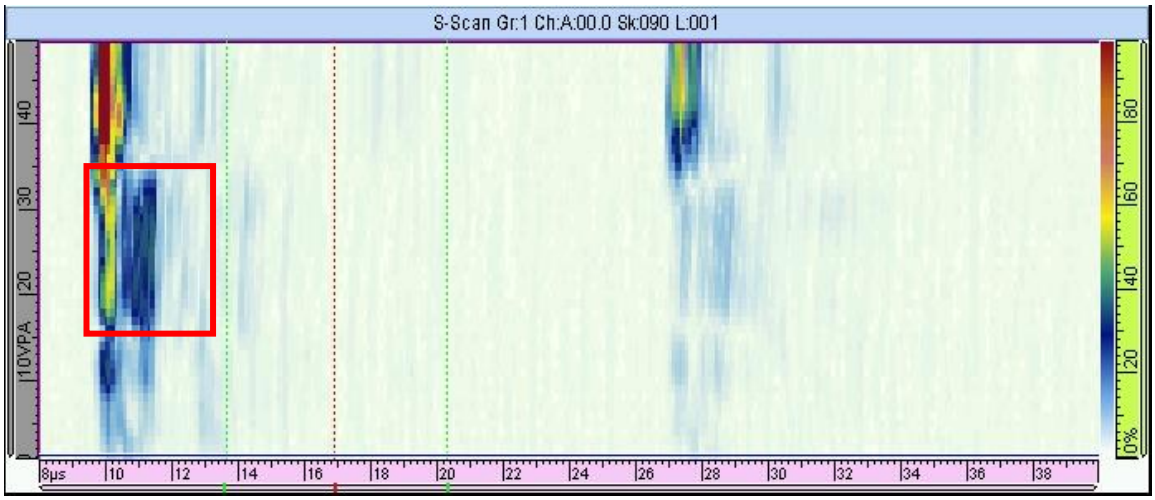

Figure 5-36. Mechanical impacts detection on propeller blade (PA 3.5 MHz)

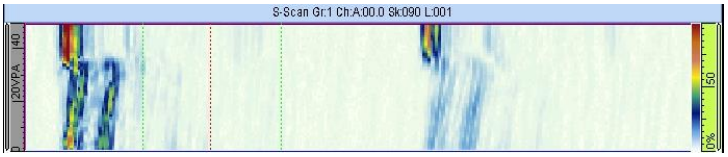

Figure 5-37. S-Scan at the point where no mechanical damage is done (PA 3.5 MHz)

1. Literature review has been performed for NDT techniques available to be used for propeller blade. Literature review helped to determine the correct NDT methods and probes type to start the theoretical and experimental analysis. During the project contact type and phased array probes used which was found as concurring with literature review as suitable solutions.

2. Sections have been cut from physical propeller blade, 3D scanned and imported to CIVA for theoretical analysis. Propeller blade's materials acoustic characteristics have been found experimentally by utilising different types and frequencies of contact probes.

3. Computerised model for propeller blade has been created using CAD files received from 3D scanner and acoustic properties set. Computerised model results compared to experimental results. Computer model has been experimentally validated.

4. Different types probes has been used to find acoustic characteristics of separate material volumes. Results driven experimental inspections determined that contact type probe with frequency of 3.5 MHz coupled with water for better acoustic penetration was found suitable to find the individual material's characteristics.

5. Phased array ultrasonic scanning has been performed on physical propeller blade comparing to model data. It was found that phased array probe with aperture of 64 elements and frequency of 3.5 MHz would be most suitable for complex shape propeller blade overall inspection and all types of flaws detection. It was also found that wedge which would be used must be flexible which would adapt to propeller blade air foil

1. Olympus flaw detection tutorial [viewed on 01.02.2019]. Access via https://www.olympus-ims.com/en/ndt-tutorials/flaw-detection/wave-propagation/

2. United Technologies Corporation. Composite blade manufacture. Inventors: Jogn M.Graff, John A.Violette. USA patent WO 1993008017 [viewed on 09.06.2017]. Access via Google Patents

3. Extende software manufacturer [viewed on 03.01.2018]. Access via http://www.extende.com/files/extende/download_files/CIVA_2017_Software_Data_Sheet_EN.pdf

4. NDT Resource centre [viewed on 03.01.2018]. Access via : https://www.nde-ed.org

5.Ultrasonic testing -NDT encyclopaedia [viewed on 03.01.2018]. Access via: http://www.ndt.net/ndtaz/content.php?id=435

6. NDT Resource centre [viewed on 03.01.2018]. Access via https://www.nde-ed.org/EducationResources/CommunityCollege/Ultrasonics/Physics/defectdetect.htm

7. NDT Resource centre [viewed on 03.01.2018]. Access via https://www.nde-ed.org/EducationResources/CommunityCollege/Ultrasonics/Physics/attenuation.htm

8. NDT Resource centre [viewed on 03.01.2018]. Access via https://www.nde-ed.org/GeneralResources/Formula/UTFormula/near_field/near.htm

9. Ultrasonic evaluation of the fibre content in glass/epoxy composites [2006], G. Wróbel, S. Pawlak, Journals of Achievements in materials and manufacturing engineering, Volume 18, issue 2. Access via: http://citeseerx.ist.psu.edu/viewdoc/download?doi=10.1.1.457.3039&rep=rep1&type=pdf

10. Jasiūnienė E, Renaldas. R, Šliteris.R, Voleišis. A, Jakas, M. Ultrasonic NDT of wind turbine blades using contact pulse-echo immersion testing with moving water container, ISSN 1392-2114 [viewed on 14.01.2018], access on: https://epubl.ktu.edu/object/elaba:6083446/

11. G. J. Gruber . Defect identification and sizing by the ultrasonic satellite pulse technology, Southwest Research Institute. [viewed on 14.01.2018]. Access via https://pdfs.semanticscholar.org/5f5c/4473de66f7f5e81d94cd5964fd958cf9c713.pdf

12. S. Chatillon, L. de Roumilly, J. Porre, C. Poidevin, P. Calmon, Simulation and data reconstruction for NDT phased array techniques, Ultrasonics 44 (2006) e951–e955. Access via science direct

13. A.G. Every, The importance of ultrasonics in nondestructive testing and evaluation, Ultrasonics 54 (2014) 1717–1718. Acess via Science direct

14. Edouard G. Nesvijski, Some aspects of ultrasonic testing of composites, Composite Structures 48 (2000) 151-155 . Access via Science direct

15. Frank Babick, Frank Hinze, Siegfried Ripperger , Dependence of ultrasonic attenuation on the material properties , A: Physicochemical and Engineering Aspects 172 (2000) 33–46. Acess via Science direct

16. Ran Li, Qing-Qing Ni, Hong Xia, Toshiaki Natsuki, Analysis of individual attenuation components of ultrasonic waves in composite material considering frequency dependence, Composites Part B 140 (2018) 232- 240. Access via Science Direct

17. Biwa S. Independent scattering and wave attenuation in viscoelastic composites. Mech Mater 2001,33(11). Access via Science Direct

18. Biwa S, Idekoba S, Ohno N. Wave attenuation in particulate polymer composites: independent scattering/absorption analysis and comparison to measurements. Mech Mater 2002,34(10):671-82. Access via Science Direct

19. Biwa S, Watanabe Y, Ohno N. Analysis of wave attenuation in unidirectional viscoelastic composites by a differential scheme. Compos Sci Technol 2003;63(2),237-47. Access via Science Direct

20. Martin Spies, Hans Rieder, Synthetic aperture focusing of ultrasonic inspection data to enhance the probability of detection of defects in strongly attenuating materials, NDT&E International 43 (2010) 425–431, Access via Science direct

21. Diamanti K, Soutis C. Structural health monitoring techniques for aircraft composite structures. Prog Aerospace Sci 2010;46:342–52. Access via Science direct

22. Bruce W. Drinkwater, Paul D. Wilcox. Ultrasonic arrays for non-destructive evaluation: A review , NDT&E International 39 (2006) 525–541. Access via Science direct

23. Weixiang Du, A review of miniaturised Non-Destructive Testing technologies for in-situ inspections, Procedia Manufacturing 16 (2018) 16-23. Acess via Access via Science direct

24. Christian Garnier, Marie-Laetitia Pastor, Florent Eyma, Bernard Lorrain, The detection of aeronautical defects in situ on composite structures using Non Destructive Testing, Composite Structures 93 (2011) 1328–1336. Access via Science direct

25. J.A. Schroeder, T. Ahmed, B. Chaudhry, S. Shepard, Non-destructive testing of structural composites and adhesively bonded composite joints: pulsed thermography, Composites: Part A 33 (2002) 1511–1517. Access via Science direct

26. Andrzej Katunin, Krzysztof Dragan, Michał Dziendzikowski, Damage identification in aircraft composite structures: A case study using various non-destructive testing techniques, Composite Structures 127 (2015) 1–9. Access via Science direct

27. Daniel Veira Canle, Ari Salmi, Edward Hæggstrom, Non-contact damage detection on a rotating blade by Lamb wave analysis, NDT and E International 92 (2017) 159–166. Access via Science direct
28. Lingyu Yu, Zhenhua Tian, Guided wave phased array beamforming and imaging in composite plates, Ultrasonics 68 (2016) 43–53. Access via Science direct

29. Gian Piero Malfense Fierro, Michele Meo, A combined linear and nonlinear ultrasound time-domain approach for impact damage detection in composite structures using a constructive nonlinear array technique, Ultrasonics 93 (2019) 43–62. Access via Science direct

30. Junliang Dong, Byungchil Kim, Alexandre Locquet, Peter McKeon, Nico Declerc, D.S. Citrin, Nondestructive evaluation of forced delamination in glass fiber-reinforced composites by terahertz and ultrasonic waves, Composites Part B 79 (2015) 667-675. Access via Science direct

31. Ružek, R., Lohonka, R., Josef Jironč, Ultrasonic C-Scan and shearography NDI techniques evaluation of impact defects identification. NDT & E International, 39(2006), 132-142. Access via Science direct

32. S.Gholizadeh , A review of non-destructive testing methods of composite materials
XV Portuguese Conference on Fracture, PCF 2016, 10-12 February 2016. Access via Science direct

33. Meola, C., & Carlomagno, G. M. (2014). Infrared thermography to evaluate impact damage in glass/epoxy with manufacturing defects. International Journal of Impact Engineering, 67(2014), 1-11.

34. V.Dattoma , Optimization and comparison of ultrasonic techniques for NDT control of composite material elements , Structural Integrity Procedia 12 (2018) 9–18. Access via Science direct

35. F. Schadow, Ultrasonic inspection and data analysis of Glass and Carbon fibre reinforced plastics, Procedia structural integrity 7 (2017) 299-306. Access via Science direct

36. V. Kappatos, G. Asfis, K. Salonitis, V. Tzitzilonis, N. P. Avdelidis, E. Cheilakou, P. Theodorakeas , Theoretical Assessment of Different Ultrasonic Configurations for
Delamination Defects Detection in Composite Components, Procedia CIRP 59 (2017) 29 – 34 , Access via Science direct

37. RuizhenYang, YunzeHe, HongZhang, Progress and trends in non destructive testing and evaluation for wind turbine composite blade, Renewable and Sustainable Energy Reviews 60(2016) 1225–1250. Access via Science direct

38. Mark Sonnenschein, Benjamin L. Wendt, Alan K. Schrock, Jean-Marie Sonney, Anthony J. Ryan, The relationship between polyurethane foam microstructure and foam aging, Polymer 49 (2008) 934-942. Access via Science direct

39. E. Ciecierska, M. Jurczyk-Kowalska, P. Bazarnik, M. Gloc, M. Kulesza, M. Kowalski, S. Krauze, M. Lewandowska, Flammability, mechanical properties and structure of rigid polyurethane
foams with different types of carbon reinforcing materials , Composite Structures 140 (2016) 67–76. Access via Science direct

40. Chiara Colombo, Laura Vergani Influence of delamination on fatigue properties of a fibreglass composite, Composite Structures 107 (2014) 325–333. Access via Science direct

41. Walid Harizi, Salim Chaki, Gérard Bourse, Mohamed Ourak, Mechanical damage characterization of glass fiber-reinforced polymer laminates by ultrasonic maps, Composites: Part B 70 (2015) 131–137. Access via Science direct

42. M.A. Caminero, S. Pavlopoulou, M. Lopez-Pedrosa, B.G. Nicolaisson, C. Pinna, C. Soutis Analysis of adhesively bonded repairs in composites: Damage detection and prognosis, Composite Structures 95 (2013) 500–517, Access via Science direct

43. P. Gaudenzi, M. Bernabei, E. Dati, G. De Angelis, M. Marrone, L. Lampani, On the evaluation of impact damage on composite materials by comparing different NDI techniques, Composite Structures 118 (2014) 257–266. Access via Science direct

44. Angelika Wronkowicz, Krzysztof Dragan, Krzysztof Lis, Assessment of uncertainty in damage evaluation by ultrasonic testing of composite structures , Composite Structures 203 (2018) 71–84 , Access via Science direct

45. A.P. Mouritz, C. Townsend, M.Z. Shah Khan Non-destructive detection of fatigue damage in thick composites by pulse-echo ultrasonics, Composites Science and Technology 60 (2000) 23-32. Access via Science direct

46. Jochen H. Kurz, Anne Jüngert, Sandra Dugan, Gerd Dobmann, Christian Boller Reliability considerations of NDT by probability of detection (POD) determination using ultrasound phased array. Access via Science direct

47. M.E. Ibrahim, R.A. Smith, C.H. Wang Ultrasonic detection and sizing of compressed cracks in glass- and carbon-fibre reinforced plastic composites, NDT and E International 92 (2017) 111–121. Access via Science direct

48. Phani Mylavarapu, Eyassu Woldesenbet A predictive model for ultrasonic attenuation coefficient in particulate composites, Composites: Part B 41 (2010) 42–47. Access via Science direct

49. A. Misra, Composite materials for aerospace propulsion related to air and space transportation, Design, Manufacturing, Analysis and Performance 2016, Pages 305-327. Access via Science direct.

50. PNDT Broshure , How Phased array work. Access via https://www.applusrtd.com.au/files/brochure/39_Howphasedarraysworks.pdf

51. Airbus NDT manual [viewed on 15.03.2018]. Access via https https://www.scribd.com/document/307160919/Airbus-Non-Destructive-Test-Manual